Mechanical Modeling and Characterization of Cancer Cells Using Optical Tweezers

by

Samaneh Khakshour

M.Sc., Khajeh Nasir Tousi University of Technology, 2009

Thesis Submitted in Partial Fulfillment of the
Requirements for the Degree of
Doctor of Philosophy

in the
School of Mechatronic Systems Engineering
Faculty of Applied Sciences

SIMON FRASER UNIVERSITY

Summer 2016

Approval

Name: **Samaneh Khakshour**

Degree: **Doctor of Philosophy**

Title: ***Mechanical Modeling and Characterization of Cancer Cells Using Optical Tweezers***

Examining Committee: **Chair:** Dr. Woo Soo Kim
Assistant Professor

Dr. Edward Park
Senior Supervisor
Professor

Dr. Timothy Beischlag
Co-Supervisor
Associate Professor

Dr. Carolyn Sparrey
Supervisor
Assistant Professor

Dr. Ash Parameswaran
Internal Examiner
Professor
School of Engineering Sciences

Dr. Stephanie Willerth
External Examiner
Associate Professor
Department of Mechanical Engineering
University of Victoria

Date Defended/Approved: June 15, 2016

Abstract

In this thesis, the development of a novel optical tweezer is described. Additionally, alterations in the mechanical properties of cancer cells associated with metastatic transformation was characterized using this technology. Cell mechanical properties can be utilized as a quantitative measure for understanding the pathophysiological behavior of cells and evaluating pharmacological treatments that modify the cell structure. Thus, an oscillating optical tweezer capable of applying time varying force and manipulating the cell cytoskeleton was developed in order to measure the mechanical properties and structural changes of single epithelial cancer cells and blood cancer cells. Employing this device would be beneficial in differentiating between normal, cancer and metastatic cancer cells and evaluating the effectiveness of different chemotherapeutic approaches.

To this end, the developed tool was utilized to conduct a systematic study of the mechanical properties of human epithelial cancer cells by mimicking the condition that causes cancer cell invasiveness and tumour cell transformation. Different signaling pathways that modulate actin organization under hypoxia were studied via analyzing the biophysical properties of cancer cells and quantifying cytoskeleton rearrangement employing the oscillating optical tweezer. It was demonstrated the optical tweezer is a novel, rapid and reliable tool for the identification and characterization of cancer cells and for evaluating therapeutic performance. Finally, a sensitivity study was applied using COMSOL to evaluate the effect of cell-bead geometries on cell mechanical responses for different cell types and optical tweezer experiments.

Keywords: Optical tweezer, single cells, cell manipulation, cancer, therapeutic agent evaluation

To my loving companion, Yaser

Acknowledgements

First I would like to express my appreciation to my senior supervisor and my mentor Professor Edward Park. I would like to thank you for guiding me and for allowing me to grow as a research scientist. I would also like to thank my co-supervisor Dr. Timothy Beischlag and my supervisor Dr. Carolyn Sparrey for your priceless advices during my PhD path. Furthermore, I would like to thank my examining committee, Dr. Ash Parameswaran and Dr. Willerth for serving as my committee members.

I would specially like to thank my lab mates Shabnam, Hadi, Mandeep, Kelly for your help and support during these years. You have always encouraged me and did not let me to loss hope or courage to finish the PhD line. I am really grateful to my dearest friend Shabnam who helped me by giving her suggestions and assistance and supply of valuable information.

A special thanks to my family, my mother-in-law, father-in-law, my mother, and father for all the sacrifices that you have made and all your support during this path. Also, I would like to express my appreciations to my siblings, Saeideh, Sara and Hamed. You have always been there for me and cheered me up. At the end I would like to express my special thanks to my husband Yaser Mohammadian Roshan who was unconditionally there for me and supported me and offered precious suggestions all the time.

Table of Contents

List of Tables

List of Figures

List of Symbols and Abbreviations

AFM: Atomic Force Microscopy

AKT: Protein Kinase B

ANOVA: Analysis of Variance

ART: Artesunate

ERK: Extracellular Signal Regulated Kinase

LNCaP: Lymph Node Carcinoma of the Prostate

MANOVA: Multivariate Analysis of Variance

MTC: Magnetic Twisting Cytometry

MTOR: Mechanistic Target of Rapamycin

NARBM: Normalized Amplitude of Resultant Bead Movement

NFkB: Nuclear Factor Kappa-Light-Chain-Enhancer of Activated B Cells

NPAF: Normalized Position Autocorrelation Function

OT: Optical Tweezer

PBS: Phosphate-Buffered Saline

Rb: Retinoblastoma

RBC: Red Blood Cell

RGD: Arginyl Glycylaspartic Acid

SCX: Scrambled

shRb: Short Hairpin Retinoblastoma

shSCX: Short Hairpin Scarambled

Chapter 1

Introduction

1.1 Background and Rationale

Biomechanics is the study of structure and function of biological systems such as cells by means of methods of mechanics. The links between biomechanics and human disease have been studied extensively. Previous studies showed that the progression of human disease is related to the alteration of mechanical properties of cells [1-17]. Therefore, the determination of cells' mechanical properties could be helpful in differentiating between normal and diseased cells and facilitate early detection of disease. Furthermore, employing mechanical approaches and modifying them properly based on the experimental conditions can be used to interpret biological responses of cellular and subcellular components such as phospholipid bilayer membrane and cytoskeleton quantitatively. Table 1.1 summarizes key examples of diseases and their mechanical effects on cells.

Recent advances in technology and the integration of these advances in an interdisciplinary fashion into the life sciences and medicine provide valuable tools in the study of cellular and molecular mechanics. These tools can be applied to the study of different disease states such as cancer. Improvements in engineering and physics have led to development of devices with the capability of measuring or generating forces and deformations in the resolution of picoNewton and nanometer ranges [18-43]. Progress in computer technologies has enabled the use of sophisticated numerical models to interpret cellular and biomolecular behaviors that are not measureable quantitatively solely by conventional experimental techniques [44-69]. Also, advances in genetics and genomics have provided new techniques for disease diagnosis and therapies. Such

knowledge can be applied to better understand cellular mechanical responses associated with certain diseases by directly targeting specific genes [1], [2].

The above advances have enabled researchers to study in-depth the influence of state of disease such as cancer on cellular and subcellular mechanics. Finding the connection between cell structure, mechanical properties, function, and human disease is the main focus of these studies [3].

In order to find the connection, first, we need to develop an appropriate tool that is capable of measuring and interpreting mechanical properties of diseased cells. In this thesis, I developed an oscillating optical tweezer (OT) that is capable of applying time varying force on cell cytoskeleton and measuring mechanical properties and structural changes of epithelial cancer cells and blood cancer cells. Employing this device would be beneficial in differentiating between normal, cancer and metastatic cancer cells and evaluating the chemotherapy performance. Moreover, employing such a device is useful as an additional research tool to further validate the conventional research results.

The second step is to conduct a systematic study of mechanical properties of cells under a full range of the disease state by mimicking *in vivo* phenomena. Such detailed systematic analysis of cells' mechanical properties, in particular for cancer, has not yet been carried out very widely, since the underlying mechanisms are very complicated [3]. In this thesis, a systematic study of mechanical properties of human epithelial cancer cells was conducted by mimicking the condition that causes cancer cell invasiveness. Such invasiveness properties cause cancer cells to become mesenchymal stem cells (Epithelial to mesenchymal transition or EMT). During the process of EMT we see changes in the cell cytoskeleton, altering the cellular structure and mechanical properties of the cells.

Employing an OT, we found the relationship between the cell structure, mechanical properties of cells and molecular mechanism that result in structural changes in epithelial cancer cells undergoing EMT. Therefore, measuring cancer cell stiffness by employing the OT can provide useful insights into the molecular mechanisms that might be critical determinants of the motile and invasive phenotype of

cancer cells. Finally, the mechanical characterization of cancer cells could provide an additional technique for cancer diagnosis and evaluating therapeutic performance.

Table 1.1. Examples human diseases and the related pathophysiological outcome from biomechanics perspective.

Human Disease	Pathophysiological Outcomes	Pertinent Reference
Arthritis	Chondrocyte stiffening and increased viscosity	[4]
Asian ovalocytosis	Erythrocyte stiffening	[5]
Asthma	Airway smooth-muscle cell stiffening and contracting	[6]
Cancer	Epithelial and fibroblast cells softening and metastasis	[7], [8], [9], [10]
Cryohydrocytosis	Erythrocyte stiffening	[5]
Elliptocytosis	Erythrocyte stiffening and increased adherence	[11]
Malaria	Erythrocyte stiffening and cytoadherence	[1] , [12], [13], [14]
Sickle cell anemia	Erythrocyte stiffening and increased viscosity	[15] , [16]
Spherocytosis	Erythrocyte stiffening and increased adherence	[17]

1.2 Previous Works

Several single cell manipulation technologies and mechanical cell modeling approaches already exist in previous literature. In this section, a variety of mechanical cell characterization methods that include experimental techniques (e.g., atomic force microscopy, optical tweezers, optical stretcher, magnetic tweezers, micropipette aspiration, and magnetic twisting cytometry) and computational approaches for investigating the mechanical cell responses are reviewed.

1.2.1 Cell Manipulation Technologies

Atomic Force Microscopy

A schematic of atomic force microscopy (AFM) is shown in Figure 1.1a, which can be used both as an imaging tool and a force sensor. The principle of AFM is based on detection of forces acting between the sample surface and the AFM's sharp tip. The tip is attached to a flexible cantilever, and any movement of the cantilever can be detected by an optical system. This method has various features that make it valuable in biology. Being able to study biological objects in their natural conditions, scanning surfaces with up to nanometer resolution, providing 3D surface topographical information are some of AFM beneficial features. AFM has been used widely to study cell mechanics such as Jurkat T lymphoma cells [18], human lung carcinoma cells [19], kidney epithelial cells [20], human platelets [21], and human bladder cells [22]. This technique can provide useful elastic properties of cells in nanoscale. However, applying force on cells may damage the cell, also the shape of the tip and its location on the cantilever might affect the force deformation results.

Optical Stretcher

The optical stretcher consists of two opposed, identical laser beams which can trap and deform an object in the middle (Figure 1.1b). If the beam size is larger than the size of the object and the refractive index of the object is larger than the surrounding medium, the trapping is stable and the total force on the object is zero. The laser power up to 800 mW in each laser source can be used, which lead to surface forces up to hundreds of pico-Newton [23]. This technique has been used to manipulate cells and

study mechanical characteristics of different cells, such as RBCs [24], fibroblasts and breast epithelial cells [25], and oral epithelial cancer cells [26]. The main advantage of this technique is that its working distance is large; therefore, it has a large trapping volume which provides a high throughput cell analysis. Its main disadvantage is its limitation to suspension cells manipulations.

Micropipette Aspiration

Micropipette aspiration can be used to study the mechanical responses of living cells. The schematic of this method is shown in Figure 1.1e. In this technique a small-diameter glass pipet is brought in to contact with a cell. Applying a known suction pressure within the pipette, causes the cell aspiration into the pipette. The range of forces that micro pipette aspiration technique can apply is in the range of 10pN-104nN which is more than other techniques. Since there can be a significant amount of evaporation in the chamber and also it demands training and skill for the experiments, this is not a perfect technique. This method has been used to study deformation behavior of different cells such as RBCs [27], neutrophils [28], chondrocytes [29], human embryonic stem cells [30]. Some of the advantages of this technique are its low cost and simplicity comparing to other techniques; however, it might deform or damage cells profoundly during experiment.

Magnetic Twisting Cytometry

Magnetic twisting cytometry (MTC) can be used to probes mechanical properties of an adherent cell by applying torque to magnetic beads that are bound to cell membrane (Figure 1.1d). The torque is generated by applying a directional magnetic field H to the beads. Using this method the relation between applied torque and angular rotation can be measured. The cell response in this method is time dependent, which makes MTC suitable for characterizing viscoelastic properties of cells, such as chick embryos cells [31], actin networks [32], RBCs [33], and endothelial cells [34]. Its main advantage is using magnetic beads as a probe, as beads can be coated with variety of molecules and ligands that are specific to a certain cell structure. However, variability of magnetic properties among bead populations and non-uniformity of the applied stress profile on cells are the main limitations of this technique.

Optical Tweezers

Optical tweezers, also known as optical traps, use a laser beam focused through a high-quality microscope objective to generate an optical trap, which is able to constrain microscopic objects (Figure 1.1c). The underlying principle of laser OTs has been known for over a century. At the beginning of the 19th century, scientists learned that light of a high power density focused laser through a microscope could be used to manipulate biological objects. In 1970, Arthur Askhin found that small particles may be trapped by the radiation pressure of a laser beam. The first demonstration of OTs with the basic three-dimensional single-beam trap configuration was reported in 1986. Later in 1987, Ashkin and his group reported trapping viruses and Escherichia coli bacteria [35]. Recent technical innovations established OTs as a biological tool for studying biological forces [36]. There are several cells that have been studied to investigate their mechanical characteristics, such as studies of the deformation characteristics of the human RBC and its membrane. RBCs in different osmotic saline solutions are stretched at various laser powers, and the relationships between the stretching forces and the induced deformations were obtained [37]. OT has been used to measure the effect of store time on force–extension relation curves for erythrocytes cells [38]. To study the shape recovery of deformed RBCs, investigators used three OTs to induce a parachute-shaped red blood cell deformation comparable to the deformation in small capillaries [39]. To measure the apparent membrane viscosity, the spatially fixed OTs trapped a silica bead bound to one RBC of two-cell spontaneously formed rouleaux, while the second OTs trapped the other RBC directly [40]. OT has also been used to measure mechanical response of a chondrocyte cells. Moreover, an increases in the intracellular calcium level of bone and cartilage derived cells were observed by applying force on these cells using OT [41]. The effect of laser trap duration and laser trapping power on sperm motility between sperm swimming force, swimming speed and speed of progression score were described [42]. The PKH membrane linkers effect on the adhesive properties of cells were determined, by using OT [43]. Mechanical properties of different parts of mouse fibroblast cell at different time are assessed by OT [44]. OT can be used to form tethers, between a living E. coli cell and a bead, which are several times longer than the bacterial length [45]. The main advantage of this technique is its non-invasiveness in terms of lack of contact between cells and laser. Moreover, being able to

coat the bead specifically for different cell structures, would allow OT to apply force on variety of cell structures. However, due to the limitation on the number of lasers, one or small number of cell location manipulation at a time is possible.

Extensive cell structure studies which have been done by OT demonstrate its ability in becoming a promising tool to study cell mechanical behaviour. Moreover, the importance of manipulating cells in a non-invasive fashion in terms of nonphysical contact between cell and the laser beam is the main reason behind our choice of OT. Therefore, in this thesis, an OT setup is utilized to perform experimental analysis on structural changes of cancer cells. The details of the OT setup used for my experiments are described in Section 2.2.1.

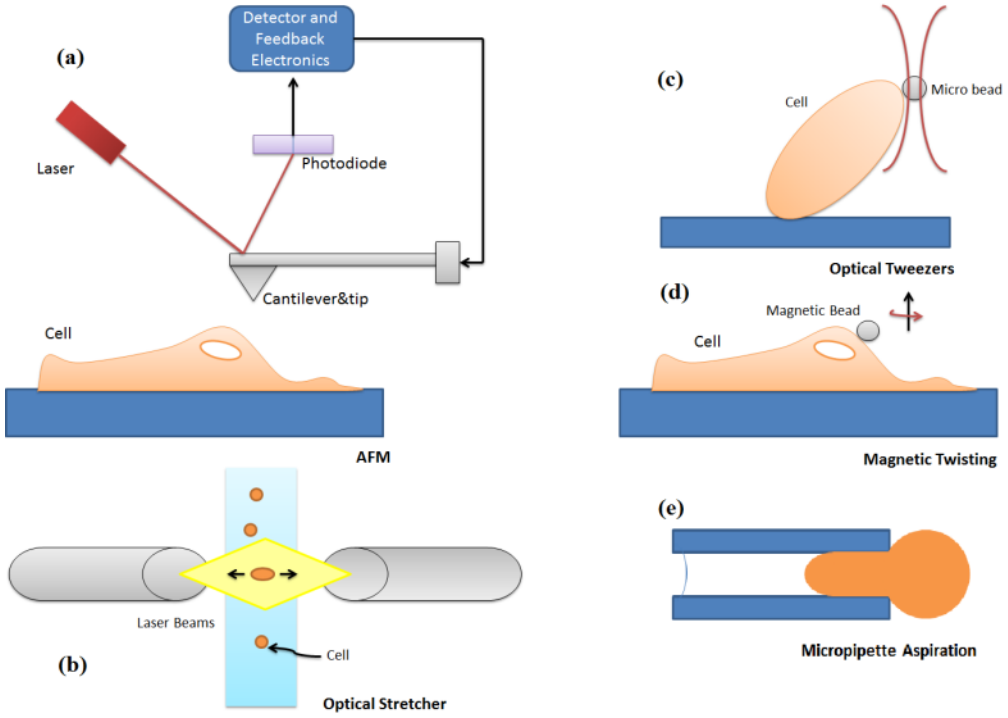

Figure 1.1. Different cell manipulation technique: (a) AFM, (b) Optical Stretcher, (c) OT, (d) MTC, (e) Micropipette Aspiration.

1.2.2 Mechanical Modeling of Cells

To perform analytical study on mechanical behaviour of cells, developing a modelling technique that can describe the cell behaviour is necessary. There are two

major approaches for cell modeling in the literature: continuum models and microstructural models. The continuum models treat cells as comprising of materials with certain continuum material properties. These models are used for characterizing biomechanical responses of cells based on experimental manipulation tools such as OT, AFM, micropipette aspiration, etc. The microstructural models treat the cells as comprising a network of microstructural elements and they are based on Monte Carlo and molecular dynamics simulation [46].

Microstructural Models

Generally microstructural models consist of a network of interconnected structures. The list of common microstructural models in the literature is as follows:

- *Open Cell Foam Model*: The open cell foam model was first proposed by Satcher et al. (1996) [47] and it assumed that the cytoskeleton is a network of interconnected struts. In this model, the structural elastic modulus is proportional to either φ or φ2 depending on whether the cell is stretched or bended, where φ is the relative foam density which can be obtained as the ratio of foam mass density to the mass density of an individual strut.

- *Tensed Cable Networks*: Tensed cable networks model considers the cytoskeleton as reticulated structures composed of cables, which cannot support compression. These cables carry initial tension, and balance to the cable tension is internally (e.g. by compression-supporting elements of the CSK), or externally (e.g. by the extracellular matrix or ECM), or by combination of both [48], [49].

- *Semiflexible Chain*: The semiflexible chain model describes how mechanical strength of cells is maintained by tension. This model is based on the idea that stretching the thermally fluctuating chain causes a reduction in number of possible chain configuration of states, which is associated with stiffening of the chain [50].

- *Dipole Polarization*: The dipole polarization model describes the active remodeling of cytoskeleton as the actin-myosin dipole. The dipoles are defined by their orientation and the magnitude of the force they exert. Actin-myosin is oriented in the direction of applied stress, and a contracting force is developed to oppose the stress and help the system to maintain the equilibrium. In this manner, the dipoles polarize in the direction of applied stress [50], [51].

- *Brownian Ratchet:* The Brownian ratchet model is based on Brownian Ratchet theory, where non-equilibrium fluctuations in an isothermal fluid can induce mechanical force and motion. Based on this model, chemical reactions generate cellular protrusive forces and mechanical motions during actin polymerization [50], [52].

- *Stress Fiber Reorganization*: It has been observed that stress fibers are pre-extended at a homeostatic level, and external forces that change the fiber length could dissociate the stress fibers [53]. Stress fiber reorganization model can be used to model the rate of stress fiber assembly. The relationship between fiber dissociation and strain rate is defined based on this model as well [54].

- *Dynamic Stochastic*: The dynamic stochastic model considers cells as elastic force dipoles and externally applied forces could change the dipole orientation and magnitude. This model is based on the idea that cells reorganize their stress fibers to maintain the optimal stress or strain and any deviation from optimal state cause internal forces within the cells to restore the optimal state [50].

- *Constrained Mixture:* The constrained mixture model considers four different events in cells to describe the cell mechanics. The diffusion of actin monomers inside the cells, stress fiber formation from the monomers, stress fiber contraction, stress fiber dissociation to monomers is the different events considered in this model. This model is used to find the relation between cell contraction and substrate stiffness [55].

Continuum Models

The main draw back of microstructural models is model complexity and limited available computational power. This issue is solved by employing the continuum models. In continuum models cell material is considered as a continuum media with the length scale of interest being significantly larger than the discrete microstructure. Some of the most common continuum models in literature is listed as follows:

- *Cortical Shell-Liquid Core:* The Cortical shell-Liquid core model was first proposed by Yeung and Evans [56]. The cell is modeled as a uniform liquid core which is assumed to be Newtonian viscous fluid, and a cortical shell which is considered as an isotropic fluid layer with static tension. The membrane theory is applied to drive the constitutive relations for cortical shell. In [57] and [58], a more complicated model that considered the contribution of nucleus was derived.

- *Shear Thinning*: The shear thinning liquid drop model was first found by Tsai et al. in 1993 [59] where they established that the apparent cytoplasmic viscosity depended on the shear rate at large deformations. The Maxwell liquid drop model was first proposed by Dong et al. in 1998 [60], in which the liquid core of the cell was assumed to have Maxwell fluid characteristics.

- *Solid*: The solid model treats cells as homogeneous, incompressible elastic solid or viscoelastic solid materials. The linear viscoelastic and elastic models were first proposed by Schmid-Schonbein et al. in 1981 and Theret et al. in 1988 [61], [62], respectively.

- *Power Law*: The previous models are all derived using the static loading of the cell; however, in real life, cells are subjected to dynamic forces in their environment. Testing the dynamic forces on adherent cells are conducted using oscillatory MTC [63], AFM [64], and OT [65]. In all techniques a sinusoidal force signal is applied, which resulted in a sinusoidal cell movement with the same frequency. Using this model the dynamic viscoelastic modulus that depended on frequency according to a weak power

law were obtained. The power law structural damping model was proposed by Fabry et al., [66] and [67], to interpret the dynamic behaviors of cells.

- *Biphasic*: The biphasic model assumes two separate phases of solid and interstitial fluid material for the cytoplasm [68]. This model was first employed for biological tissue by Mow et al. (1980) [69]. The solid phase was assumed as linear elastic and the fluid phase as an inviscid fluid. The proposed theory suggested that the changes of momentum between two different phases caused by friction are partially responsible for the cells viscosity.

The continuum models are the main mechanical models for representing cell behaviour. The material nonlinearity can be considered in these models in order to simulate cell mechanical responses. Moreover, the contact and boundary conditions can be incorporated accurately in these models. Since a microbead with a radius of 3 μm as a handle to manipulate cells was used in this thesis, the length scale of the region of applied force is larger than the discrete nature of cytoskeleton network (50-100 nm). Therefore, continuum models best describe cell behaviours based on OT experimental measurements. As a continuum model, first we developed a static model based on shell theory in order to account for any bending moments that may arise from the use of an OT in the mechanical characterization of the membrane of suspended cells. However, as cells are subjected to dynamic force in their environment, a viscoelastic model that describes the dynamic behaviour of cells was developed later. Comparing this dynamic model to other static continuum models in the literature, it enabled us to measure the power-law coefficient of cells that is an intrinsic property of the cell cytoskeleton, using oscillating OTs. Thus, such model could be a more accurate representation for cell mechanical responses and properties.

1.3 Summary of Contributions

In the first “development” phase of this project, a proper tool for single cell manipulation and characterization of mechanical properties of cells was developed. To

develop such a tool, an OT system in concert with numerical models was employed to measure and analyze the structural properties of single cells. Two different forms of cell manipulation were employed using the OT to better understand and interpret a cell's mechanical responses. In the first form, a constant force was applied on a single cell and the mechanical response of the cell was analyzed utilizing shell theory. The related results are demonstrated in Chapter 2 [70]. In the second form, a cyclic force was applied and dynamic properties of cell structure was analyzed and the results are represented in Chapter 3 [71]. Both states of cell manipulation and characterization were employed on Jurkat cells to demonstrate the performance of the developed tool and its usage in a drug efficacy study.

The corresponding contributions related to this phase of project are as follows:

1. Modifying existing models to develop a proper model for characterizing mechanical properties of suspended cells under constant force. This will help to overcome the non-feasibility problem in the previous methods by taking into account of the effect of bending moment (Chapter 2 [70]).

2. Optimizing a numerical model by reducing the number of free parameters for estimating key mechanical parameters of suspended and adherent cells under cyclic force (Chapter 3 [71]).

3. Modifying the OT setup by adding an extra camera and applying video processing techniques to better analyze the OT results (Chapter 3 [71]).

4. Demonstrating quantitative indicators of therapeutic efficacy by establishing the relationship between the Jurkat cell' cytoskeleton stiffness and different ART dosages, as well as indicating the effect of chemotherapy on cells' power-law coefficient (Chapter 3 [71]).

In the next "application" phase of the project, the above tool was employed to provide a systematic study of mechanical responses of cancer cells as a function of cell signaling, cyto-adherence, and migration; different states of epithelial to mesenchymal transition of malignant cancer cells. Rb is a tumor suppressor gene, and loss of Rb

(common in many solid tumours) in hypoxic conditioned cancer cells increases cancer invasiveness. Applying the developed tools to measure and interpret mechanical properties of such cells not only helped in finding the connection between structural changes in cancer cells and their invasiveness but also allowed to validate activated targets and pathways that promote metastasis. Therefore, applying these tools helped us for detecting and validating novel therapies to prevent metastasis. The related results are demonstrated in Chapter 4 (submitted in Scientific Reports (2016)).

The corresponding contributions related to this phase of project are as follows:

5. Characterizing the connection between loss of Rb in hypoxic conditioned cells and increase in invasiveness using the developed tool (Chapter 4).

6. Identifying the related signaling pathways that are activated in response to loss of Rb in hypoxia using the developed tool (Chapter 4).

1.4 Thesis Outline

The outline of this thesis along with the background and summary of works that have been done during this project is provided in the following sections. Each chapter is simply a reproduction of my published or submitted papers.

1.4.1 Chapter 2: Mechanical Characterization of ART treated Jurkat Cells Using Optical Tweezers (Constant Stretching)

In this chapter, mechanical properties of Jurkat cells and drug treated cells is measured and analyzed by OT in concert with shell theory. Image processing technique is used to measure cell deformation at different laser powers. Shell theory is applied to model mechanical properties of cells and the nonlinear differential equations were solved in MATLAB. Comparing the results of the model and the experimental measurements, we demonstrated the performance of the proposed model and effectiveness of OT to evaluate the effect of ART on cell membrane mechanical features.

1.4.2 Chapter 3: Probing Mechanical Properties of Jurkat Cells Under the Effect of ART Using Oscillating Optical Tweezers (Cyclic Loading)

In this chapter, the effect of chemotherapy on cells cytoskeleton is analyzed via studying cells mechanical properties. In order to do so, the OT system is optimized to measure oscillaion. Employing OT, we applied a sinusoidal force on beads attached to cells cytoskeleton. Computer Vision System Toolbox in MATLAB is utilized for tracking beads movement. A numerical model is optimized by reducing the number of free prameters and utilized to estimate key mechanical features of cells cytoskeleton. By fitting the experimental data to the numerical model, a power-law behaiviour is observed in cells mechanical responses over a range of frequencies.

1.4.3 Chapter 4: Hypoxia and Cell Structural Changes: Rb Links Hypoxia to Actin Reorganization in Cancer Cells as Measured by an Optical Tweezer

In this chapter, the effect of hypoxia and loss of Rb on the cell cytoskeleton organization is studied. Hypoxia, a characteristic common to most solid tumors, modulates actin organization via multiple molecular pathways. Analyzing the effect of hypoxia on the biophysical properties of cancer cells is beneficial for studying different modulatory signaling pathways by quantifying cytoskeleton rearrangements. In order to analyze the biophysical variations of cells in response to loss of Rb under hypoxia we measured the human LNCaP prostate cancer cells mechanical properties by utilizing the oscillating OT. We have demonstrated that LNCaP cell stiffness is increased after 72 h of exposure to hypoxia. We measured the effect of inhibition of the extracellular signal-regulated kinase (ERK) and the protein kinase B (AKT) and NF-κB pathways on LNCaP cells mechanical responses as well. The results demonstrated that inhibition of ERK and AKT but not NF-κB prevented the hypoxia-inducible reorganization of stress fibers in Rb-negative cells. These results suggest that loss of Rb, in a HIF-1α dependent fashion, is an upstream regulator of ERK and AKT signaling pathways that drive the motile function of metastatic cells. Thus, the mechanical characterization of cancer cells by employing OTs could provide an additional technique for cancer diagnosis and evaluating therapeutic performance.

1.4.4 Chapter 5: A Sensitivity Study of Cell-Bead Geometry on Cell Mechanical Responses using Finite Element Analysis

In this chapter, a finite element model of an adherent cell attached to a microbead under dynamic loading is developed for cell manipulation by an OT. Experimental results of LNCaP cells by employing the oscillating OT are obtained and utilized as the cell material constants in the finite element model. This model is employed to study the structural dynamics behavior of LNCaP cells and to characterize the sensitivity of cell mechanical response to cell-bead geometries, and the finite element analysis results for different cell and bead sizes are reported. This sensitivity study shows the importance of evaluating the effect of cell-bead geometries on cell mechanical response for different cell types and OT experiments.

1.4.5 Chapter 6: Summary, Conclusions and Suggestions for Future Work

A summary of this thesis project is presented in this chapter. Based on the experimental results, theoretical studies and simulations general conclusion related to the outcome of this thesis along with the suggested future works are provided.

Chapter 2

Mechanical Characterization of ART treated Jurkat Cells Using Optical Tweezers (Constant Stretching)

Jurkat cells derived and immortalized from acute lymphoid leukemia, is a common type of blood cancer and chemotherapy is the initial treatment of choice. Quantifying the effectiveness of a chemotherapeutic drug at the cellular level plays an important role in the process of the treatment [72]. In this chapter, an OT was employed to characterize the mechanical properties of Jurkat cells exposed to artesunate (ART) as a chemotherapy. Jurkat cells were chosen as they were readily available in our lab and they provide a good model to verify the capability of the tool. A mathematical model was developed to describe the mechanical characteristics of the cell membrane and its features. By comparing the modeling results against experimental results from the OT, the elastic modulus of the Jurkat cells before and after ART treatment was calculated. The results demonstrate an increase in the cell stiffness after treatment. Therefore, the elastic modulus of a cell membrane may be a useful biomarker to quantify the effectiveness of a chemotherapeutic agent. The results are presented in [70].

2.1 Mechanical Model of Cells

Membrane theory has been extensively used for the mechanical characterization of cell membranes [73]- [74]. This theory is a simplified version of the shell theory in which the transverse tensions and bending moments are neglected, and only the in-plane stress resultants are retained in the analysis. In the proposed method, the shell theory is applied to determine a mechanical model of the suspended cell membrane, as a complete analysis, which might include the relative contribution of uneven distribution

of stress in our case [75], [76]. Equilibrium equation are used to model the suspended cell deformation behavior as,

$$k_s T_s + k_\varphi T_\varphi = p + \frac{E_B}{\sigma}\left(\frac{d^2(\sigma k_s)}{ds^2} - \frac{d}{ds}\left[\left(k_\varphi\right)\frac{d\sigma}{ds}\right]\right) \quad (2.1)$$

$$\frac{dT_s}{ds} + \frac{1}{\sigma}\frac{d\sigma}{ds}\left(T_s - T_\varphi\right) = -E_B k_s\left(\frac{dk_s}{ds} + \frac{1}{\sigma}\frac{d\sigma}{ds}\left(k_s - k_\varphi\right)\right) \quad (2.2)$$

where T_s , T_φ , k_s , k_φ are the principal tensions and curvatures; $\sigma(s)$ is the radial position of the membrane; E_B is the scalar bending modulus; and p is the normal pressure acting on the membrane, and it is calculated as the force of OT divided by the contact area [75]. The shape for cells before deformation is assumed to be spherical, and Mooney-Rivlin constitutive material which has been widely applied in literature to represent cells biomembrane is used in this study [77]. The principal tensions for the Mooney-Rivlin material is expressed as,

$$T_s = 2h_0 C\left(\frac{\lambda_1}{\lambda_2} - \frac{1}{(\lambda_1\lambda_2)^3}\right)\left(1 + \alpha{\lambda_2}^2\right) \quad (2.3)$$

$$T_\varphi = 2h_0 C\left(\frac{\lambda_2}{\lambda_1} - \frac{1}{(\lambda_1\lambda_2)^3}\right)\left(1 + \alpha{\lambda_1}^2\right) \quad (2.4)$$

where λ_1 and λ_2 are the principal stretch ratios, C and α are defined in terms of Mooney-Rivlin constants, i.e. C_1 and C_2, where $\alpha = \frac{C_2}{C_1}$ and $C = C_1$, and h_0 is the shell thickness [77]. For homogeneous, incompressible, isotropic elastic material, $C = E/6(1 + \alpha)$, where E is the elastic modulus. The set of non-linear differential equations in (2.1) and (2.2) are solved using the 4th order Runge-Kutta and multiple shooting methods. C and α are obtained by optimization. The relation between different force and deformation ratios, as well as cell deformation shape can be achieved by solving the above equations.

2.2 Experiment

2.2.1 Optical Tweezer Setup

The OT experimental setup (mmi Cell Manipulator, MMI AG, Zurich, Switzerland) is illustrated in Fig. 2.1. A continuous wave 3W, Nd:YAG laser emitting light at a wavelength of 1064 nm was used and the Nikon TE2000 inverted microscope was utilized. A dichroic mirror was used to reflect the laser beam into the 100× objective and focus on the sample. A two dimensional motorized stage driven by stepper motors with 78 nm positioning accuracy was used and the stage movement was controlled by visual feedback. A CCD camera was used for monitoring the experimental process. All the optical and mechanical components were placed on an anti-vibration table.

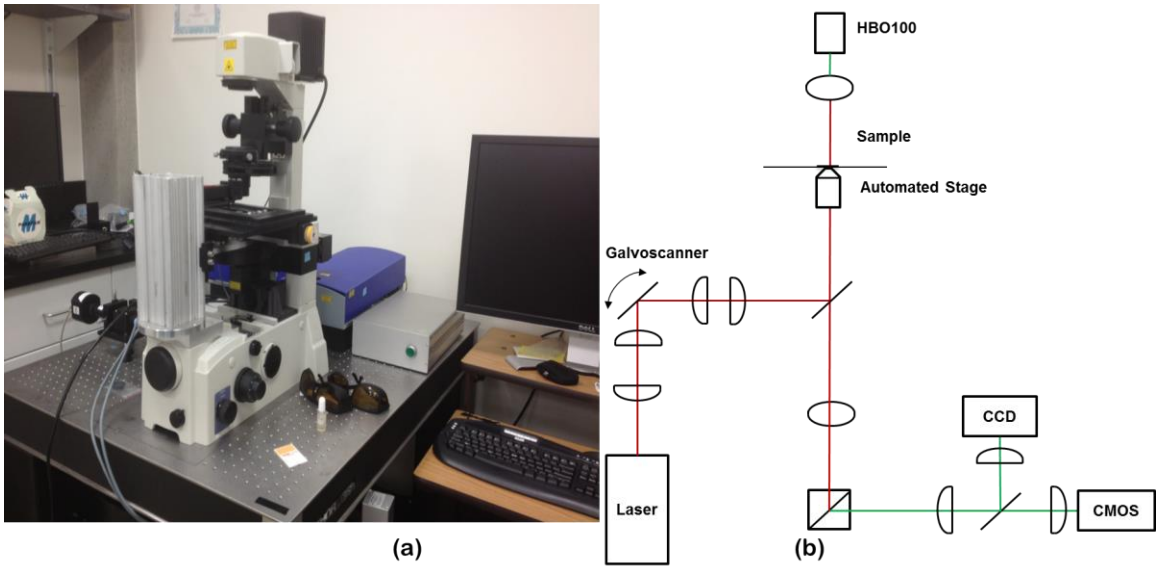

Figure 2.1. OT setup: (a) a picture and (b) a schematic.

2.2.2 Experiment Preparation

Jurkat cells were cultured in RPMI-1640 supplemented with 1% penicillin and 10% FBS at 37°C in a humidified atmosphere of 5% CO2, and fresh culture medium were added every 2 to 3 days. After five passages, cells were cultured in four different dosages of ART (3.125, 6.25, 12.5, 25μg/ml) for 24 hours. Microbeads were adhered to

cell membranes and were used as a handle for cell manipulation [9]. Streptavidin-coated polystyrene beads (0.5 mg/ml) with radii of 1.55 μm (Bangs Lab, Fishers, IN) were washed in PBS three times and incubated with 0.4 mg/ml biotin-conjugated concanavalin A (Con A, Sigma) at 4°C for 40 minutes with gentle mixing. Jurkat cells were washed in PBS three times. The antibody-coated beads were then rinsed and added to the washed Jurkat cell suspension, which was incubated at 25°C for 1 h to allow for the adhesion between beads and cells.

2.2.3 Force Calibration

The OTs system can be calibrated using an escape force method [78]. In this technique, the force required to move a trapped microbead is calibrated against a known viscous drag force. The calibration procedure involves trapping a microbead in fluid at a measured height, h, above the glass slide surface. The fluid and height of the trapped bead from the slide surface will be kept unchanged throughout calibration and mechanical deformation. As the microscope stage is translated, the fluid exerts a viscous drag force on the trapped bead. The viscous drag force equals the trapping force when the bead just escapes the trap. Using the stage velocity, at the point of escape of the trapped bead, the drag force, which is the opposite of the escape force, is estimated as,

$$F = \frac{6\pi\eta R v}{1 - 9/16(R/h) + 1/8\left(\frac{R}{h}\right)^3 - 45/256\left(\frac{R}{h}\right)^4 - 1/16(R/h)^5} \tag{2.5}$$

where R is the bead radius, η is fluid viscosity, v is the stage velocity beyond which the bead escaped the trap, and h is the separation distance of the bead from coverslip surface. We used phosphate buffered saline (PBS) as our fluid which has η=0.9 mPa·s at 25°C. During our calibration and cell stretching experiment the separation distance of the bead from the coverslip was kept at 5 μm. Correlation of laser power with force was determined from repeated trials at five different laser powers (Fig. 2.2).

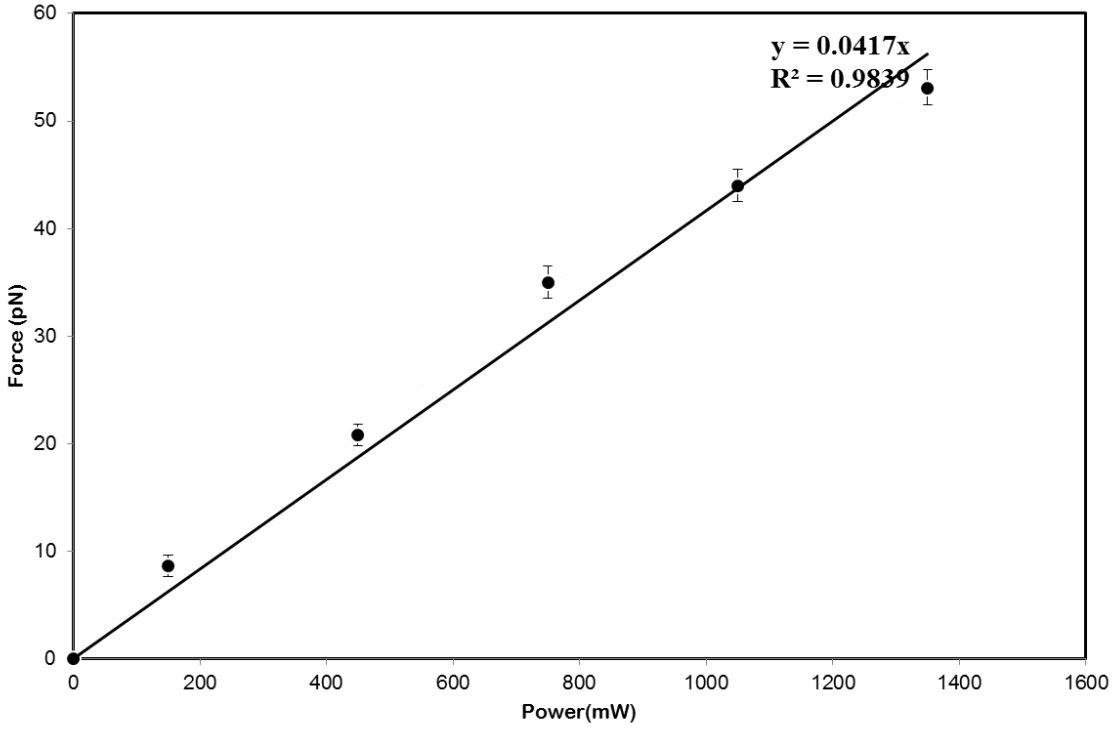

Figure 2.2. Calibration results of trapping force for a 1.5 μm bead (R2=0.98).

2.3 Jurkat Cell Stretching Using the Optical Tweezer

The beads, which were adhered to the Jurkat cell membranes, were used as a handle and trapped by a laser beam to minimize the optical damage. The cell stretching process required anchoring a small portion of the cell to the chamber. In order to attach the cells to the slide, the glass slides were coated with poly-L-lysine (Sigma). The bead which was attached to the cell membrane was trapped by the laser beam. Then, the stage was moved at a velocity of 2 μm/s to diminish the extra viscous drag force exerted on the trapped bead. By moving the stage, the part of the cell that was attached to the chamber will move, while the bead remains fixed in the laser trap, and the Jurkat cells were stretched. The trapping force was equal to the pulling force at the certain maximum deformation. The maximum deformation was measured when any excess stretch led to escape of the bead from the trap.

Cell deformation was measured at different laser power. Increasing the laser power could lead to more deformation in the cell membrane as illustrated in Fig. 2.6. The stretching force was acquired by the calibrated force-power relation in Fig. 2.2. Also, for each level of laser power, the cell deformation was acquired by image processing techniques, in which the change in cell diameter was measured to quantify cell deformation. The images were analysed using the Image Processing Toolbox™ in MATLAB® to perform object edge detection. To do this, Sobel edge detector was applied to find cell edges. Two examples of cell edge detection for non-deformed and deformed cells are illustrated in Fig. 2.3 and 2.4 respectively. During the experiment five different cells were stretched at each laser power, and the results were averaged. Cell deformations were obtained from the stretched cell images when the maximum deformation was observed by image processing.

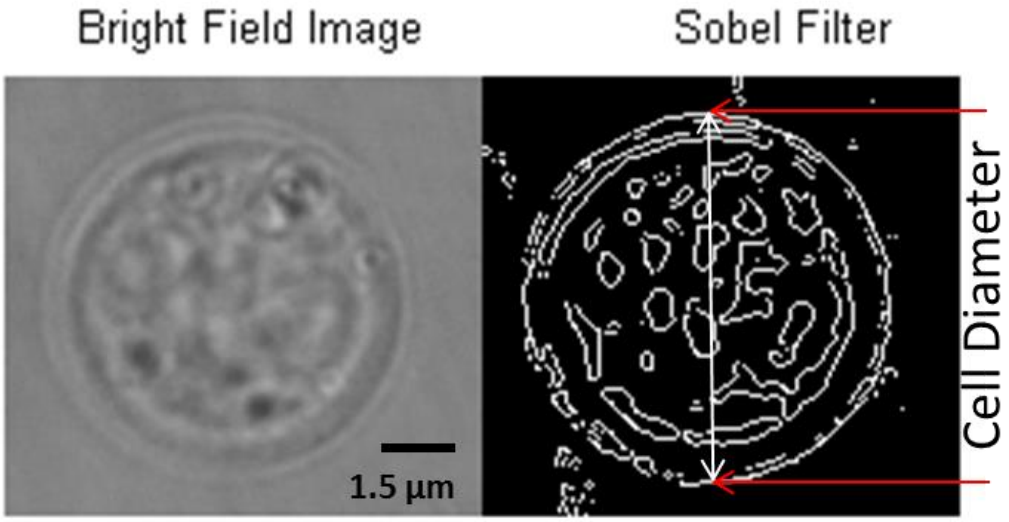

Figure 2.3. Measuring cell diameter using Sobel edge detector.

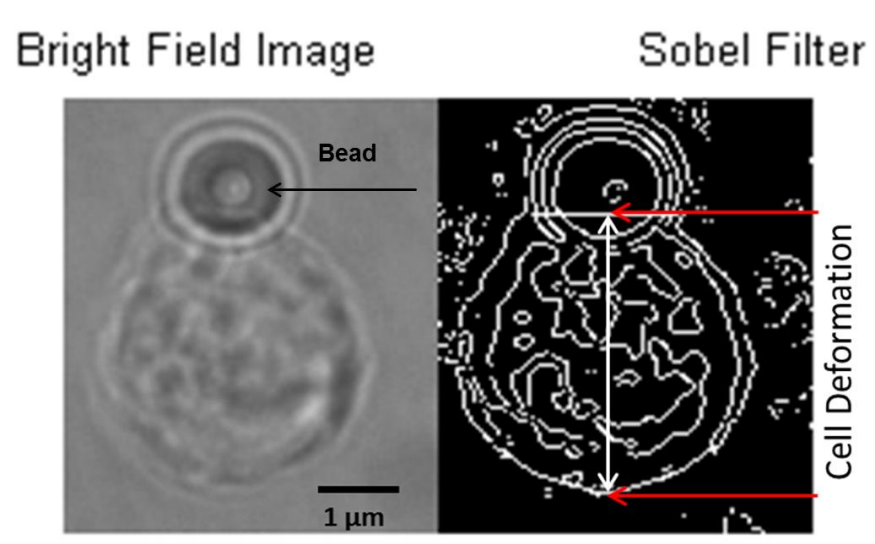

Figure 2.4. Measuring cell deformation using Sobel edge detector.

2.4 Results and Discussions

The cell radii were measured for 150 Jurkat cells and the results are presented in Table 2. The contact radius was measured 0.8 µm from the image of an adhered bead to the cell membrane (Figure 2.5). The membrane thickness was approximated as 7nm [79]. Using these parameters the force-deformation relation based on the proposed mechanical model were obtained. These results are from the assumption of uniform deformation, which is an approximation for now and we will continue to look at the effect of this error in future studies.

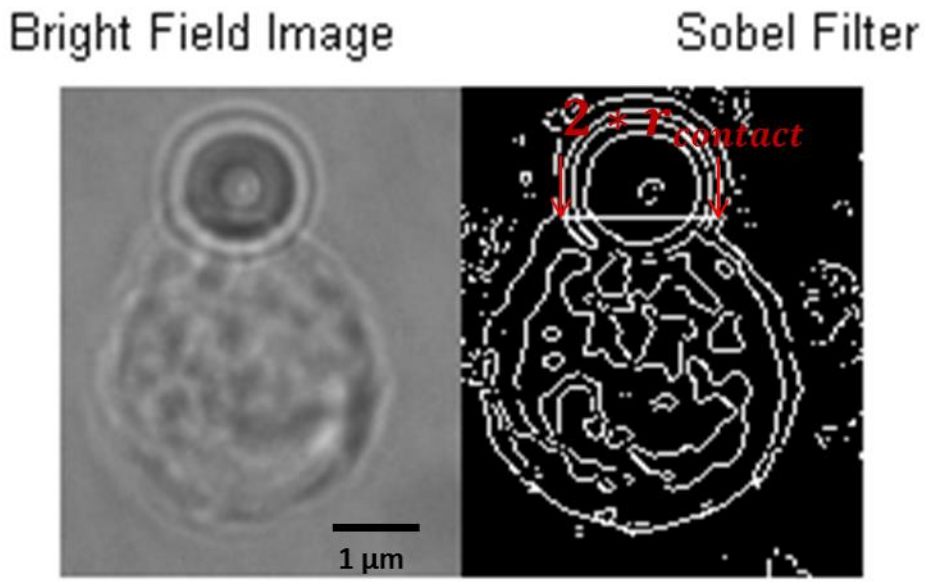

Figure 2.5. An example of measuring cell contact radius.

To obtain the cell properties from our experimental data, an identification procedure was used. The mechanical properties of cells (C and α) can be identified when the deviation parameter between modeling and experimental data is minimized. The elastic modulus is reported so that we can compare it with previous results in this area.

The mechanical modeling results as well as experimental results for the control group and drug treated Jurkat cells are shown in Fig. 2.7. Utilizing the experimental results along with modeling, the elastic moduli of un-treated Jurkat cells was estimated to be 0.224 ± 0.04 kPa, which was increased to 0.588 ± 0.11 kPa after treatment with 25 µg/ml ART. These results show similar behavior as 0.254 ± 0.035 kPa and 0.648 ± 0.037 kPa for Jurkat cells and, treated cells which is reported in [80]. A paired-samples t-test was conducted for each group of ART treated cells and control group to compare the effect of ART on the elastic modules of cell membrane. The result for 3.12 ug/ml ART treated cells shows a not-significant difference, $t(4)=2.00$, $p=0.0801$, while showing a significant difference for other groups of treated cells. For example the result for 6.25 µg/ml ART treated cells is $t(4)=5.62$, $p=0.0013$, which suggests that the ART treatment affect the elastic modulus of the Jurkat cells membrane. The elastic moduli of cells

exposed to different dosages of ART are illustrated in Fig. 2.8. These results demonstrate that the ART treated cells' elastic moduli increased in a dose-dependent fashion in contrast to the control group.

Comparing the deformation results for the control and drug treated cells, at the same stretching force, revealed that the control group deformed more severely than the ART-treated cells, therefore the cell stiffness increased with chemotherapy.

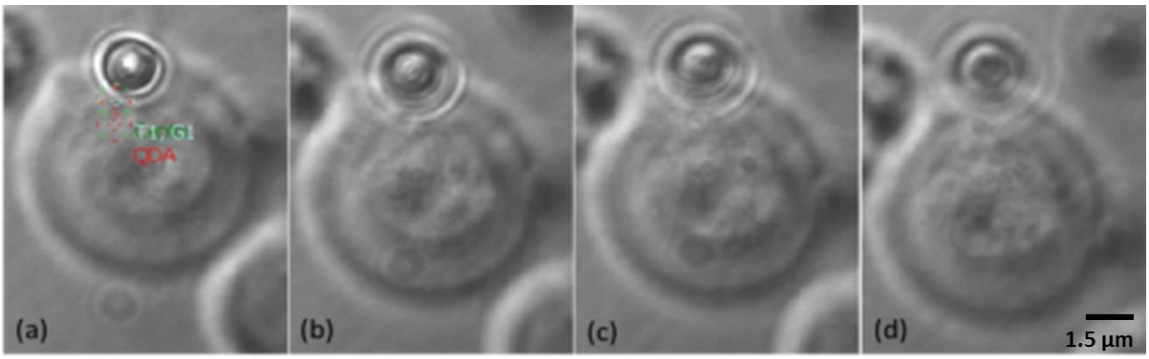

Figure 2.6. Jurkat cell deformation at four different levels of stretching forces. (a) 0pN, (b)6.3pN, (c) 18.9pN, (d) 31.5pN.

Table 2.1. Cell radii measured for 30 Jurkat cells in each group.

Cell	Radius (µm)
Control Group	5.73 ± 0.52
3.12µg/ml ARTesunated	4.9 ± 0.44
6.25µg/ml ARTesunated	4.5 ± 0.37
12.5µg/ml ARTesunated	4.1 ± 0.31
25 µg/ml ARTesunated	3.5 ± 0.26

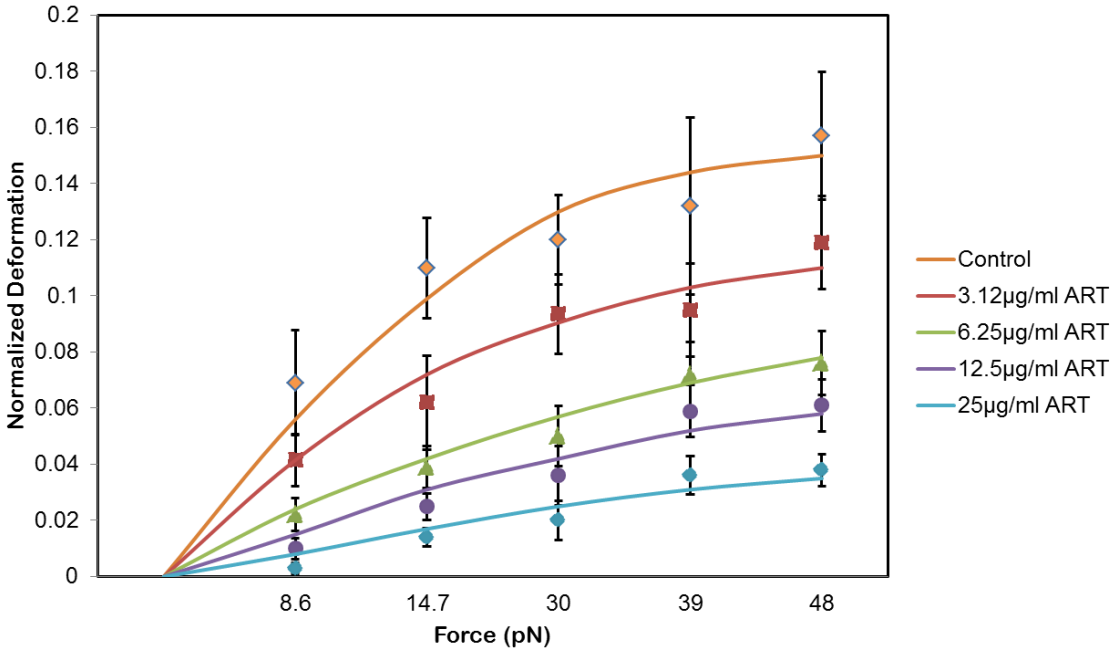

Figure 2.7. **Mechanical responses of Jurkat cells and 3.12 μg/ml, 6.25 μg/ml, 12.5 μg/ml, 25 μg/ml ARTesunated Jurkat cells from both experiment (points) and numerical simulation (solid line). Deformation in the cells is normalized to undeformed cell diameter (The error bars are in terms of standard deviation).**

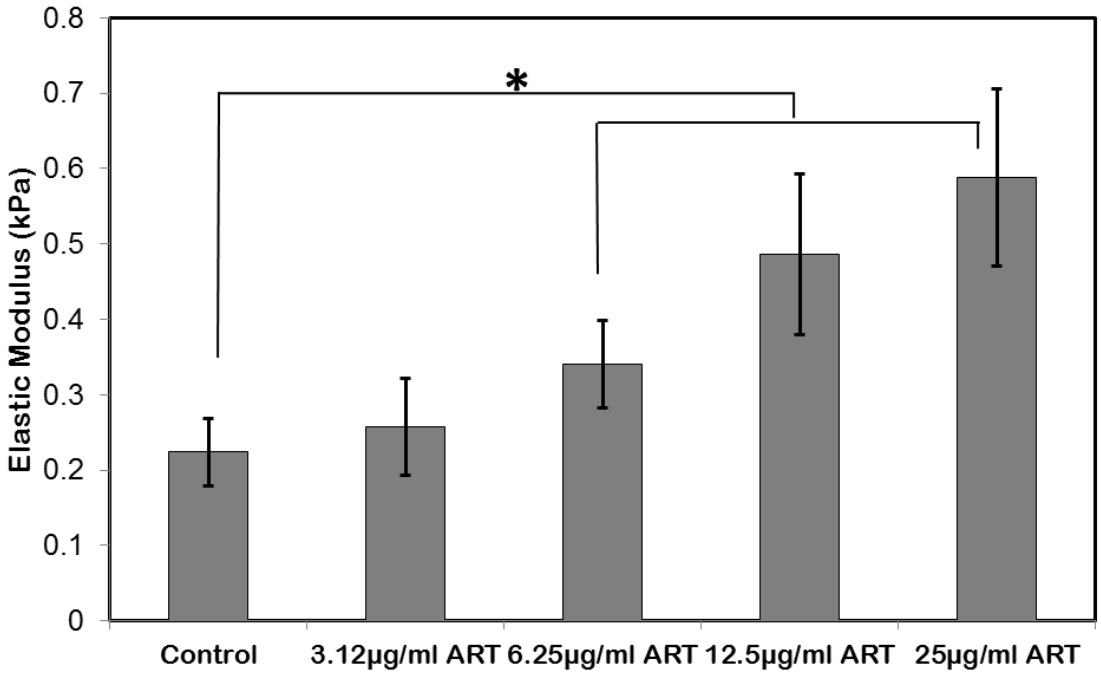

Figure 2.8. Effect of ART on average elastic modulus of Jurkat cells (The error bars are in terms of standard deviation).

2.5 Conclusion

An OT was used to measure mechanical properties of Jurkat cells exposed to ART. Previous studies [80] showed that ART could inhibit the growth of Jurkat cells, and increasing the concentration of ART could increase the inhibition rate. The result of this study is in agreement with the previous studies.

Force-deformation relation was measured for cells exposed to different concentrations of ART. Our results showed that the mechanical properties of the Jurkat cells changed when exposed to ART. Treated cell normalized deformation (0.038) was less than control cell deformation (0.157), when applying 48 pN force. The elastic modulus was 0.588±0.11 kPa in ART treated cells and 0.224±0.04 kPa in the control group. These results clearly show that the cell stiffness increased after the chemotherapy. Therefore, measuring the elastic modulus of cells, with the combined use of the OT and our numerical model as a tool, could serve as a useful biomarker to quantify the effectiveness of a chemotherapeutic agent.

Chapter 3

Probing Mechanical Properties of Jurkat Cells Under the Effect of ART Using Oscillating Optical Tweezers (Cyclic Loading)

In this chapter, an oscillating OT was employed to characterize the frequency-dependent mechanical properties of Jurkat cells exposed to the chemotherapeutic agent, artesunate (ART). A motion equation for a bead bound to a cell was applied to describe the mechanical characteristics of the cell cytoskeleton. By comparing between the modeling results and experimental results from the OT, the stiffness and viscosity of the Jurkat cells before and after the ART treatment were obtained. The results demonstrate a weak power-law dependency of cell stiffness with frequency. Furthermore, the stiffness and viscosity were increased after the treatment. Therefore, the cytoskeleton cell stiffness as well as power-law coefficient can provide a useful insight into the chemo-mechanical relationship of drug treated cancer cells and may serve as another tool for evaluating therapeutic performance quantitatively. The results are presented in [71].

3.1 Experimental Setup and Methods

3.1.1 Optical tweezer setup

The oscillating OT experimental setup (mmi Cell Manipulator, MMI AG, Zurich, Switzerland) is the same as the previous section. The only difference is that a CCD camera and a CMOS camera were connected to the left side of the inverted microscope by utilizing a beam splitter. The CCD camera was used for monitoring the experimental process, whiles the CMOS high-speed camera (up to 500 fps), with a limited region of interest was used for bead motion tracking at high frequencies.

3.1.2 System calibration

The calibration of the OT is an essential step in evaluating the force applied to the microbead. The first step in calibrating the system was determining the trap stiffness constant, k_{OT}, of the OT. Utilizing the stiffness constant and bead displacement measurement, the OT force can be obtained. According to the equipartition theorem, the trap stiffness constant was calculated as follows [81], [82]:

$$\frac{1}{2}k_{OT}\langle x^2\rangle = \frac{1}{2}k_B T \tag{3.1}$$

where k_B is the Boltzmann's constant, T is the absolute temperature (300°K), x is the trapped bead displacement, and $<.>$ indicates a time average. Exposure time and frame rate of the CMOS camera were set to 1.25ms and 30 frames per second, respectively. The frame rate of the camera does not affect the stiffness constant measurement of the system. However, the exposure time affects the precision of the position measurement and therefore, has an effect on the accuracy of the stiffness constant. The exposure time was determined after a series of experiments with the exposure time ranging between 0.1 ms and 30 ms. To determine the stiffness of the system, a microbead was trapped and the bead's displacements was measured for 250 frames (Figure 3.1). The variance of histogram of the trapped bead displacement (Figure 3.1b) is used to derive $< x^2 >$. The results are then used utilizing Eq. (3.1) to calculate the trap stiffness constant, k_{OT}. The repeatability of this experiment was tested on 20 different beads.

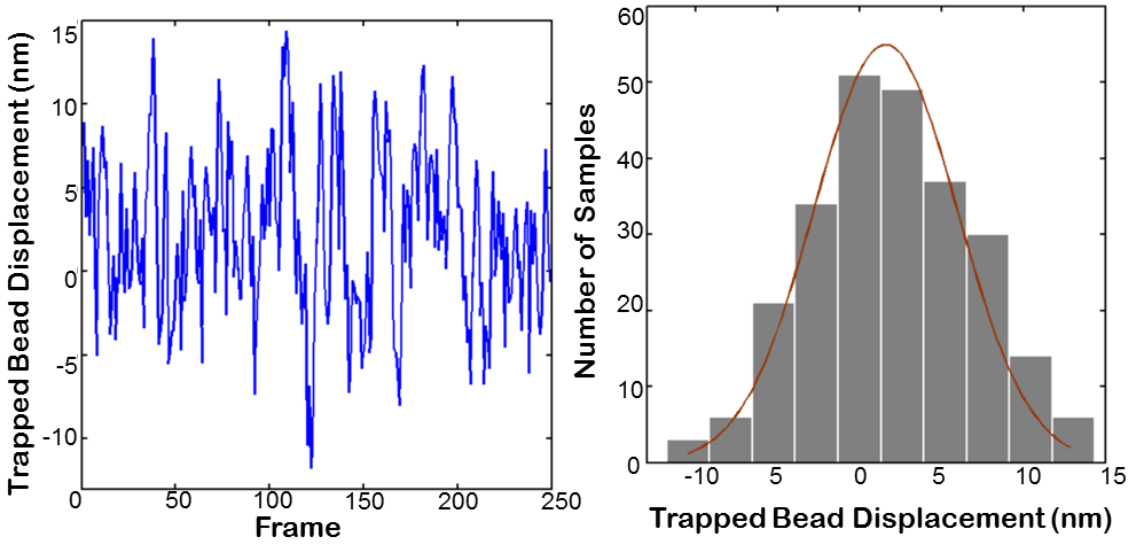

Figure 3.1. A sample displacement variation of a trapped bead over 250 frames is illustrated on left side, and trapped bead displacement histogram is shown on the right side.

3.1.3 Oscillating cell-bonded microbeads using the optical tweezer

The cell manipulation process required anchoring a small region of the cell to the slide surface below. In order to attach the cells to the slide, the glass slides were coated with poly-L-lysine (Sigma). A microbead was trapped with the OT and attached to the surface of a cell. In order to test if the bead attachment was stable, the laser beam was shut off for several seconds. If the bead did not escape, it could be assumed that there was adherence between the cell and the bead. The beads that adhered to the Jurkat cell membranes were then used as a handle and trapped by the laser beam. Changing the angle of the galvanomirrors moved the trapped beads back and forth in a sinusoidal manner, which applied a time varying force on the cells. Note that the application of the time varying force was done by controlling the bead displacement in Eq. (3.2). The oscillatory movement of the bead causes cytoskeletal deformation of the cell. The cell resists the deformation by producing internal stresses that are directly related to the cell mechanical properties [83]. Thus, cell mechanical properties could be calculated by applying a time varying force and measuring the resultant bead motion. The amplitude of the applied oscillating force remained constant during the whole experiment, and was

equal to 33 pN. Jurkat cell mechanical responses were measured at different frequencies (0.1 Hz, 1 Hz, 10 Hz, and 100 Hz) of applied force. A total number of 79 cells were tested for the experiment. Four different dosages of ART treated cells (6.25, 12.5, 25, 50 µg/ml) and a control group of cells (each group employing between 15 and 17 cells) were chosen and the effect of sinusoidal forces on their mechanical responses were analyzed. To test the repeatability of the measurements, the whole experiment was repeated for three different cell populations. New cells were manipulated during each experiment of repeatability test.

3.1.4 Data Analysis

For the analysis of the experimental data, the bead motion equation was used to calculate the cell mechanical properties in the frequency domain. The bead that was bound to the surface of the cell membrane was first trapped and then oscillated by the laser beam. The motion equation of the bead can be described by [84]:

$$mx'' + 6\pi\eta_{med}r_{bead}x' + r_{cont}\eta_{cell}x' + \frac{Y}{2r_{bead}^2}(x - X_0)^{\nu} + k_{OT}x = k_{OT}Asin(2\pi ft) \qquad (3.2)$$

where m is the bead mass (m = 28.27 pg), η_{med} is the viscosity of the surrounding medium which is PBS ($\eta_{med} = 10^{-3}\,Pas$), $r_{bead} = 1.55\,\mu m$ is the polystyrene bead radius, and $r_{cont} = 0.25{\sim}0.45\,\mu m$ is the radius of the contact of the bead on the cell membrane, which is measured from the images of the experiment. The whole cells were assumed to have viscoelastic properties with a viscosity coefficient of η_{cell}, while Y is a constant proportional to the stiffness of the cells. X_0 is the displacement of the bead on the cell membrane caused by the fluid-like behaviour of the cell. k_{OT} is the spring constant of the OT which was calculated using the equipartition theorem, Eq. (3.1). A and f are the amplitude (A = 0.437 µm) and frequency (f = 0.1, 1, 10, or 100 Hz) of the applied displacement oscillation, respectively. Finally, the exponent ν is related to the degree of non-linearity of the cell membrane's material. In Eq. (3.2), Y, η_{cell}, X_0, and ν are the unknown parameters that will be identified using the experimental results and an optimization approach presented below.

3.1.5 Measurement of bead motion

In response to a time varying sinusoidal trapping force, the beads oscillated back and forth along with the oscillating force. The bead displacement was recorded by the CMOS camera on the inverted microscope with a camera adapter of 1× magnification. The camera frame rate was set to 440 frames per second (fps).

The images were analysed using the Computer Vision System Toolbox™ in MATLAB® to perform object detection, feature identification, and bead tracking. To do this, a system object for reading and displaying the video was created in the toolbox. Then, the first frame of the object was read and the region of the bead was selected, followed by applying the minimum eigenvalue corner detector of the toolbox to locate the corners of the bead. Finally, by using the Kanade-Lucas-Tomasi (KLT) point tracker, the point's positions for all frames of the videos were tracked and used to measure the bead motion.

3.1.6 Optimization

The Curve Fitting Toolbox™ of MATLAB® was used for fitting the experimental data. Using the least squares method, the best-fit curve of the bead displacement for each experiment was obtained. Figure 3.2 illustrates a sample result of the bead motion curve fitting. In order to identify the unknown parameters, Y, η_{cell}, X_0, and ν, in Eq. (3.2), the following procedure was carried out. First, Eq. (3.2), which is a non-linear differential equation, was solved using the 4th order Runge Kutta method. Then, a mean square error (MSE) approach was utilized as the regression tool for comparing the solution of Eq. (3.2) and the best-fit curve of the bead displacement obtained from the experiment. Finally, an iterative genetic algorithm (GA) approach was used to minimize the error between the two curves by optimizing the unknown parameters.

The repeatability of this automated technique is determined and the absolute difference between two test results showed negligible variation or non-variation at all. Using this image processing algorithm the bead position was measured.

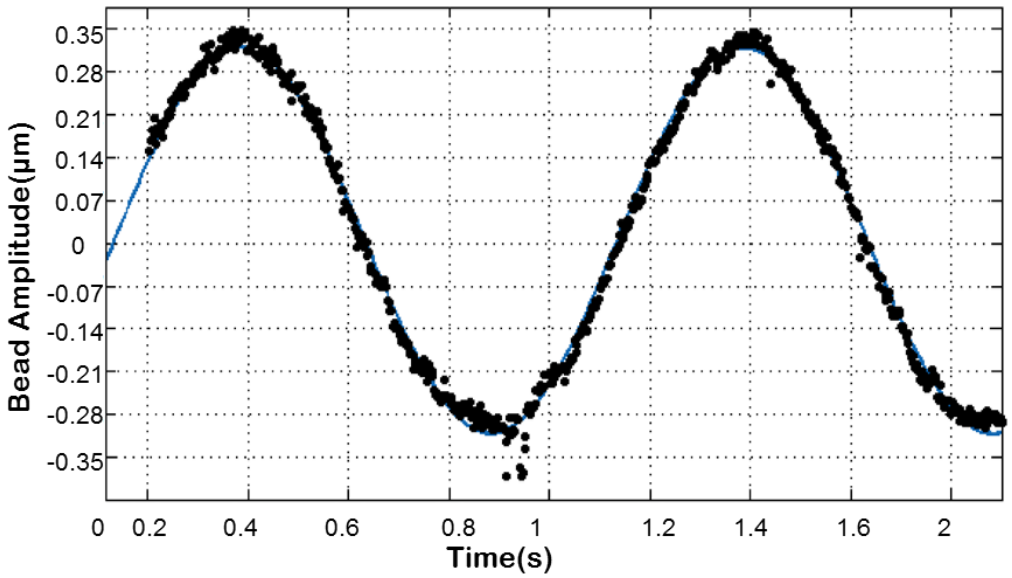

Figure 3.2. Sample curve fitting result for the bead's oscillatory displacement.

3.1.7 Power-law rheology

According to Fabry et al. [9], various types of cells' mechanical responses over a wide range of time scale are governed by a common behaviour that is called power-law rheology. The power-law rheology is based on the fact that, cell stiffness shows a power-law dependency on excitation frequency. The power-law rheology of living cells is related to the cell's stiffness and power-law exponent. These two parameters are dependent on each other, where soft cells have a larger power-law exponent, which makes them to appear more fluid-like, while stiff cells have a smaller power-law exponent which makes them to appear more solid-like [10]. In our study, the power-law dependency of Jurkat cells exposed to ART was analyzed. Among the four different parameters of cells (Y, η_{cell}, X_0, and ν), Y, which is the coefficient proportional to the stiffness, changed according to a power-law, f^{x-1}, with respect to the changes in the applied force frequency.

3.1.8 Statistics

Analysing the statistics of the results has two objectives. The first one is to estimate the cell mechanical parameters Y, η_{cell}, X_0, and ν, while the second one is to find if the number of free parameters can be reduced. Four different models, which were obtained based on Eq. (3.2), were analyzed. In the first model, all parameters were set free and there were no constraints. In the second model, $X_0$was held constant across the different ART dosages and the control group, while the other parameters remained as treatment-dependent. In the third model, $X_0$and ν remained constant for all cell conditions, while η_{cell} was set as treatment-dependent. In the last model, three parameters (η_{cell}, X_0, and ν) were constant across all cell conditions. As the changes in Y are considerably more significant than those of the others with respect to different cell conditions, Y was not held constant in any of these models.

3.2 Experimental Results and Discussion

The experimental results showed that, the bead displacement amplitude, which is inversely proportional to the cell stiffness, varied widely between the Jurkat cells of each group: (i) control–not treated with ART, (ii) treated with 6.25 µg/ml of ART, (iii) treated with 12.5 µg/ml of ART, (iv) treated with 25 µg/ml of ART, (v) treated with 50 µg/ml of ART. A histogram of all bead displacements revealed a log-normal distribution. The probability functions of the bead displacement amplitude for all cell conditions at 1 Hz frequency are illustrated in Fig. 3.3. The median of bead displacement amplitude for the control group was 0.79 µm, with the standard deviation of 0.017 µm. Increasing the dosage of ART caused a decrease in the bead displacement amplitude. In the case of the groups of Jurkat cells treated with 6.25, 12.5, 25, and 50 µg/ml of ART, the medians of the bead displacement amplitude were 0.74± 0.016 0.66± 0.011, 0.57± 0.010, and 0.47 ± 0.008µm, respectively. The median values of the bead displacement amplitude decreased with the increase in the dosage as a result of the increase in cell stiffness. The results related to the repeatability of the experiment showed negligible changes in the standard deviation values (<15%), with the median value for each group not varying day to day.

The median of each cell group bead displacement along with the solution of Eq. (3.2) were used to identify a set of free parameters for each cell group. The goodness of the fit was satisfactory ($r^2 = 0.95$); however, we noticed that the degree of changes in three parameters, i.e. η_{cell}, X_0, and ν, were not comparable to the variation of Y at different cell conditions, for which ν remained almost constant, X_0 increased two-fold, η_{cell}, increased three-fold; while Y increased by more than twenty-fold in comparing the drug treated cells to the control condition. Thus, these results indicate that the number of parameters could be reduced without decreasing the goodness of the fit.

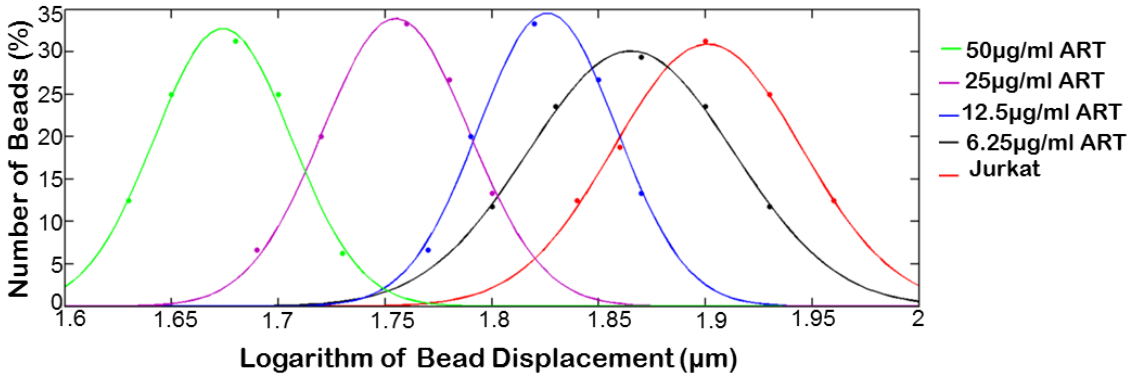

Figure 3.3. Probability function of the bead displacement amplitude for Jurkat cells treated with different dosages of ART, compared to the control group. Dotted data are the experimental results, while solid lines are the fitted curves.

In order to identify the unknown parameters and find if the number of parameters can be reduced, four different statistical models were proposed in the Statistic section. All four models were compared using the F-test and the results are shown in Table 3.1.

Table 3.1. Statistical results of four different models.

	Model 1	Model 2	Model 3	Model 4
r^2	0.95	0.95	0.96	0.95
r_{ss}	0.391	0.888	0.427	0.819

To test the independency of three parameters of η_{cell}, X_0, and ν to the drug treatment, the residual variance of fit of data to Eq. (3.2) was analyzed. Thus, we have analyzed how well Eq. (3.2) will be fitted to the median data, for each one of the four different models. The residual variance of fit of data for Model 1 and Model 3 were not significantly different from each other; therefore, Model 3 is preferred as the number of parameters is less than Model 1. The residual variance of fit of Models 2 and 4 were slightly larger than that of Models 1 and 3 (Table 3.1). Since Model 3 showed the best fit of the four different models, it can be concluded that the viscosity coefficient of the cells varied in response to the drug treatment and dosage. Finally, the estimated cell parameters, obtained by fitting Eq. (3.2) to the experimental data under control conditions, as well as the Jurkat cells treated with the different dosages of ART, are shown in Table 3.2.

Under control conditions there was a weak power-law dependency of Y on frequency (Figure 3.4). When the Jurkat cells were treated with ART, Y increased, while still maintaining a low power-law dependency on frequency (Figure 3.5). Increasing the dosage caused Y to further increase. The power-law dependency of the Jurkat cells treated with ART decreased with increasing dosage (Figure 3.6).

According to the results, the changes in cell stiffness and viscosity are dosage dependant, as shown in Table 3.2, and Figures 3.4 and 3.5. Both the stiffness and viscosity increased with increasing dosage. In order to test if there is a significant difference between different treatment dosages groups of cells, a MANOVA test was applied on different cell groups based on the stiffness and viscosity coefficients. Wilk's Lambda measure was used to determine the F-value. Since, the estimated p-value was < 0.05, we can conclude that there is a significant statistical difference between the five different groups of cells. Moreover, the power-law coefficient, which is an intrinsic property of the cytoskeleton, decreased with increasing the dosage, which implies the cell structure transitioning from a liquid-like state to a solid-like state, according to Fabry et al. [85]. The results of the power dependence of stiffness are also in good agreement with previously reported studies, which used other measurement techniques [86], [85], [87], [88], [89].

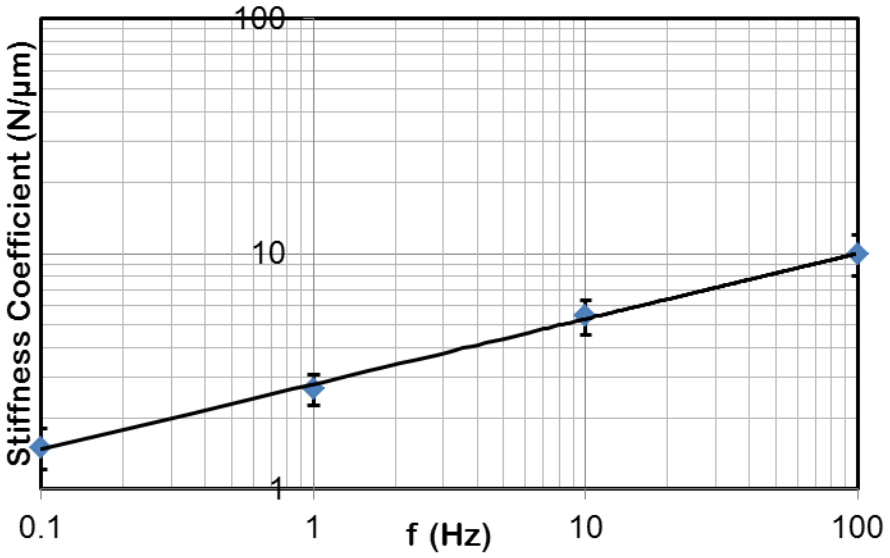

Figure 3.4. **Stiffness vs. frequency under control condition for frequencies between 0.1-100 Hz. Each data point represents the median value of 20 cells.**

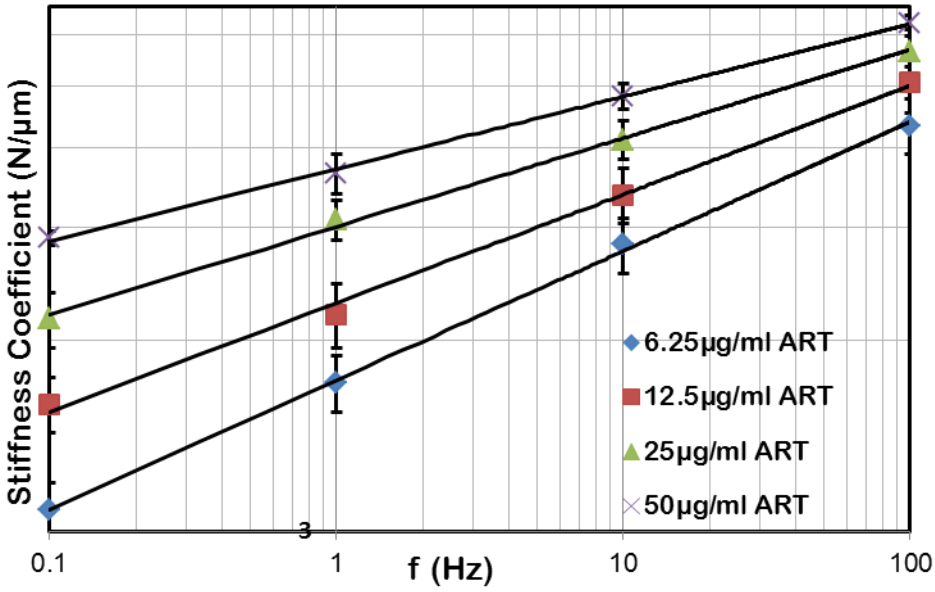

Figure 3.5. **Stiffness coefficient vs. frequency for Jurkat cells treated with different dosages of ART.**

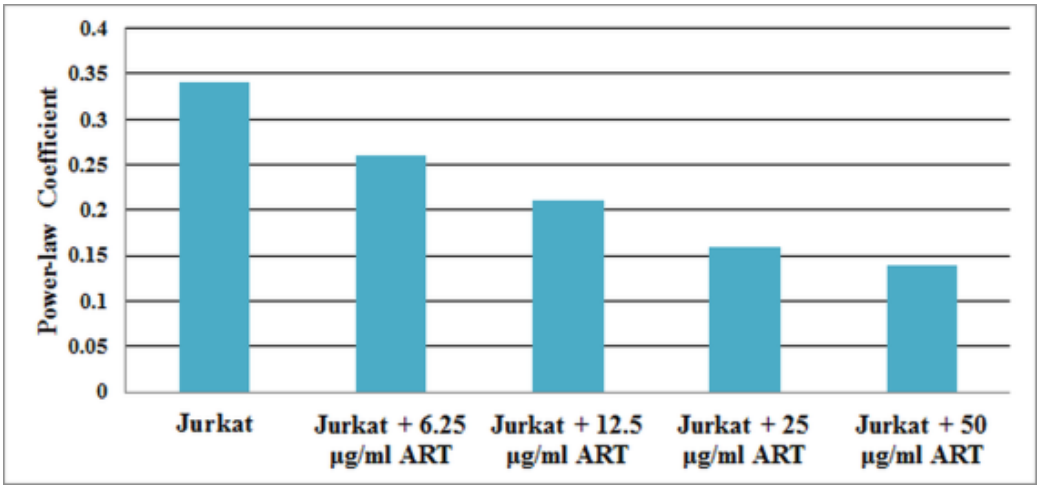

Figure 3.6. Power-law coefficient for control group and four different dosages of ART treated Jurkat cells.

Cai et al. [80] has reported an inhibition rate of more than 50% when the dosage of ART applied on Jurkat cells is more than 12.5 µg/ml, after 24 h exposure, and further increasing the ART concentration also decreased the cell growth and division rate significantly. Their results showed that ART can increase cell stiffness as well. Similarly, we observed a reduction in cell viability with increasing drug dosage after 24h exposure, where the mechanism of cell death due to ART may be through apoptosis, which includes morphological changes such as cell shrinkage, blebbing, and stiffening. Cells with morphological changes were seen at all drug dosages, while the number of cells with these changes was increased with increasing drug dosage significantly.

The concentrations of ART that are selected in this study resulted in inhibition rate of > 50% [80]. A statistical analysis (ANOVA) was performed for studying the effect of different frequencies on cell stiffness at each group of cells. The power-law coefficient was decreased from 0.34 in the non-treated Jurkat cells to 0.14 in the cells treated with 50 µg/ml ART. The Jurkat cell's mechanical properties such as stiffness coefficient and the power-law coefficient were changed significantly after the exposure to different dosages of the chemotherapeutic agent, which proves structural changes within the cells due to chemotherapy. These variations in stiffness and power-law coefficient at different drug concentrations may be related to the cytoskeleton reorganization.

As mentioned previously, a FEA was carried out in COMSOL to test the validity of the derived material parameters in accurately simulate the ART-treated Jurkat cell biomechanics. As shown in Figure 3.7, the maximum amplitude of bead motion predicted by the FEA are in a good agreement with the experimental results, which verifies the accuracy of the proposed numerical cell parameters estimation method.

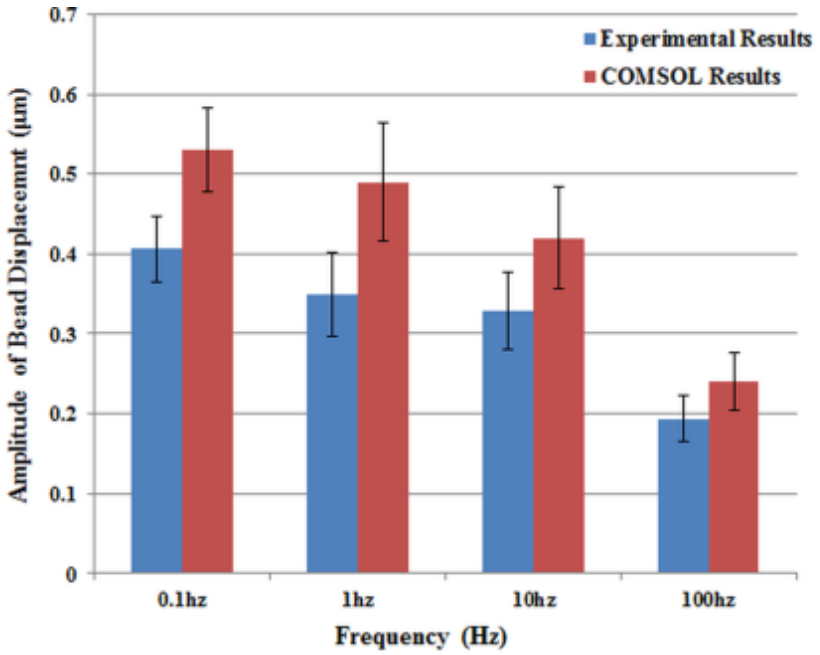

Figure 3.7. Comparing bead displacement amplitude for FEA and experimental results. (Jurkat cells treated with ART).

The immunofluorescent microscope images of the non-treated cells and drug treated cells are shown in Figure 3.8. The results show a variation between F-actin structures of non-treated cells and drug treated cells. The F-actin distribution is larger in cells exposed to ART, compared to the non-treated cells, which is in agreement with the alterations in the mechanical properties between these two different cell groups. These results confirm the contribution of the F-actin in regulating the mechanical properties of drug treated cells.

Furthermore, Figure 3.8 demonstrated a significant shrinkage in treated cells comparing to non-treated cells. According to our results related to the cell's mechanical

properties, stiffness coefficient increased with in treated cells comparing to non-treated cells. Therefore, there might be a relation between cell size and cells stiffness in this case.

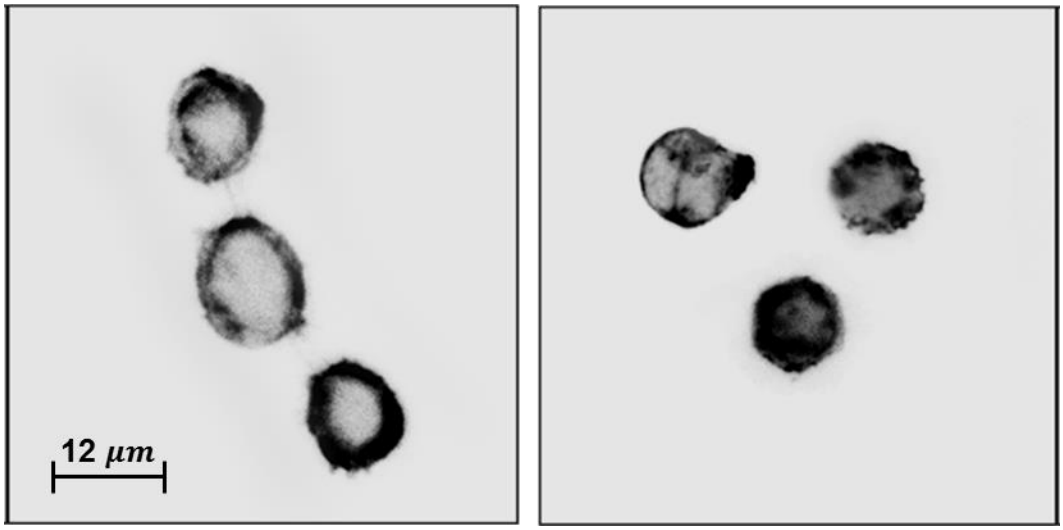

Figure 3.8. Sample immunofluorescnet images of the Jurkat cells (right: cells exposed to 50 µg/ml ART, left: non-treated cells).

The proposed method may serve as an easier and faster quantitative indicator in evaluating therapeutic effect on cytoskeletal proteins in comparison to biochemical fractionation and immunoblotting. However, there is a need to perform the analysis on variety of cell types and different chemotherapeutic agents before a generalized conclusion can be made. Also, the effect of chemotherapy may cause inter cellular mechanisms that may not directly affect the cell stiffness. For example, Li et al. [90] suggested that ART causes translocation of β-catenin and inhibition of unrestricted activation of Wnt/β-catenin pathway. Nevertheless, changes in cell mechanical responses due to drug effects are an indicator of cell behaviour deviation. Quantifying the behaviour deviation by performing mechanical characterization can be used as a complementary method to understand such responses. Therefore, the proposed method

can potentially serve as a tool for a comprehensive cell mechanical characterization study with respect to various treatments.

Table 3.2. Estimated cell parameters under the control condition and four different dosages of ART.

Cell Condition	X_0 (nm)	ν	η_{cell} (Pa·s)
Jurkat cells	7.71 (sd = 1.03)	3.01 (sd = 0.013)	0.018 (sd = 0.013)
Jurkat + 6.25 µg/ml ART	6.85 (sd = 0.95)	3.02 (sd = 0.014)	0.044 (sd = 0.008)
Jurkat + 12.5 µg/ml ART	6.14 (sd = 1.2)	3.02 (sd = 0.018)	0.064 (sd = 0.009)
Jurkat + 25 µg/ml ART	5.29 (sd = 0.91)	3.05 (sd = 0.013)	0.069 (sd = 0.011)
Jurkat + 50 µg/ml ART	3.68 (sd = 1.3)	3.05 (sd = 0.019)	0.085 (sd = 0.015)

3.3 Conclusion

In this chapter, the effect of different doses of ART on Jurkat cells stiffness and viscosity over four decades of frequency was analyzed. The stiffness of both untreated and ART-treated Jurkat cells increased with increasing frequency according to a weak power-law dependency. Moreover, the power-law coefficient decreased with increasing dose.

The results demonstrate that significant stiffening occurs in cancer cells after chemotherapy, which might be due to actin microfilament dynamic reorganization during apoptosis [91], [92]. This suggests that clinical observations may be performed with an oscillating OT combined with numerical simulations to quantify the mechanical properties of cancer cells following exposure to chemotherapeutic agents, in order to quickly assess the efficacy of the treatment. In addition, white blood cell stiffening after chemotherapy is a treatment complication that could lead to leukostasis and other vascular complications in some leukemia patients. Tracking the mechanical characteristics of white blood cells using OTs may provide an early indicator of such complications. As a previous study [91] showed, the cytoskeleton reorganizes during the process of apoptosis induced by chemotherapeutic agents acting on leukemia cells. Therefore, measuring mechanical changes, such as the magnitude of cell stiffness, allows for monitoring the drug effect on cytoskeletal proteins as well. As a result, a powerful method for quantifying the effect of anti-cancer drugs and prevention of clinical complications following chemotherapy may be established by connecting cell mechanics with biological functions.

Chapter 4

Hypoxia and Cell Structural Changes: Rb Links Hypoxia to Actin Reorganization in Cancer Cells as Measured by an Optical Tweezer

In this chapter, the effect of hypoxia and loss of Rb on the cell cytoskeleton organization is studied. Hypoxia modulates actin organization via multiple pathways. Analyzing the effect of hypoxia on the biophysical properties of cancer cells is beneficial for studying modulatory signaling pathways by quantifying cytoskeleton rearrangements. We have characterized the biophysical properties of human LNCaP prostate cancer cells that occur in response to loss of Rb under hypoxic stress using an oscillating OT. Hypoxia increased cell stiffness in a fashion that was dependent on activation of the extracellular signal-regulated kinase (ERK) and the protein kinase B (AKT)- mammalian target of rapamycin (MTOR) pathways. Inhibition of either the ERK1/2, AKT or MTOR prevented hypoxia-inducible reorganization of stress fibers in Rb-negative cells. These results suggest that loss of Rb, in a HIF-1α dependent fashion, affects ERK/AKT-MTOR signaling and drives motility in transformed cancer cells. Thus, the mechanical characterization of cancer cells using an OT could provide an additional technique for cancer diagnosis/prognosis and evaluating therapeutic performance. The related results are submitted in Scientific Reports (2016).

4.1 Materials and Methods

4.1.1 Materials and reagents

RGD peptide, wedelolactone, U0126 and A6730 were purchased from Sigma-Aldrich (ON, Canada). The microbeads were purchased from Bangs Laboratory (ON, Canada).

4.1.2 Cell culture and exposure to hypoxia

The production of control shSCX- and knock-down sh-Rb-LNCaP cells was described previously [93]. Cells were maintained in RPMI 1640 medium with L-Glutamine (BioWhittaker, Lonza), supplemented with 10% FBS and 1% 100 units/ml potassium penicillin- 100 $\mu g/ml$ streptomycin sulphate. For hypoxia treatment, cells were split to 90% confluency and placed into a humidified, hypoxia incubation chamber and maintained in 5% CO2, and 1% O2 at 37°C. For normoxia treatment, cells were kept in a humidified incubation chamber and maintained at 37°C with 5% CO2, and 20% O2.

4.1.3 Antibodies and immunoblotting

LNCaP cells were left at normoxia (20% O2) or incubated under hypoxic conditions (1% O2) for 24 h. Cells were then treated with either vehicle (DMSO) or drug (2 μM A6730 or 10 μM U0126) and then left at normoxia or hypoxia for a further 48 h. Cells were harvested and the protein concentration estimated by the RC DC Protein Assay (Bio-Rad). Equal amounts of total protein from the samples were resolved on a SDS-acrylamide gel then transferred to polyvinylidene fluoride (PVDF) membrane. Membranes were incubated with diluted primary antibodies in 5% w/v skim milk powder, 1X TBS, 0.1% Tween-20 at 4°C with gentle shaking, overnight. Primary antibodies used were anti-α-tubulin (mouse monoclonal, Santa Cruz Biotechnology Inc., SC-8035), anti-pan-AKT (rabbit monoclonal, Cell Signaling Technology, 4691), anti-phospho-AKT (Ser473) (rabbit monoclonal antibody, Cell Signaling Technology, 4060), anti-phospho-AKT (Thr308) (rabbit monoclonal, Cell Signaling Technology, 13038), anti-p44/p42 (ERK1/2) 137F5 (rabbit monoclonal, Cell Signaling Technology, 4695) and anti-phospho-p44/p42 MAPK (ERK1/2) (T202/Y204) (rabbit polyclonal, Cell Signaling Technologies, 9101). Horseradish peroxidase conjugated anti-mouse or anti-rabbit IgG (Santa Cruz Biotechnology Inc.) and Luminata Crescendo Western HRP substrate (EMD Millipore) were used for detection.

4.1.4 Transwell migration assay

Control scrambled or shRb LNCaP cells were treated with hypoxia (1% O2) or maintained at normoxic conditions and treated with either vehicle or drug (10 μM U0126, 2 μM A6730 or 10 nM INK128) for 96 h. After 96 h, cells were washed, trypsinized, counted on a Haemocytometer and then seeded on ThinCerts (Greiner Bio-One) with 8.0 μm pore size at 1X104 cells per cell culture insert. The cells were maintained in serum-free RPMI 1640 with L-glutamine in the upper chamber whereas the lower chamber contained RPMI 1640 media with L-glutamine and 50% FBS. Cells were treated as stated above for a further 96 h and then total migrating cells were counted using an Olympus CKX41 light microscope.

4.1.5 Microscopy and immunofluorescence

Cells were seeded on coverslips in twelve-well plates and grown to 60% confluency. Cells were fixed with 4% paraformaldehyde in 1x PBS. Cells were permeabilized with 0.1% Triton X-100 in 1x PBS. Cells were incubated with 1% BSA in PBS (for how long). FITC conjugated anti-Vinculin probe and Rhodamine phalloidin was then added to this solution and incubated for 1 h at room temperature. Cell morphology was observed using an Olympus IX-81 inverted fluorescence microscope (Olympus Canada). MetaMorph software (Olympus Canada) was used to capture the cell morphology.

4.1.6 Oscillating optical tweezer mechanical characterization

The stiffness of LNCaP cells were measured using an oscillating OT as described previously [71]. Briefly, the RGD-coated microbeads bound to the cell surface

were trapped by the laser tweezer and then moved back and forth via oscillating laser trap with various frequencies of 0.1, 1, 10 Hz. As the bead moves sinusoidally, the cell develops internal stress and resistance to the bead motion that depends on the cell's mechanical properties. The resultant bead displacement in response to the force applied by the tweezer was measured optically and the bead motion equation was used to calculate the cell shear modulus and viscosity in the frequency domain.

The cell relaxation time can also be measured by a microbead linked to a cell in viscous solution trapped by the OT. Movement of the trapped bead due to viscous drag force of the surrounding solution as well as the thermal noise of the laser causes a cell to develop an internal stress that also depends on the cell's mechanical properties. The bead motion in response to such forces is measured and by performing autocorrelation analysis on the bead position signal, we can find the cell relaxation time as derived in next section.

4.1.7 Data Analysis

In order to analyze the experimental data and calculate the changes in cell mechanical properties, a bead motion equation was used as described previously [71]. The cell relaxation time was calculated by measuring fluctuations in the position of trapped beads linked to the cell cytoskeleton. By analyzing the normalized position auto-correlation function of trapped bead signal fluctuations in time domain, relaxation time was determined. The trapped bead motion equation can be described by:

$$x' + (1/\tau_0)x = \xi(t) \tag{4.1}$$

$$\tau_0 = \frac{(\gamma+\beta)}{k_1} \tag{4.2}$$

$$\gamma = 6\pi a \eta_{med} \tag{4.3}$$

$$\beta = r_{cont}\eta_{cell} \tag{4.4}$$

where η_{med} and η_{cell} are the viscosity coefficients of the surrounding medium and the cell structure, and k_1 is the laser stiffness coefficient, and τ_0 is the relaxation time. Integrating both sides of the above equation with respect to time, we arrived at:

$$x(t) = e^{-t/\tau_0} \int_{-\infty}^{t} \frac{1}{(\gamma+\beta)} \xi(\tau') e^{\frac{\tau'}{\tau_0}} d\tau' \quad (4.5)$$

Calculating the normalized position autocorrelation function, and using the properties of $\xi(t)$ we arrived at:

$$< \xi_i(t) > = 0 \quad (4.6)$$

$$< \xi_i(t)\xi_j(t') >= 2\gamma\beta k_B T\delta(t-t') \quad (4.7)$$

$$< x_i(t)x_i(t+\tau) >= e^{\frac{-\tau}{\tau_0}} \quad (4.8)$$

Thus, by performing autocorrelation analysis on bead fluctuations and fitting the experimental results to the exponential function, we can determine the cell relaxation time.

4.1.8 Statistical analysis

All Data are represented as means ± standard deviation (SD), and for statistical analysis we used an ANOVA test for comparing more than two groups of samples' mean. *P<0.05* was considered as statistically significant.

4.2 Results

4.2.1 Hypoxia and loss of Rb exhibit dynamic change in cell stiffness

To determine the effect of hypoxia and loss of Rb on the organization of the LNCaP cell cytoskeleton, we examined the normalized amplitude of resultant bead movement (NARBM) in response to an OT applied force at a frequency of 1Hz in scrambled short-hairpin (shSCX) and short-hairpin-Rb knock-down (shRb) cells under hypoxic and normoxic conditions (24, 48, 72 h). Measuring the NARBM in response to the OT applied force demonstrated a time-dependent response in bead displacement (Figures 4.1, 4.2 and 4.3) that was significantly decreased in cells exposed to hypoxia at all times. By contrast, cells exposed to 72 h of hypoxia exhibited a significant difference between shRb cells under hypoxia and the other groups of cells. These observations suggest that hypoxia promotes time dependent changes in cell structure that was measureable by tracking bead displacement in response to the OT's applied force. Additionally, these results indicate that structural remodeling observed in LNCaP cells in response to hypoxia that was observed by the RGD coated bead displacement, was due to actin remodeling and polymerization. The bead displacement is limited by the quantity of actin tethered to the bead; therefore, an increase in actin polymerization and reorganization leads to a decrease in observed bead displacement.

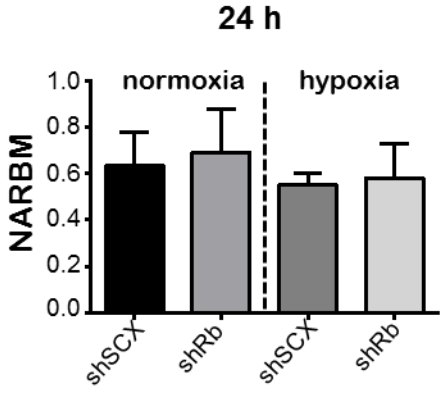

Figure 4.1. Variation in measured NARBM (Normalized Amplitude of Resultant Bead Movement) of shRb and shSCX LNCaP cells after 24 h of exposure to hypoxia.

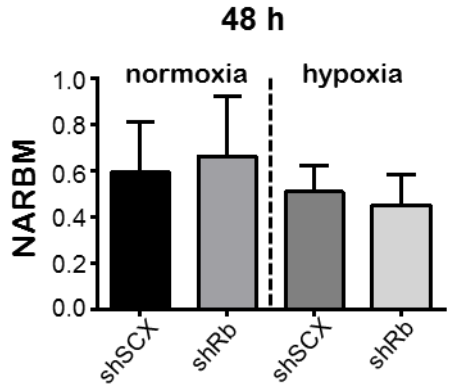

Figure 4.2. Variation in measured NARBM (Normalized Amplitude of Resultant Bead Movement) of shRb and shSCX LNCaP cells after 48 h of exposure to hypoxia.

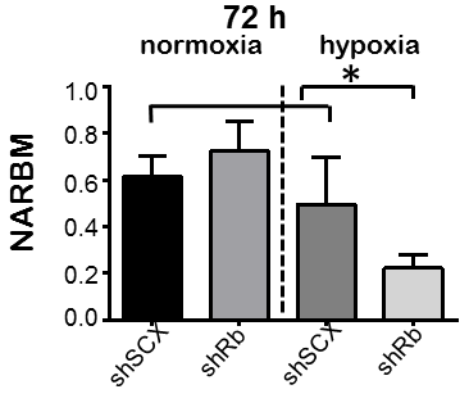

Figure 4.3. Variation in measured NARBM (Normalized Amplitude of Resultant Bead Movement) of shRb and shSCX LNCaP cells after 72 h of exposure to hypoxia. Error bars represent ±S.D. *p<0.05.

The measured bead displacements for each group of cells, after 72 h of exposure to hypoxia and normoxia, along with the solution of bead motion equation were used to identify each group of cells' viscoelastic properties [71]. According to our results (Figure 4.4), shear modulus alterations for each group of cells were frequency dependent with a weak power-law dependency. Comparing the shear modulus at all applied frequencies of 0.1 Hz, 1 Hz, and 10 Hz, there exist a significant difference between hypoxia treated shRb cells and the other groups of cells. Both cell groups (shRb and shSCX) under hypoxia showed an increase in their shear modulus compared to the normoxic cells, while the shRb group of cells showed the most significant increase

in cell shear modulus at all frequencies (Figure 4.4). The viscosity coefficient response was not frequency dependent; however, there was a significant difference between the hypoxic shRb cells and all other treatments (Figure 4.5). In addition, the differences between normoxic shSCX and hypoxic shSCX were not significant. Finally, the viscosity coefficient was increased for the hypoxic conditioned cells compared to the cells cultured in normoxia. The power-law coefficient, which is an intrinsic cytoskeletal property, decreased under hypoxia for shRb and shSCX compared to their normoxic conditioned cells. Thus, our results suggest that hypoxia alters the mechanical properties of Rb-ve cells, which is a quantifiable measure of cellular structural changes.

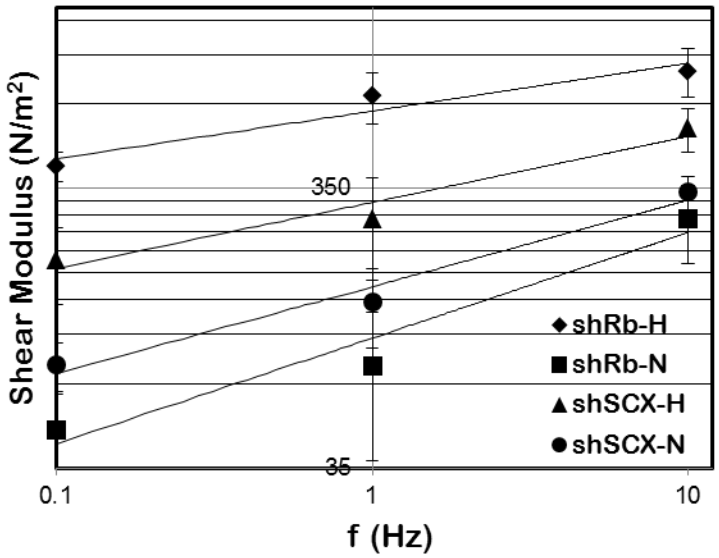

Figure 4.4. Variation in shear modulus after 72 h of exposure to hypoxia at different frequencies of applied force (0.1, 1, and 10 Hz). Error bars represent ±S.D.

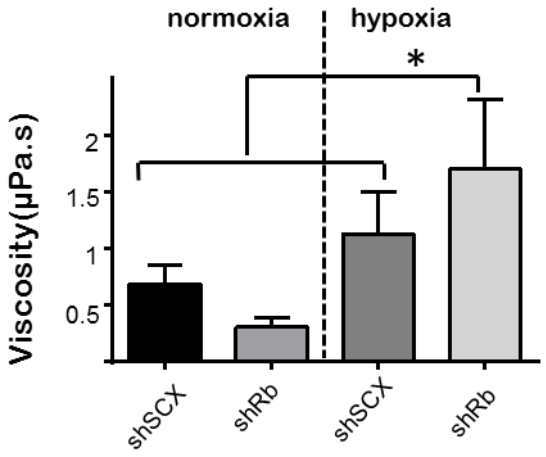

Figure 4.5. Variation in viscosity of shRb and shSCX LNCaP cells after 72 h of exposure to hypoxia. Error bars represent ±S.D. *p<0.05.

4.2.2 Hypoxia and loss of Rb exhibit significant change in cell relaxation time

To further assess the effect of hypoxia and Rb-loss on the organization of the LNCaP cytoskeleton, we measured the relaxation time of control and Rb-ve cells by monitoring the random movement of trapped beads anchored to the cell cytoskeleton [94]. More details about the derivation of relaxation time are presented in the data analysis section of the *Materials and Methods*.

The normalized position autocorrelation function (NPAF) of bead movement for the different groups of cells was plotted in Figure 4.6. The autocorrelation results were analyzed by fitting with exponential functions. According to these results, the time scale varied for different groups of cells; however, those under hypoxic stress demonstrated a higher relaxation time compared to the normoxic cells (Figure 4.7). Moreover, cell viscosity coefficient was derived based on the relaxation times. These results, illustrated in Figure 4.8, also showed a significant difference between the hypoxic treated shRb cells and the other groups of cells. Accordingly, these findings are in agreement with our previous results.

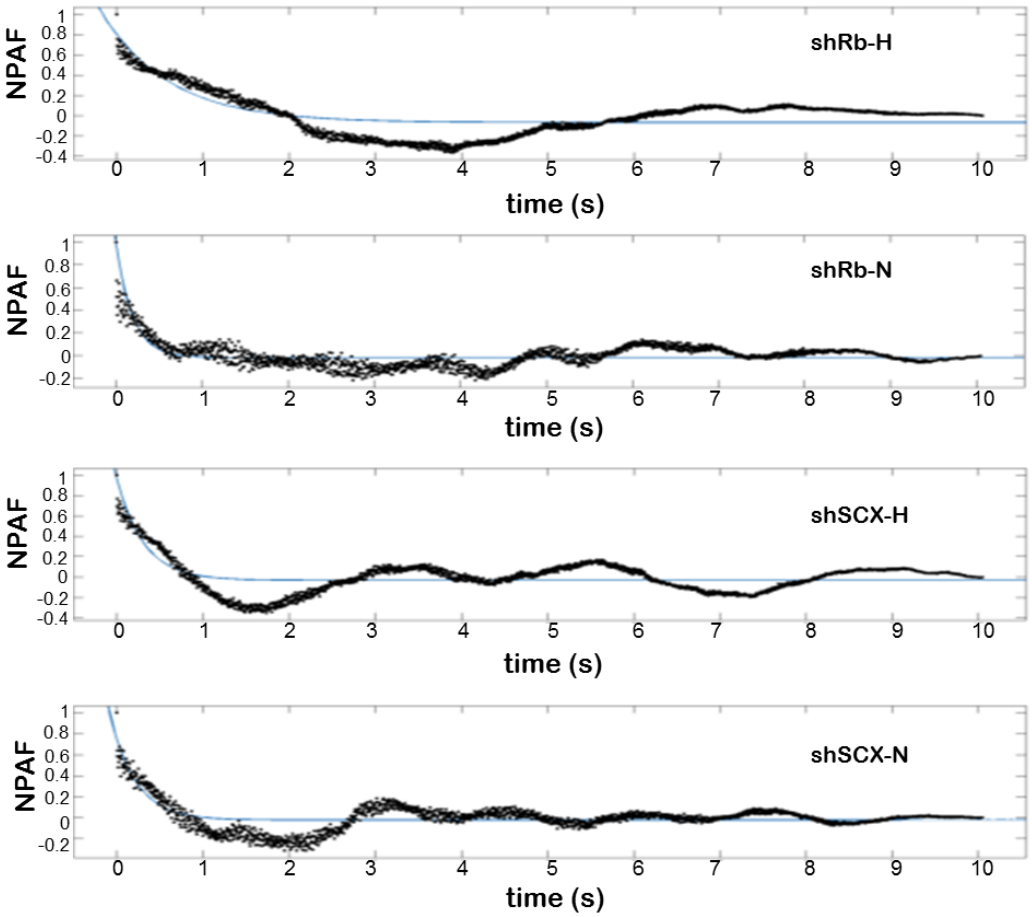

Figure 4.6. **NPAF (Normalized Position Autocorrelation Function) of beads fluctuations along with their exponential fit for shRb and shSCX LNCaP cells after 72 h of exposure to hypoxia or normoxia.**

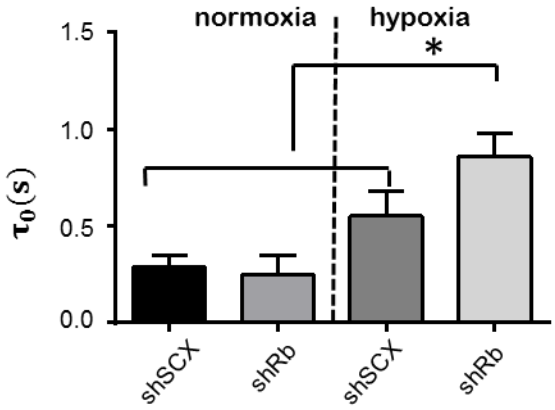

Figure 4.7. Relaxation time variation between different groups of cells (shRb, shSCX) after 72 h of exposure to hypoxia and normoxia.

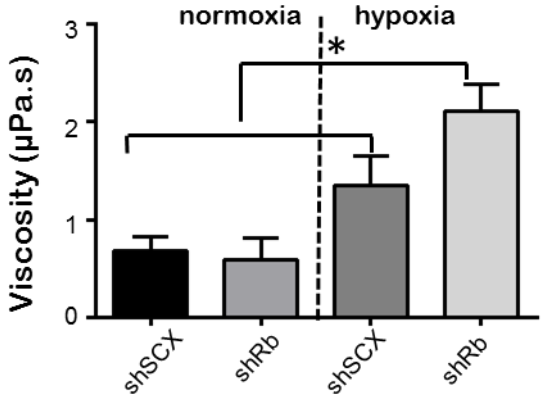

Figure 4.8. Estimated viscosity from the measured relaxation time for different groups of cells (shRb, shSCX) after 72 h of exposure to hypoxia or normoxia. Error bars represent ±S.D. *p<0.005.

4.2.3 Cell stiffness response is dependent on ERK

Next we wanted to determine the pathway responsible for actin reorganization. Gene ontology analysis of the LNCaP transcriptome identified the ERK1/2 pathway as a likely regulator of hypoxia-inducible cell motility in Rb-knock-down cells [95]. In order to determine if the ERK pathway is responsible for actin reorganizations, cells were treated with 10 μM of the MEK1/2 inhibitor U0126. Cell mechanical properties were determined

by applying time varying force on beads anchored to the cytoskeleton, employing the OT and measuring bead displacement. The shRb cells under hypoxic stress showed a significant increase in shear modulus compared to the control scrambled (shSCX) cells (Figure 4.9). While there was no significant difference between shSCX or shRb cells maintained under normoxia and treated with or without U0126, hypoxic shRb cells treated with U1026 demonstrated a significantly lower shear modulus compared to untreated hypoxic shRb cells (Figure 4.9). Moreover, the results related to cell viscosity demonstrate a significant difference between hypoxic shRb cells treated with or without U0126 as well (Figure 4.10). Immunoblots of whole cell lysates determined that both shSCX and shRb LNCaP cells treated with hypoxia expressed elevated levels of phosphorylated ERK1/2 protein. Importantly, addition of 10 μM U0126 blocked ERK1/2 phosphorylation (Figure 4.11). These results suggest that hypoxia increased cell stiffness in Rb knock-down cells in an ERK-dependent fashion. Inhibition of the ERK pathway using U0126 prevented reorganization of stress fibers, which was observed as decreased cell shear modulus. Furthermore, we studied the effect of the NFkB pathway on actin disruption by treating cells with 15μM of wedelolactone; an NFkB inhibitor that blocks the phosphorylation and degradation of IκBα. The mechanical responses of the cells were again calculated upon applying time varying force on beads adhered to LNCaP cells using the OT and measuring bead displacement. The result showed no significant differences between cells treated with or without wedelolactone (Figures 4.12 and 4.13). According to these results, the NFkB does not play a role in actin reorganization of Rb knock-down LNCaP cells in response to hypoxia.

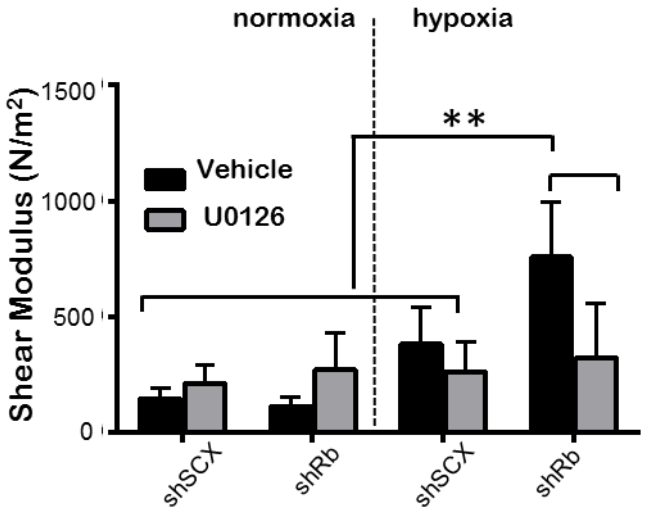

Figure 4.9. **Variation in shear modulus of shRb and shSCX LNCaP cells after 72 h of exposure to hypoxia and treated with or without 10 μM U0126. **p<0.001.**

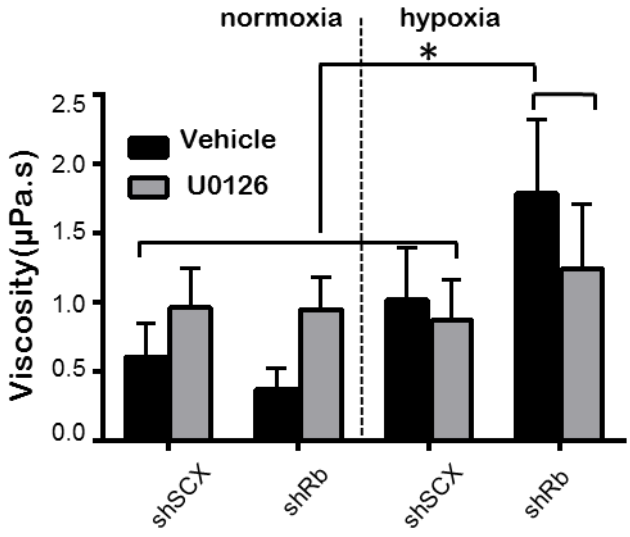

Figure 4.10. **Variation in viscosity of shRb and shSCX LNCaP cells after 72 h of exposure to hypoxia and treated with or without 10 μM U0126. *p<0.05.**

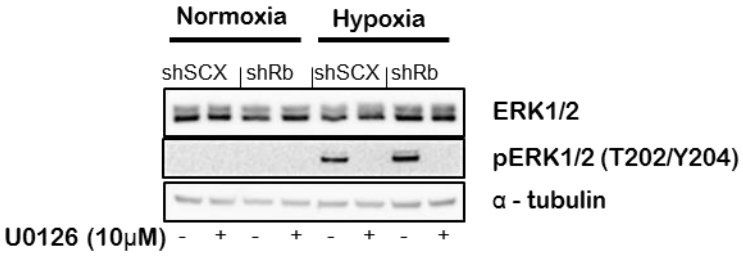

Figure 4.11 **Cells were immunoblotted with the indicated antibodies against ERK pathway.**

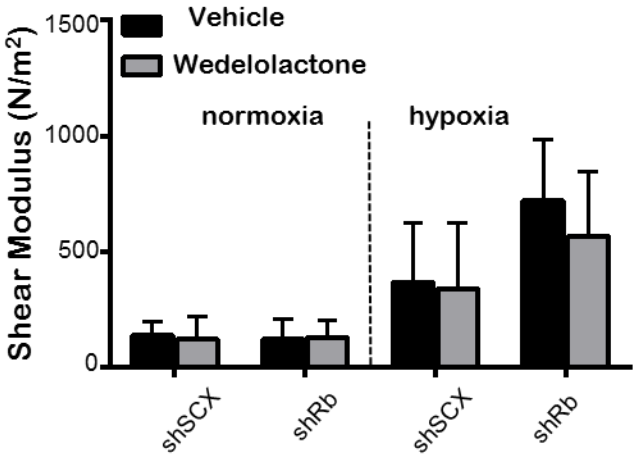

Figure 4.12. **Variation in shear modulus of shRb and shSCX LNCaP cells after 72 h of exposure to hypoxia and treated with or without 15 μM wedelolactone.**

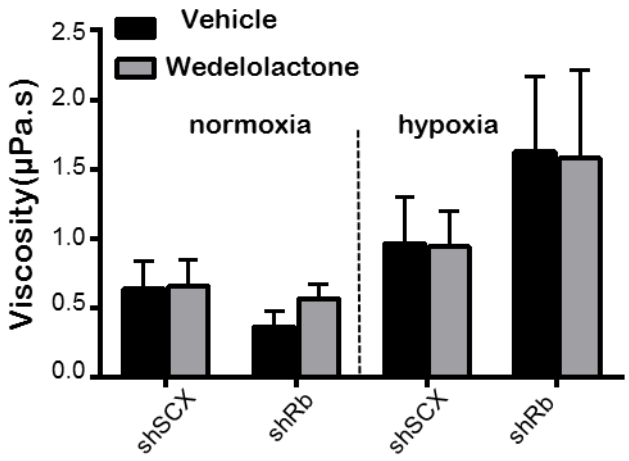

Figure 4.13. Variation in viscosity of shRb and shSCX LNCaP cells after 72 h of exposure to hypoxia and treated with or without 15 μM wedelolactone. Error bars represent ±S.D.

In order to validate our results, immunofluorescent microscopy of 10 different groups of cells, (shSCX and shRb cells maintained under normoxia or hypoxia and treated with or without inhibitors), was performed using rhodamine phalloidin as an actin probe. The results are illustrated in Figure 4.14. The shRb cells treated with hypoxia demonstrate significant actin polymerization and this strongly supports the results we obtained from our mechanical characterization studies. Furthermore, according to this data, pre-treatment of cells with U0126 prevented the hypoxia-inducible reorganization of stress fibers in the shRb cells (Figure 4.14). Therefore, our results suggest that the ERK but not the NFkB pathway contributes to actin reorganization.

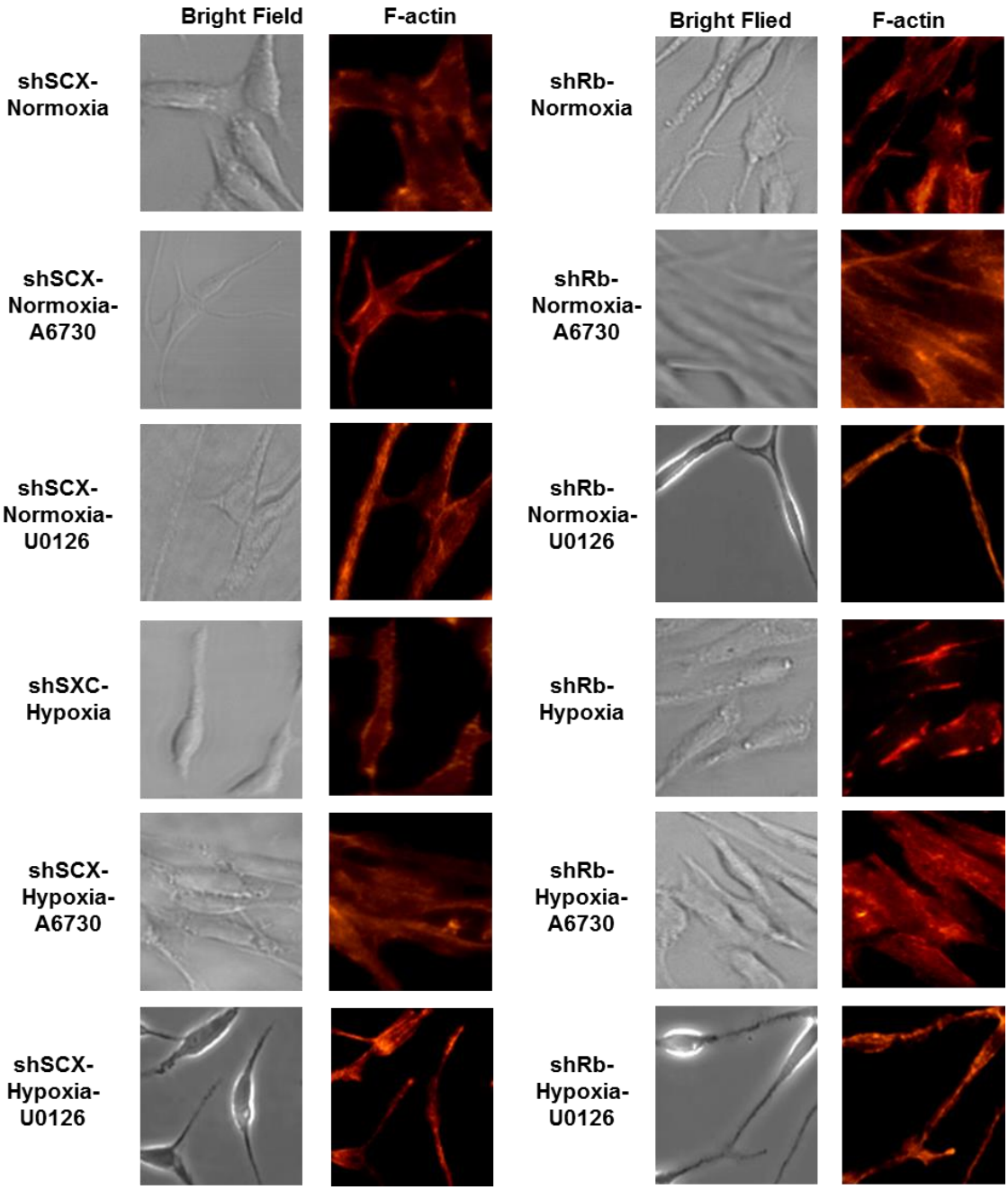

Figure 4.14. **shRb and shSCX LNCaP cells were exposed to 72 h of hypoxia or normoxia and treated with or without 10μM U0126 or 2μM A6730. Actin organization is visualized using rhodamine phalloidin and an Olympus IX-81 inverted fluorescence microscope.**

4.2.4 Cell stiffness response is dependent on AKT

In order to further validate our results we examined the role of AKT, a regulator of actin organization that works in parallel and cross-talks with the ERK1/2 signalling pathway [96, 97]. Our measurements of changes in shear modulus and actin polymerization as assessed by immunofluorescent microscopy were in good agreement. We treated control and shRb-LNCaP cells with the specific MEK1/2 inhibitor, U0126, and observed a significant increase in shear modulus of shRb cells cultured in hypoxia compared to shRb cells. Additionally, cells treated with 2 μM A6730, an inhibitor of AKT demonstrated similar alterations (Figure 4.15 and 4.16).

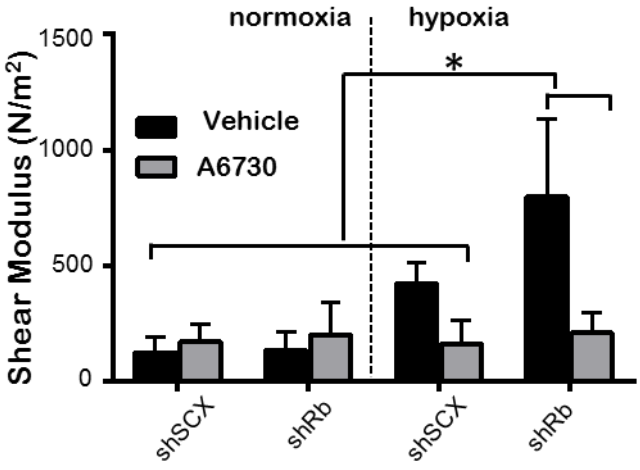

Figure 4.15. Variation in shear modulus of shRb and shSCX LNCaP cells after 72 h of exposure to hypoxia and treated with or without 2 μM A6730. *p<0.005.

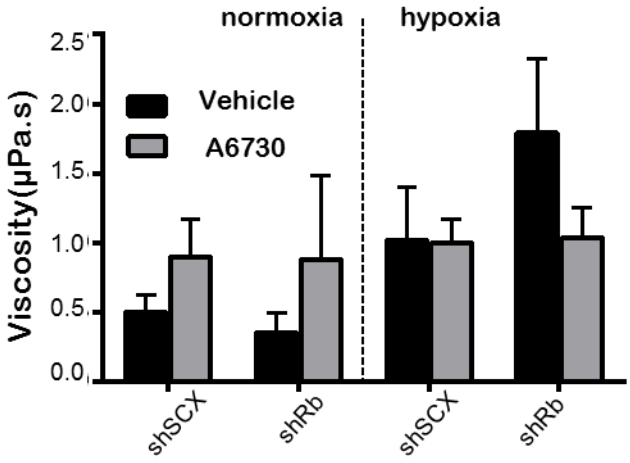

Figure 4.16. Variation in viscosity of shRb and shSCX LNCaP cells after 72 h of exposure to hypoxia and treated with or without 2 μM A6730.

Immunoblotting of total cell lysates using an affinity purified antibody specific for total and phosphorylated AKT is shown in Figure 4.17. As shown in this Figure, the shRb cells cultured in hypoxic conditions showed higher levels of phosphorylated AKT compared to all other groups of cells. This phosphorylation was prevented by treatment with A6730. Furthermore, we validated these results with immunofluorescence microscopy of cells treated with A6730 (Figure 4.14). The results demonstrate that both A6730 and U0126 prevented the hypoxia-inducible reorganization of stress fibers in shRb cells.

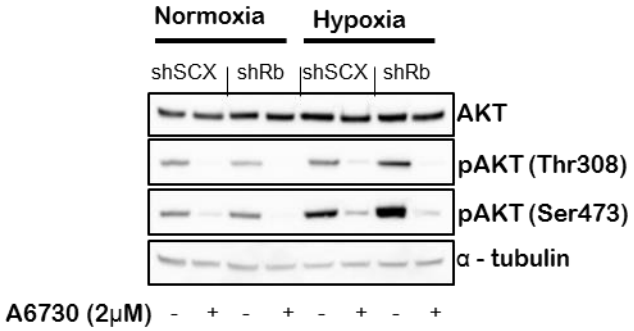

Figure 4.17. Cells were immunoblotted with the indicated antibodies against AKT pathway.

Moreover, we determined the role MTOR might play in this phenomenon. MTOR is a downstream effector of AKT and ERK pathways and a regulator of actin organization

[98, 99]. The shear modulus of LNCaP cells treated with or without 10 nM INK128, a specific inhibitor of MTOR, and incubated under normoxic or hypoxic conditions were measured (Figures 4.18 and 4.19). We observed a significant increase in the shear modulus of shRb cells cultured in hypoxia compared to shRb cells treated with INK128, which is in agreement with our observations using A6730 and U1026. Thus, our results demonstrate that both ERK-MTOR and AKT-MTOR signalling pathways are responsible for actin reorganization and cell motility observed in Rb negative hypoxic cells.

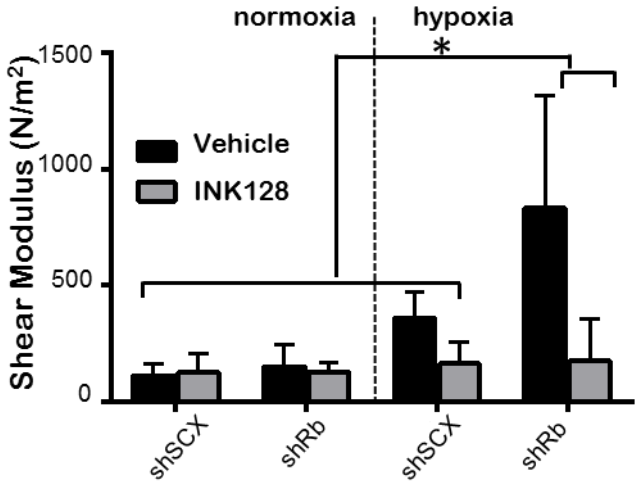

Figure 4.18. Variation in shear modulus of shRb and shSCX LNCaP cells after 72 h of exposure to hypoxia and treated with or without 10 nM INK128. *p<0.005.

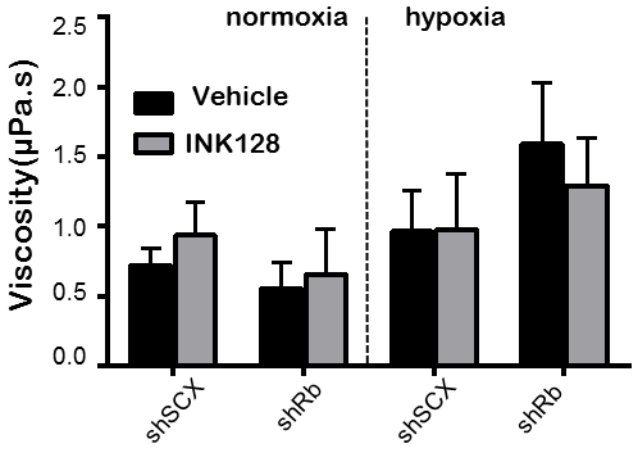

Figure 4.19. Variation in viscosity of shRb and shSCX LNCaP cells after 72 h of exposure to hypoxia and treated with or without 10 nM INK128. Error bars represent ±S.D.

4.2.5 Hypoxia inducible migration is dependent on ERK, AKT and MTOR

Gene ontology analysis [95] and a growing body of evidence in the literature [100, 101] suggest that the AKT and ERK signaling pathways control cell migration and metastasis in shRb LNCaP cells exposed to hypoxia. To determine if actin reorganization correlates with increased cell migration, we treated shRNA LNCaP cells with hypoxia or normoxia and used a cell migration assay to measure the total number of migrating cells. Indeed, shRb LNCaP cells exposed to hypoxia migrated at a significantly higher rate compared to scrambled negative controls and to normoxic shRb cells (Figure 4.20). Additionally, treatment with 10 μM U0126, 2 μM A6730 or 10 nM INK128 significantly impeded hypoxia-inducible migration in shRb LNCaP cells compared to the untreated control (Figure 4.21). Taken together, these data support our hypothesis that the ERK1/2 and AKT pathways may crosstalk through MTOR to control migration and invasion in hypoxic prostate cancer cells lacking Rb. Moreover, the cell migration data is in agreement with the OT data and this strongly supports the use of our oscillating OT as an accurate method to detect cells with migratory phenotypes.

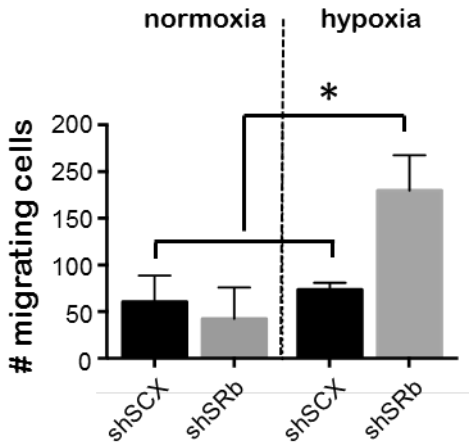

Figure 4.20. Total number of migrating cells for shRb and shSCX LNCaP cells after exposure to hypoxia or normoxia. *p<0.05

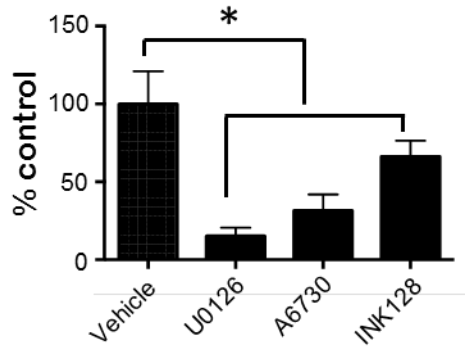

Figure 4.21. Total number of migrating cells for shRb LNCaP cells treated with hypoxia and with DMSO, 10μM U0126, 2μM A6730 or 10nM INK128. Error bars represent ±S.D. *p<0.05

4.3 Discussion

In this study we examined the alteration in biophysical properties of transforming prostate cancer cells after loss of Rb under hypoxic conditions using an oscillating OT. Our results indicate that loss of Rb protein in prostate cancer cells under hypoxic condition increases invasiveness and alters cytoskeletal proteins dynamics by activating the downstream signaling modules. The over-activity of either the ERK1/2 or AKT pathway facilitates alterations in the cytoskeleton that, in turn, promotes motility and results in structural changes and actin protein reorganization. These alterations were

monitored by measuring the resultant movement of beads anchored to the cytoskeleton and extrapolating those measurements to estimate cell stiffness. Inhibition of either the ERK1/2 or AKT-MTOR pathways prevented actin reorganization that may contribute to cancer cell transformation and motility.

In order to analyze alterations in the mechanical properties of control and Rb-knock-down LNCaP cells, resultant bead movements were measured under hypoxic and normoxic conditions using an oscillating OT [71]. The results show time dependent changes in bead movement for cells (shSCX and shRb) cultured under hypoxia for 72 h while there were no significant differences for cells cultured in normoxia for the same amount of time. Moreover, these changes in bead movement were more profound for shRb cells compared to control shSCX cells. Changes in bead movement correspond to changes in actin organization, where decreased movement is a result of reorganization and stabilization of actin and an increase in cell tethering forces at focal adhesion sites. Increased actin polymerization near the focal adhesion sites translates to an increased tethering of beads to these sites resulting in decreased bead movement. The fluorescence microscopy of cells using rhodamine phalloidin was in agreement with the measured mechanical properties of cells that also suggest the contribution of actin reorganization in transformed cancer cells mechanical responses. Furthermore, increased cell migration in hypoxic shRb LNCaP cells suggests that there is a correlation between increased cell migration and actin reorganization.

Activation of the ERK1/2 pathway has a profound effect on actin disruption in many cell types [102, 103, 104, 105, 106]; however, these findings were mainly based on structural evidence. Consistent with these structural observations, we measured and analyzed mechanical properties of cells and investigated the role of the ERK pathway on actin reorganization. Our results show that ERK activation is responsible for actin reorganization. Furthermore, we measured the effect of inhibiting the AKT pathway, and analyzed the cell structural changes as well as alterations in mechanical properties of cells. The results were in good agreement with results regarding the inhibition of ERK pathway. Therefore, we conclude that activation of AKT pathway is also responsible in actin reorganization and inhibiting this pathway using A6730 result in restoration of actin cytoskeleton. Based on our results, the parallel activation of both the ERK and AKT

pathways are responsible for actin reorganization in Rb-ve hypoxic cancer cell lines. Moreover, we measured the effect of inhibiting MTOR, the downstream effector of AKT and ERK pathways, on cell mechanical properties alteration. Since the results of inhibiting MTOR pathway was in agreement with either of the ERK or AKT pathway inhibition, we conclude that MTOR is the downstream effector of both the ERK and AKT pathways for actin reorganization in Rb-ve hypoxic cancer cell lines.

The evidence presented here suggests that loss of Rb in hypoxic prostate cancer cells increases actin reorganization and migration through ERK-AKT-MTOR signaling (Figure 4.22). Several studies have demonstrated crosstalk between PI3K/AKT/MTOR and MAPK/ERK signaling pathways [107, 108, 109]. However, depending on the stimulus, the pathways may have cooperative, inhibitory or separate biological functions. For example, MEK1, MEK2 and MEK5 inhibitors enhance AKT activation possibly involving phosphorylation of GAB1 induced by ERK2 and inhibition of recruitment of PI3K to the EGF receptor [110]. Alternatively, it has been reported that AKT can phosphorylate inhibitory sites in Raf, and consequently down regulate ERK1/2 [111]. Conversely, cross-activation has also been reported. In this instance, Ras-ERK regulates PI3K, and MTORC1 which results in cross activation of PI3K-MTORC1 [112]. Furthermore, the ERK1/2 and AKT promote MTORC1 activity by inhibiting TSC1/2's GAP function [113].

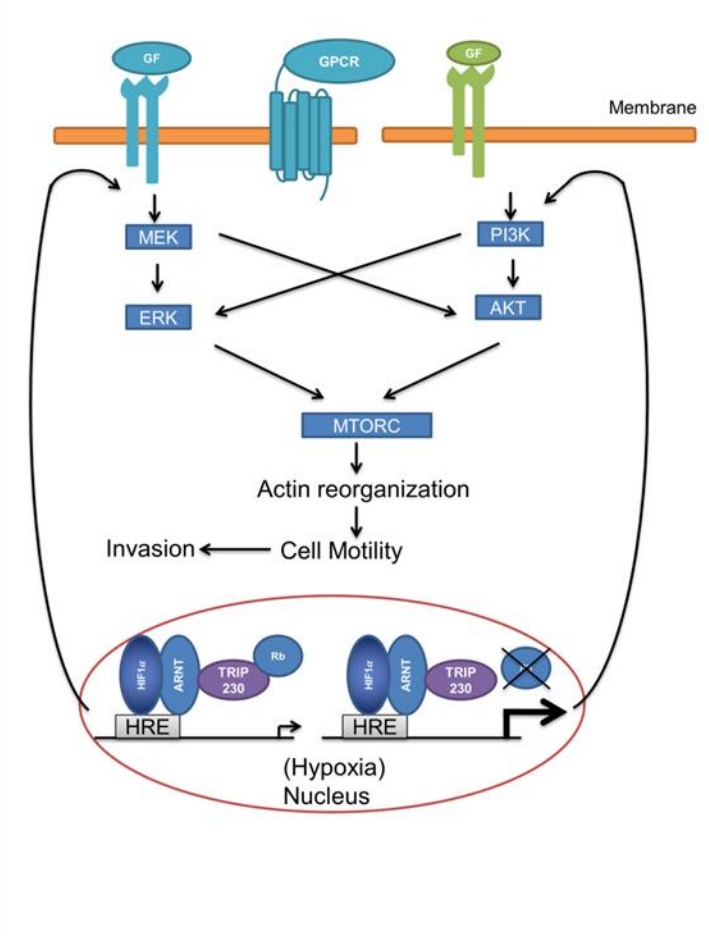

Figure 4.22. Loss of Rb in hypoxic prostate cancer cells increases actin reorganization and migration through ERK-AKT-MTOR signaling. GF: growth factor; GPCR: G protein coupled receptor; HRE: hypoxic response element; ARNT: aryl hydrocarbon receptor nuclear translocator.

Previously, we determined that loss of Rb dysregulates HIF1-mediated transcriptional responses [93] and that Rb loss in conjunction with hypoxia leads to the acquisition of a more invasive and neuroendocrine phenotype in prostate cancer cells [95]. We identified several putative upstream regulators of ERK1/2 and AKT-MTOR signaling that may contribute to prostate cancer cell transformation, such as CXCR4, HTR5A and KISS1 receptor (KISS1R) [95]. Furthermore, loss of Rb expression and hypoxia sensitized prostate cancer cells to kisspeptin-10, a potent KISS1R agonist [95]. Although KISS1/KISS1R interactions have been linked to both pro- and anti-metastatic processes, KISS1R expression in breast cancer cells increases cell invasion and

metastasis [114, 115]. Additionally, KISS1R signaling activates ERK1/2 through β-arrestin [116] and stimulates invadopodia formation in triple negative breast cancer via β-arrestin and ERK1/2-dependent mechanisms [117]. The KISS1R-ERK1/2-invadopodia paradigm requires further investigation in prostate cancer, however, we speculate that some Rb-negative prostate cancer cells under hypoxic stress may become more invasive in a similar fashion.

MTC and AFM have been employed previously to measure alterations in the mechanical properties of cancer cells in order to characterize the pathways responsible for actin reorganization [118], [119, 120, 121]. Stiffness of pulmonary microvascular endothelial cells exposed to hypoxia was measured using MTC. These investigators determined that hypoxia increased cell stiffness and therefore regulates endothelial cell contraction [118]. Cytoskeletal dynamics were measured in skin, bladder, prostate and kidney cell lines. These results suggested that metastatic cancer cells exhibit increased cell stiffness and this increased cell stiffness is required to facilitate the vascular invasion [119, 120, 121]. Cervical and liver carcinoma cells mechanical response to anticancer drugs, colchicine or cytarabine, were measured and their results demonstrated a correlation between the degree of mechanical changes in cells and the drug dosages [119, 120, 121]. Therefore, employing MTC and AFM could provide useful insights into cancer cells' cytoskeletal dynamics, alterations and metastatic processes. Comparing OT to the other technologies, its main advantage is being a noninvasive technique that can apply a uniform stress on cells that could aid in measuring cellular mechanical alterations more accurately. To our knowledge, this is the first use of a cyclic OT to measure biophysical alterations in cancer cells in order to determine the transformational and migratory phenotype of cells. Our results demonstrate that employment of OT could provide a *de nova* technique for evaluating cancer therapeutic performance by quantifying alteration in cell structures and assessing the specific contribution of different signalling pathway to cell migration.

Our study suggests therapeutic agents that target the factors regulating the hypoxic signals that result in the untoward activation of the ERK and AKT pathways might be suitable to prevent prostate cancer metastasis. Clinical trials of AKT and ERK inhibitors have demonstrated unacceptable toxicities [122, 123]. Thus, targeting

deregulated upstream factors may be more selective in treating prostate cancers. Finally, these results highlight the utility of the OT in characterizing and identifying the transformation of cancer cells as a reliable, rapid and accurate alternative to conventional time consuming methods.

4.4 Conclusion

In this chapter, the oscillating OT was used to measure mechanical properties of Rb-negative LNCaP prostate cancer cells exposed to hypoxia. Stiffness and viscosity was analyzed for different group of normoxic and hypoxic cells. Our results showed that hypoxia and the loss of Rb caused variation in cells mechanical properties. Rb-negative hypoxic cells stiffness increased significantly comparing to other groups of cells. Moreover, the inhibitory effect of ERK, AKT and NFkB pathways on cells structural changes is measured utilizing the oscillating OT. Our results demonstrated that inhibition of both ERK and AKT pathways prevented the structural changes in LNCaP cells. These results suggest that loss of Rb, in a HIF-1α dependent fashion, affects ERK/AKT-MTOR signaling and drives motility in transformed cancer cells.

Chapter 5

A Sensitivity Study of Cell-Bead Geometry on Cell Mechanical Responses using Finite Element Analysis

In this chapter, a finite element model of a cell attached to a microbead under dynamic loading is developed for cell manipulation by an OT. The cell material constants applied in the model are obtained from oscillating OT experiments, which demonstrate a power-law dependency of cell stiffness with frequency. This model is employed to characterize the sensitivity of cell mechanical response to cell-bead geometries, and the finite element analysis results for different cell and bead sizes are reported. This sensitivity study shows the importance of evaluating the effect of cell-bead geometries on cell mechanical response for different cell types and OT experiments.

5.1 Methods

5.1.1 Cell Geometry

We developed a finite element model (FEM) to represent adherent cells and simulate the application of oscillating OT forces to a microbead attached to a cell. The cell is represented by a cylinder of radius R_{cell}=20 μm and height h_{cell}. A bead with a radius r_{bead} is embedded on top of the cell. We restricted our simulation to half of the cell volume by using a symmetrical plane (vertical).

The cell-bead geometry parameters that we considered are cell height h_{cell}, bead radius r_{bead}, and bead half-embedding angle in cell φ (refer to Fig. 5.1 for the illustration of φ), which were suggested by Mijailovich et al. [124] as to the parameters that play a main role in cell mechanical responses.

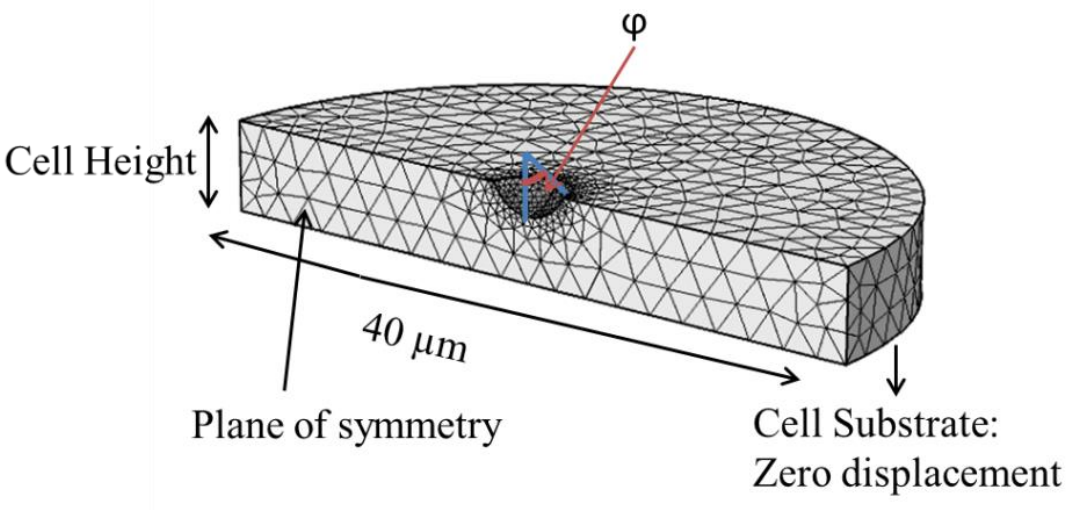

Figure 5.1. Finite element mesh of the cell volume in COMSOL.

5.1.2 Finite Element Model

The shear modulus of the cell in frequency domain can be represented as a power-law model:

$$|G(\omega)|=G_0(\omega)^{\alpha} \tag{5.1}$$

where ω is the frequency of the applied force. G_0 is a scale factor for the shear modulus and α is the power-law parameter, which are obtained from the oscillating OT experimental results.

Herein we simulated the power-law model by fitting the Maxwell Prony series expansion and used the Prony series to study cell mechanical responses in COMSOL. The Maxwell Prony series in frequency domain is defined as follows:

$$|E(\omega)| = |E_0 + \sum_{i=1}^{N} \frac{E_i {\tau_i}^2 \omega^2}{1+{\tau_i}^2\omega^2} + j\sum_{i=1}^{N} \frac{E_i \tau_i \omega}{1+{\tau_i}^2\omega^2}| \tag{5.2}$$

where E_i and τ_i are Prony coefficients, and N is the number of Prony terms.

5.1.3 Boundary Conditions

The boundary conditions that were applied are shown in Fig. 5.1 and can be summarized as follows:

- A zero displacement on the bottom surface of the cell was applied to model the full cell attachment to a rigid substrate.
- All other surfaces of the cell is assumed to have a free boundary condition.
- A vertical plane of symmetry is applied onto the cell.
- An extrusion coupling is used to map the bead elements to the cell, in the area where the bead is attached to the cell.

5.2 Experiment

5.2.1 Optical Tweezer Experimental Setup

An oscillating OT experimental setup (mmi Cell Manipulator, MMI AG, Zurich, Switzerland) was employed for this experiment. The technical details of the setup were described previously in [70]. In summary, a continuous wave 3W, Nd:YAG laser emitting light at a wavelength of 1064 nm was used with a Nikon TE2000 inverted microscope. A CCD camera and a CMOS camera were utilized to monitor the experimental process and to track the motion of the bead, respectively.

5.2.2 Cell Culture and Bead Preparation

LNCaP cells were maintained in RPMI 1640 medium (BioWhittaker, Lonza), supplemented with 10% FBS and 1% potassium penicillin. LNCaP cells are a cell line of androgen-sensitive human prostate adenocarcinoma cells commonly used in cancer research. Polystyrene microbeads were coated with RGD (Sigma-Aldrich) according to the manufacturer's protocol.

5.2.3 Experiment Procedure and Particle Tracking

Glass cover slips were coated with Poly-L-lysine (Sigma) to facilitate the cell attachment. The cells were plated in RPMI 1640 and incubated at 37ºC over night. Medium was replaced the next day with PBS and RGD coated microbeads. Cells with microbeads attached to their surfaces were chosen for the oscillating OT experiment. The bead was trapped with the laser beam and a sinusoidal force with periods of 10s, 1s, and 0.1s was applied to the bead while recording the bead position with the CMOS camera at 50fps. Ten cells were selected on the chamber and the experiment was concluded within 30 min. The video recordings of the bead motion were then analyzed using the Computer Vision System Toolbox™ in MATLAB®, to perform object detection, feature identification, and bead tracking as proposed in our previous work [125].

5.3 Results and Discussion

5.3.1 Model Parameters

Equation 5.2 was fitted to Eq. 5.1 with N=4 for which the best fitting results were obtained. An iterative Genetic Algorithm (GA) was applied to estimate the Prony coefficients by minimizing the fitting error. The effectiveness of the fitting of the power-law model to the Prony series can be observed by comparing the fitting results in Fig. 5.2.

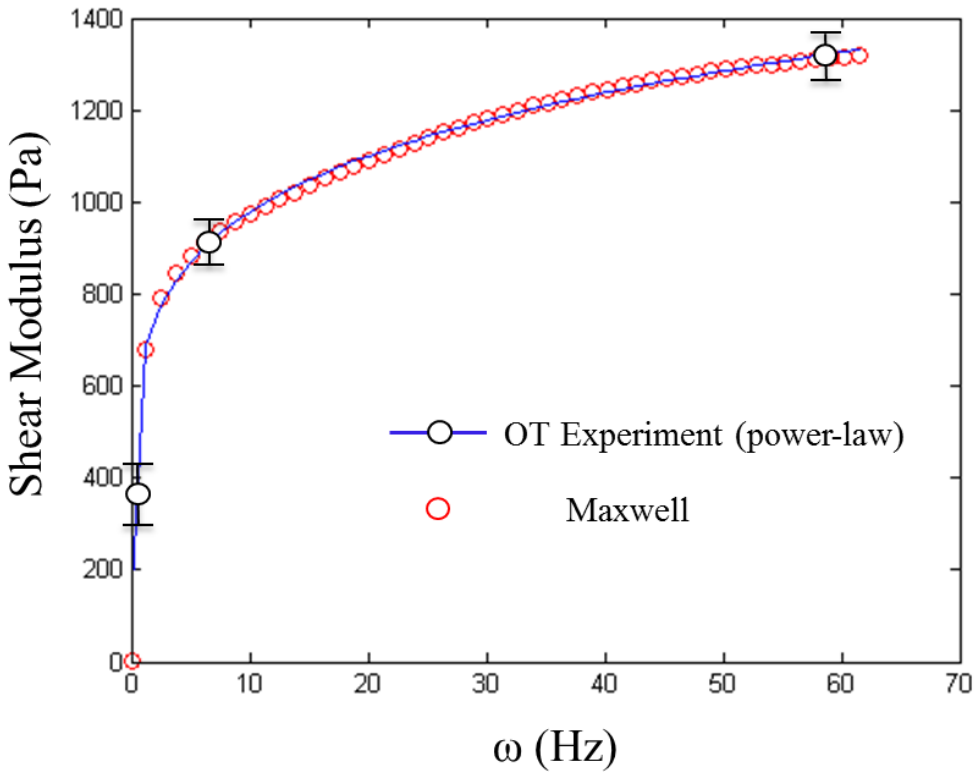

Figure 5.2. Fitted Maxwell parameters to power-law model from oscillating OT experimental results.

5.3.2 Mesh Sensitivity Study

A mesh sensitivity study was applied to consider the independence of the results from the mesh. A tetrahedral element was chosen to mesh the cell. The cell is composed of two domains with different mesh sizes: 1) the region where the bead is attached (bead-cell region) and 2) the rest of the cell. Three different mesh sizes, i.e. extremely fine, extra fine and fine, were chosen for the bead-cell region, and two different mesh sizes of normal and fine were chosen for the rest of the cell. Therefore, a total number of six different mesh combinations were analyzed. All six combinations gave the same result for the bead center translations and the maximum von Mises stresses with a maximum error of <1% and <7%, respectively, except for the two mesh combinations for which the fine mesh size was chosen for the bead-cell region (and the

normal or fine mesh size for the rest of the cell). As a conclusion, all the results of the subsequent FEA were obtained using the extra fine-normal mesh.

5.3.3 Spatial Distribution of Cell Deformation with Variation of Cell Height, Bead Radius and Embedding Angle

Figure 5.3 illustrates the effect of variation in the bead radius (r_{bead}), cell height (h_{cell}) and embedding angle (φ) on the spatial distribution of cell's local deformation. The amplitude of the applied force was kept constant in all cases. The FEA results show that increasing the cell height from 2 to 5 μm for r_{bead}=1.5 μm and φ =35º cause increase (9%) in the maximum cell deformation; and this increase is more pronounced for r_{bead}=2.5 μm (30%). In comparison, the increase in the bead radius from 1.5 to 2.5 μm for h_{cell}=5 μm and φ =35º demonstrates a sharp decrease of 71% in the maximum cell deformation. Furthermore, increasing the embedding angle from 35º to 65º causes a decrease in the maximum cell deformation for all cases. A more precise analysis of cell-bead geometry variation effect on cell mechanical response is studied in the following sections.

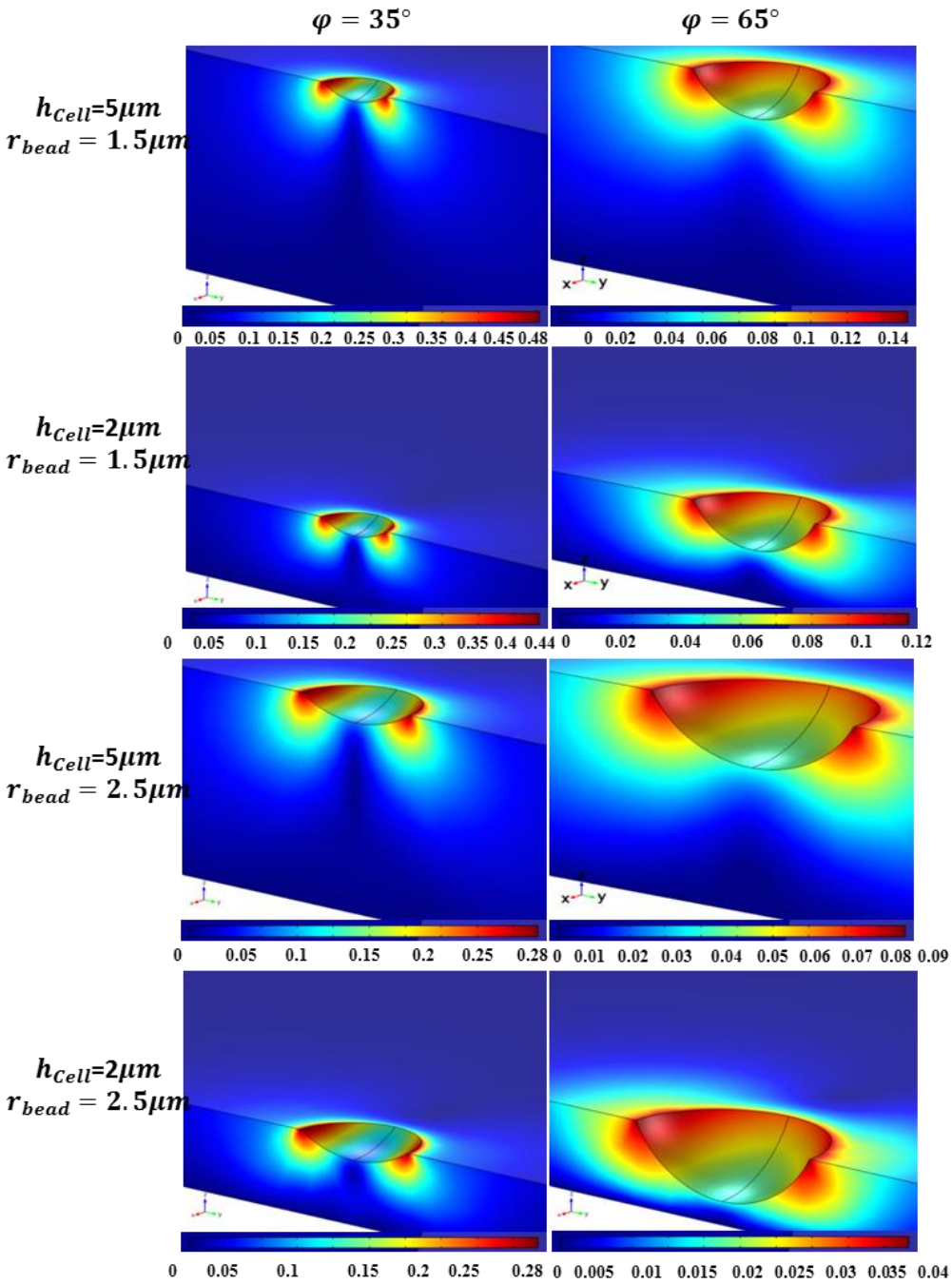

Figure 5.3. **3D color maps showing the spatial distribution of cell's local deformation in neighborhood of the bead. Six different cell-bead geometries have been considered.**

5.3.4 Influence of Bead Radius on Cell Mechanical Response

In this section, the effect of variation in the bead radius on cell mechanical response is investigated specifically. The cell response is simulated for 10 different bead radii (0.5 μm ≤ r_{bead} ≤ 5 μm). According to the FEA results shown in Fig. 5.4, increasing the bead radius causes decrease in the bead center translation. Variation of the bead center translation is not significant for bead radius between 3 μm and 5 μm; however, it is a significantly nonlinear function of bead radius if it is less than 3 μm. Therefore, the bead size can have an affect on the cell response and it is important to consider its effect in OT experiments.

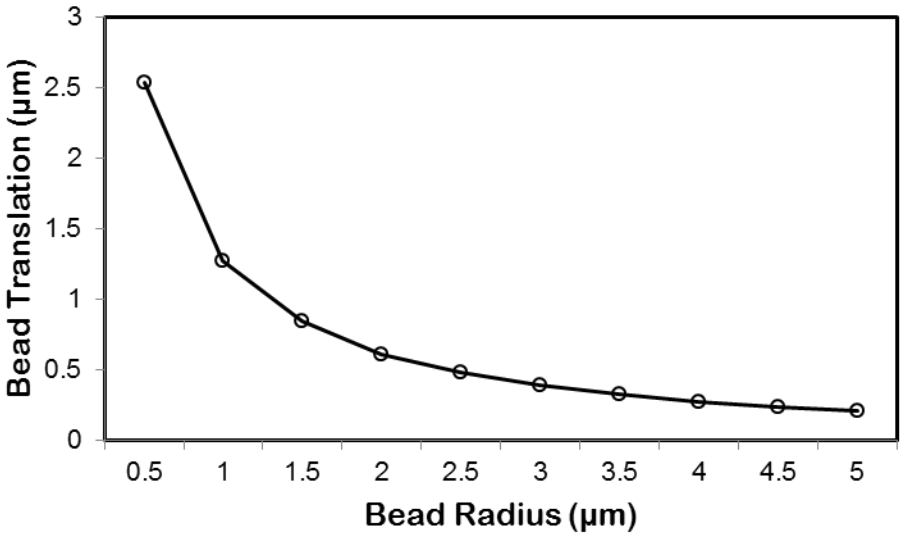

Figure 5.4. Influence of bead radius on bead center translation with cell height of 5μm and embedding angle of 35°.

5.3.5 Influence of Cell Height on Cell Mechanical Response

Figure 5.5 illustrates the influence of variation in the cell height (1 μm ≤ h_{cell} ≤ 5 μm) on the bead center translation for different bead radius (1.5 μm ≤ r_{bead} ≤ 4.5 μm). Based on the FEA results, increasing in cell height causes an increase in bead center translation for all cases; however, the rate of the increase depends on the bead radius. The bead center translation increases most significantly from h_{cell}=1 μm to 2 μm for all

cases, and especially so for the larger bead size. For example, this increase is <30% for r_{bead}=1.5 µm and 170% for r_{bead}=4.5 µm. The variation of the bead center translation for h_{cell} between 3 µm and 5 µm and r_{bead}=1.5 µm is <2%; however, it increases as the bead radius increases, e.g., <15% for r_{bead}=4.5 µm. Therefore, different cell heights cause variations in cell mechanical response. Moreover, the minimum variation is observed for r_{bead}=1.5 µm. Since measuring the cell height accurately needs sophisticated tools, the use of a smaller bead helps in decreasing the variation in cell responses. However, in order to simulate a cell by continuous models and considering the discrete nature of cell cytoskeletal proteins, the bead size needs to be considerably larger than the protein network mesh of (50-100 nm). Various studies have measured cell heights, and the results show that for epithelial cells, the height in all cases is over 5 µm, while it is 25.8 µm in average for prostate cancer cells [126], [127]. However, endothelial cell height is reported to be around 2.3 µm [128]. Therefore, the consideration of the variations in cell height is an important factor to consider when choosing the bead size to study cell mechanical responses using an OT.

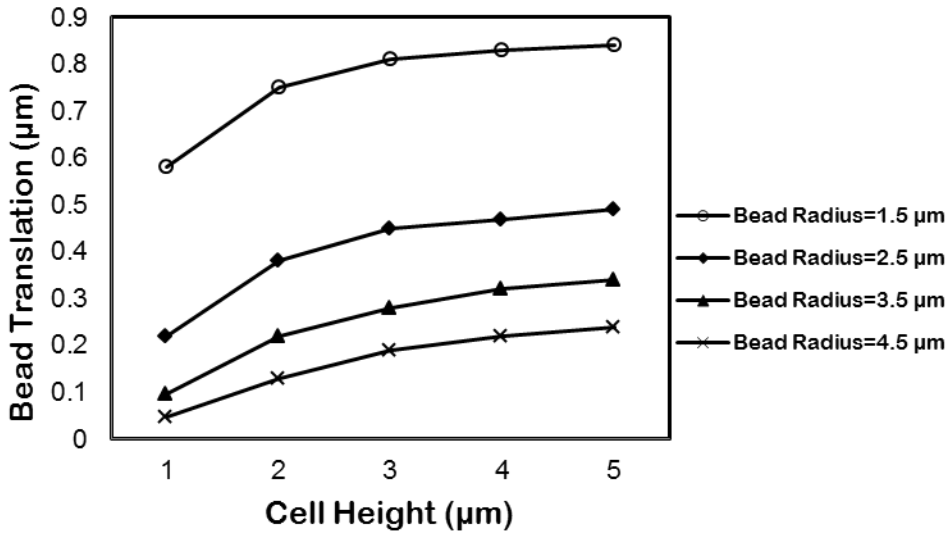

Figure 5.5. Influence of cell height and bead radius on bead center translation with embedding angle of 35°.

5.3.6 Influence of Embedding Angle on Cell Mechanical Response

The effect of variation in the bead-cell embedding angle on the bead center translation is shown in Fig. 5.6, for 16 different angles (15º≤φ≤85º). The results are illustrated for two different bead size: r_{bead}=1.5 and 2.5 μm. Increasing the embedding angle causes decreases in the bead center translation for all cases. However, there is no significant difference in the rate of the variation in the bead center translation between different bead radii. One factor that causes variability on the embedding angle during an OT experiment is that the contact surface between the bead and cell increases over time. In order to reduce this variation from one cell to other cells during an experiment, it is necessary to carry out the experiment on all cells in a short period of time.

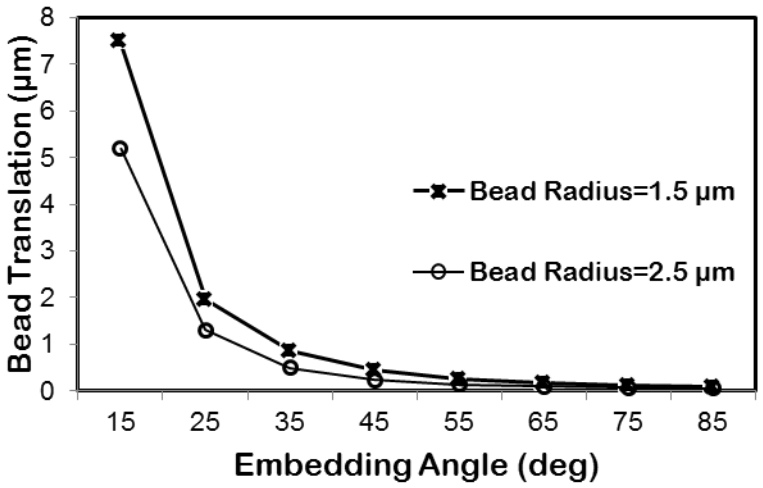

Figure 5.6. Influence of embedding angle on bead center translation with cell height of 5μm.

5.4 Conclusion

The proposed FEM, which is based on the power-law rheology, provides insights into the mechanical properties of cell cytoskeleton under time varying (i.e. oscillating)

mechanical stimuli. The model parameters were identified from oscillating OT experiments and were employed to study the structural dynamic behavior of LNCaP cells. A sensitivity analysis was performed via FEA to study the effects of the cell-bead geometry on cell mechanical responses. Bead radius, cell height and bead embedding angle variations on cell mechanical responses were considered. Conducting such a sensitivity study is important in evaluating the effect of varying cell-bead geometries on cell responses for different cell types in OT experiments.

Chapter 6

Conclusion

6.1 Summary

During this project we employed an OT to measure the mechanical properties of cells. Different numerical methods were used to simulate and analyze cells mechanical parameters. The main focus of this project was measuring alterations in cancer cell structure due to chemotherapy and cancer cell transformation using an OT. The key contributions of this dissertation can be summarized as follows:

1. Previous models were modified to develop a proper model for characterizing the mechanical properties of suspended cells under constant force. This will help to overcome the non-feasibility problem in the previous methods by taking into account the effect of (the) bending moment (Chapter 2 [70]).

2. A numerical model was optimized by reducing the number of free parameters for estimating key mechanical characteristics of suspended and adherent cells under cyclic force (Chapter 3 [71]).

3. The OT setup was optimized by adding an extra camera and applying video processing techniques to better analyze the OT results (Chapter 3 [71]).

4. We demonstrated quantitative indicators of therapeutic efficacy by establishing the relationship between the Jurkat cell' cytoskeleton stiffness and different

ART dosages, as well as indicating the effect of chemotherapy on cells' power-law coefficient (Chapter 3 [71]).

5. The connection between loss of Rb in hypoxic conditioned cells and increase of invasiveness was established using the combination of the OT and the numerical model. The results were verified by immunofluorescence microscopy (Chapter 4 submitted in oncogene).

6. The related signaling pathways that are activated in response to loss of Rb in hypoxia were identified using the combination of the OT and the numerical model. The results were verified by immunoblotting and immunofluorescence microscopy (Chapter 4 submitted in oncogene).

The outcome of this dissertation demonstrated the capability of employing an OT for measuring the efficacy of therapeutic agents on cancer cells by providing a quantitative indicator of their structural changes. The detailed summary of chapters 2-5 are described as follows:

6.1.1 Chapter 2: Constant Stretching

Acute lymphoid leukemia (ALL) is a type of blood cancer, which is characterized by the rapid proliferation of transformed lymphoblasts, and is the most common type of blood cancer in children [72]. Early treatment of the disease is essential, since the increased number of malignant cells could spill over into the blood stream and spread to other organs of the body. The most common treatment for leukemia is chemotherapy. Finding and analyzing the effectiveness of drugs with less toxicity on normal cells is indispensable for completely curing the cancer. Artesunate (ART) is an herbal compound which is conventionally used for malaria treatment. It also has anti-cancer effects, especially against leukemic cells (e.g., Jurkat cells–an immortalized line of human T lymphocyte cells) and colon cancer cells, as reported by the Developmental Therapeutics Program of the U.S. National Cancer Institute [129]. Previous studies have revealed the effect of ART on leukemia apoptosis, while having modest side effects on normal cells [130].

One report has suggested that exposing cells to pharmacological agents can cause membrane disorder changing its mechanical properties [131]. In Cai et al. [80], morphological changes of Jurkat cells exposed to ART were analyzed using AFM. Their results demonstrated that ART causes damage to the Jurkat cell membrane and changes the cell's mechanical properties, thus inhibiting cellular proliferation. Based on this report [80], analyzing the mechanical properties of the Jurkat cell membrane may serve as a useful biomarker to quantify the effectiveness of ART on leukemia as a chemotherapeutic agent.

In order to carry out a quantitative study of cell membrane mechanics, a numerical model is needed. In the literature, different mechanical models based on membrane theory have been developed to describe the biomechanical responses of cells. For instance, mechanical properties of microcapsules filled with liquid were analyzed by Carin et al. [73]. A variety of techniques have been used to experimentally characterize the response of suspended cells to mechanical loading. Mechanical characterization has been performed using two indentors or microinjection techniques to investigate suspended tomato cells [132] and zebra fish embryos at different developmental stages [133], respectively. Also, the effect of osmotic condition on red blood cells' (RBCs) mechanical properties was studied by Tan et al. [9] via mechanical modeling and manipulating the RBCs using OTs. The large deformation of a spherical membrane inflated by an incompressible fluid in contact with frictionless rigid conical indenter was analyzed by Sohail and Nadler [134]. As a more recent development, mechanical properties of human embryonic stem cells in cardiac differentiation were analyzed using OTs in Tan et al. [74]. In all of these studies, [73]- [74], the membrane theory is applied to model the mechanical properties of the cells. In membrane theory, the transverse tensions and bending moments are neglected for brevity, and only the in-plane stress resultants are retained in the analysis. However, the biological membrane's bending moment, which arises because of the non-uniform distribution of the stress over the cross section due to the external force, may have an effect on the accuracy and non-singularity of the model [75]. In this chapter, the more comprehensive shell theory is applied to determine the mechanical response of a suspended cell membrane, in order to account for any bending moments that may arise from the use of an OT in the mechanical characterization of the membrane of Jurkat cells.

To verify the accuracy of the model, an OT was employed. The OT is a powerful tool that can be employed to measure the mechanical characteristics of micron-sized objects by applying force and deformation on the order of picoNewtons (pN) and nanometers (nm), respectively. In this study, mechanical properties of Jurkat cells exposed to different dosages of ART are measured by a combination of OTs and a numerical model. Comparison of the results demonstrates the performance of the proposed model and the effectiveness of the OT to evaluate the effect of ART on cell membrane mechanical features.

6.1.2 Chapter 3: Cyclic Loading

Cytoskeletal proteins, inside the plasma membrane, are linked by molecular junctions which give the cell a complex and dynamic structure [135]. The cytoskeleton is responsible for cell growth, division, motility, and signaling, as well as the cell mechanical properties [136]. Since the cytoskeleton is the target of some anti-cancer drugs, these drugs can also influence mechanical integrity [137], [138]. As anti-cancer drugs stiffen the cancer cells [139], quantifying mechanical properties of cancer cells exposed to chemotherapy can provide insight into the mechanistic action of drugs on cells which is important from two points of view. First, biochemical changes within the cell due to chemotherapy-induced cell death, such as actin reorganization, can be related to and quantified by the mechanical changes in cells [91]. Therefore, measuring mechanical changes such as the magnitude of cell stiffness, allows for monitoring the drug effect [140]. Second, quantifying the deformability of cancer cells with respect to different dosages of chemotherapy can be helpful in further studying the vascular implications such as leukostasis that might arise from chemotherapy [139]. Therefore, mechanical characterization of cells may serve as an easier and faster quantitative indicator in evaluating therapeutic effect on cytoskeletal proteins, and also as a potential indicator for overall cell health, in comparison to biochemical fractionation and immunoblotting techniques.

The analysis of the drugs with less toxicity on normal cells is indispensable for curing the disease. Studying the effective concentration of drugs on different types of cancers has been extensively done at the biochemical and molecular levels [138], [141],

[142]. In order to combat cancer, an in-depth understanding of the dynamic functional processes such as cytoskeleton reorganization and mitotic changes are needed, which are available through both biochemical and mechanical cues. Therefore, integrating mechanical and physiological properties of cells can result in better understanding of the biophysical aspects of cancer. The relationship between variations in cell stiffness and loading frequency has been used to quantify the health or integrity of a cell and is described by power-law rheology [85]. Many cell types have been characterized using a variety of stimulation methods in the literature. For instance, mouse fibroblast cells were measured with an AFM [143], human bronchial epithelial cells were measured with AFM [144], kidney epithelial cells were measured with laser tracking microrheology [86], and mouse embryonal fibroblast cells were measured with a magnetic tweezer [145].

In this study, Jurkat cells, derived and immortalized from an acute lymphoid leukemia which is the most common type of blood cancer in children, was chosen as our demonstrative example [72]. Early treatment of the disease is essential, since the increased number of malignant cells could spread to other organs of the body. Previous studies have revealed the effect of Artesunate (ART) on Jurkat cell apoptosis, while having modest side effects on normal cells [130]. There is an established overall relationship between cytoskeletal structure and cell mechanics as well; ART has been suggested to effect the cytoskeleton of Jurkat cells [80]. Thus, we hypothesize that quantifying the changes in the mechanical properties of Jurkat cells following exposure to ART utilizing OTs and power-law rheology will provide the foundation for a new method of quantifying treatment efficacy. To accomplish this we defined a series of specific objectives as to 1) optimize an OT system to measure oscillation, 2) optimize a numerical model by reducing the number of free mechanical parameters, and 3) estimate key mechanical parameters by fitting the experimental data to the numerical model. The main contribution of this study is that, in our knowledge, it is the first work to apply the power-law theory to analyse alteration in mechanical properties of cancer cells exposed to a chemotherapeutic agent using oscillating OTs. Specifically, by establishing the relationship between the Jurkat cell mechanics and ART dosages, the effect of the chemotherapy on the cells' cytoskeleton stiffness and the power-law coefficient which can be quantitative indicators of therapeutic efficacy, is demonstrated.

6.1.3 Chapter 4: Hypoxia and Cell Structural Changes

In cancer and in particular, the tumor microenvironment, hypoxia is a pathological condition in which a significant region of tumor is deprived of adequate oxygen supply, which is associated with increased risk of metastasis [146] [147]. Invasion and metastasis are complex and life threatening processes that transform anchored cells into mobile cells. A critical step in cancer cell invasion and metastasis is cytoskeletal reorganization [148]. Recent studies on the effect of hypoxia on cell function revealed new information about the relationship between hypoxia and actin protein reorganization that underlies the invasive cancer cell phenotype [149] [150] [151] [152]. Modulation of actin organization under hypoxic conditions is complex and multiple pathways contribute to their alteration [153] [154] [155] [156] [157]. Elucidating different modulatory signaling pathways that alter actin organization and mediate the invasive cancer cell phenotype may prove a useful avenue for the development of novel anti-cancer therapeutic agents.

The hypoxic signal mediated by the HIF-1α-ARNT/HIF-1β transcriptional complex [158] induces expression of genes associated with advanced stages of tumor growth and metastasis [159] [160] [95][14-16]. The retinoblastoma protein (Rb) is a tumour suppressor protein that is associated with the HIF-1α-ARNT complex and is a key regulator of the hypoxic response [161]. Subsequently, loss of Rb function results in biochemical changes that promote invasiveness in cancer cells [93].

Studying different signaling pathways that modulate actin organization under hypoxia is possible via analyzing the biophysical properties of cancer cells and quantifying cytoskeleton rearrangement [118]. Extracellular signal-related kinase (ERK) and protein kinase B (AKT) signaling pathways are important intracellular regulators of cell growth, proliferation, and malignant transformation [162]. The ERK pathway plays an important role in actin organization and it can cause increase cell motility and invasiveness by directly targeting actin proteins [163][21]. Moreover, AKT signaling can influence cell migration by modulating actin as well [100]. Furthermore, the hypoxic signal mediated by the HIF-1α-ARNT transcriptional complex also causes expression of genes associated with tumor growth and metastasis. Gene ontogeny suggests that the

Rb-HIF1 complex mediates the ERK1/2, AKT and NFκB signaling pathways, and therefore, may result in actin impairment and reorganization [95].

Here we report cytoskeletal changes in human LNCaP prostate cancer cells that occur in response to loss of Rb under hypoxic stress using an oscillating OT (OT). LNCaP cells were selected as we have shown previously that hypoxia regulated Rb-knock-down cells are capable of undergoing neuroendocrine differentiation and adopting an invasive phenotype [95]. After interrogation of the LNCaP transcriptome in Rb knock-down cells, we have identified the top up and down regulated genes in LNCaP cells that are involved in metastasis and NED [95]. Nevertheless, we know little about actin structural changes and motile properties or the pathways that induce the invasive phenotype of Rb-ve LNCaP cells. In order to quantify the cytoskeletal remodeling and stiffness of control and Rb-ve LNCaP cells, movement of microbeads that bind to cell surface integrin receptors were measured.

6.1.4 Chapter 5: Sensitivity Studies using Finite Element Analysis

Cell mechanical properties are critical in a variety of cell functions such as spreading, contraction, crawling, and wound healing [164] [165] [166]. The central feature of cell mechanics is defined by their deformability. Previously, the relationship between variations in cell shear modulus and loading frequency, which can be modeled using power-law rheology, has been used to quantify the health or integrity of living cells [167]. The mechanical behavior of cells is an important quantitative measure for understanding the pathophysiological behavior of cells and evaluating the pharmacological treatments that modify the cell structure.

Mechanical characterization of different cell types has been performed by a variety of methods in the literature. For example, mouse fibroblast cells were explored with an AFM [168], human bronchial epithelial cells were studied by MTC [169], kidney epithelial cells were studied by laser tracking microrheology [170][7], and mouse embryonal fibroblast cells were tested with a magnetic tweezer [171]. OTs (OT) can measure mechanical properties of cells by applying force on a microbead attached to the

cell surface [70]. The relationship between the applied force and the lateral bead displacement can be used to determine the cells' shear moduli.

Previous studies showed that cell mechanical response may vary with bead radius, cell height, and bead embedding angle. Mijailovich et al. [124] computed the effect of three different cell heights (1, 5, 20 μm) on cell mechanical responses for a given bead radius of 4.5 μm. Their results showed a dependency of cell elastic modulus on cells height and bead embedding angle for MTC experiments. Ohayon et al. [172] established a correcting coefficient for cell elastic modulus to consider the effect of cell height, bead radius, and embedding angle based on MTC experimental results. Numerical simulation carried out by Karcher et al. [173] showed that cell heights of >5 μm have little effect on the cell mechanical properties related to MTC experiments [173]. Niu et al. [174] showed that, in order to accurately study cells mechanical properties using AFM, the effect of cell height and indentation depth of the probe should be considered [174]. These studies provide proof that considering the effect of geometrical parameters is important in order to increase the accuracy of such cell mechanical characterization experiments. Hence, since OT are another tool that is used for measuring cell mechanical properties, the results of the above sensitivity studies could be extended to cover the OT experiments.

In order to study the effect of variations in geometrical parameters on cell mechanical properties obtained from OT experiments, a finite element analysis (FEA) is carried out. In this chapter, a three-dimensional (3-D) finite element model (FEM) incorporating a power-law material model is applied to describe cell mechanical responses when the cytoskeleton is stimulated in oscillating OT experiments. A FEA is carried out to study different cell-bead geometries in order to analyze the sensitivity of cell mechanical responses on these parameters. The main contribution of this work lies in demonstrating the influence of cell-bead geometry on cell mechanical responses for oscillating OT experiments using FEA.

6.2 Recommendation for Future Work

Based on the current research and results that were obtained during this project, the following ideas may be considered as future work.

6.2.1 Technological Improvements

The current technology of OTs can be improved by combining with other spectroscopic and imaging techniques. For example, Raman spectroscopy which is an efficient and non-destructive technique that can be used to investigate changes at a molecular level. Therefore, combing the OT with Raman spectroscopy will help in identifying variations in cells molecules while manipulating cells mechanically or chemically. Fluorescence Resonance Energy Transfer microscopy (FREM) can be applied to investigate the precise location and nature of molecular interactions in living cells. Combining this technology with OT could be beneficial in investigating regenerative medicines. For example, molecular interactions that are critical for regulating stem cells functions can be monitored while a stem cell niche is being created using an OT. Advanced imaging technology such as multi photon microscopy, that provides a three-dimensional imaging, can be combined with the OT in order to enhance the capability of the OT in detecting manipulated cells images. For example cell height, cell-bead embedding angle and other geometrical parameters can be monitored precisely using such techniques.

Moreover, OTs can be easily combined with microfluidic devices. Culturing single cells in microfluidic devices would aid in producing more homogenous cell culture for manipulation experiments. Microfluidic devices in combination with OT can be applied to study how cells respond to their neighbouring cells, environment, pharmacological agents or mechanical stimuli. One more advantage of combining these two technologies is in increasing the cell sorting efficiency and throughput by employing multiple laser beams. Using pattern recognition algorithms, we can also automate particle detection and sorting in these technologies.

Holographic OTs can also be used in order to create three dimensional complex tissue structures. Creating such architecture is beneficial in detailed study of cellular

functions especially in the field of stem cells. Stem cells can be cultured and propagated in an environment that resembles their endogenous environment. Holographic OTs can be applied to place the stem cells, the nitche cell and the extracellular components at their functional locations so the connection and interaction between certain molecules would regulate stem cells functions.

6.2.2 Computational Improvements

A key direction for advancement in computational models lies in developing multiscale models. These models could be developed to characterize the combinational effect of molecular interactions, as well as cell layers, single cells or even tissue level mechanics. These models consider separate formulations for different length scales and the combination of these formulations would describe the chemical and mechanical responses of cells. The main challenge in developing such models is in coupling different length scales together.

Moreover, complex geometries and three dimensional loading could be considered for modeling more realistic cellular structure. Applying load at different cell locations and considering the variations in the cell's response at different cell locations would aid in providing models that represent cell heterogeneity.

A general model that can be applied for charactrizing mechanical responses of all types of cells under different experimental conditions, needs to be established. One step for establishing such a model is considering cell-bead geometrical parameters.. Based on our sensitivity study, the bead size affects the mechanical responses of cells; therefore, it is necessary to consider the effect of the bead radius on the computation model. Moreover, various cells have different cell heights and in order to increase the accuracy of the model, we need to consider the effect of the cell height. Cell-bead embedding angle is another parameter that is necessary to be applied to the computational model. Considering all these parameters in the computational model will increase the accuracy as well as providing a general paradigm that can be applied to analyze the response of different cell types.

References

[1] F. K. Glenister, "Contribution of parasite proteins toaltered mechanical properties of malaria-infected red blood cells," *Blood,* vol. 99, pp. 1060-1063, 2002.

[2] J. Mills, M. Diez-Silva, D. Quinn, M. Dao, M. Lang, K. Tan, C. Lim, G. Milon, P. David, M.-P. O., S. Bonnefoy and S. and Suresh, "Effect of plasmodial RESA protein on deformability of human red blood cells harboring Plasmodium falciparum," *PNAS,* vol. 104, no. 22, pp. 9213-9217, 2007.

[3] S. Suresh, "Biomechanics and biophysics of cancer cells," *Acta Biomater,* vol. 3, no. 4, pp. 413-438, 2007.

[4] W. R. Trickey, "Viscoelastic properties of chondrocytes from normal and osteoarthritic human cartilage," *J. Orthop. res.,* vol. 18, pp. 891-898, 2000.

[5] M. J. King, "Rapid flow cytometric test for the diagnosis of membrane cytoskeleton-associated haemolytic anaemia," *Br. J. Haematl.,* vol. 111, pp. 924-933, 2000.

[6] S. S. An, "Do biophysical properties of the airway amooth muscle in culture predict airway hyperresponsiveness?," *Cell Mol. Biol.,* vol. 35, pp. 55-64, 2006.

[7] J. Guck, "Optical deformability as inherent cell marker for testing malignant transformation and metastatic competence," *Biophys. J.,* vol. 88, pp. 3689-3698, 2005.

[8] M. Lekka, "Elasticity of normal and cancerous human bladder cells studied by scanning force microscopy," *Eur. Biophys.J.,* vol. 28, pp. 312-316, 1999.

[9] F. Wottawah, "Characterizing single suspended cells by optorheology," *Acta*

Biomater, vol. 1, pp. 263-271, 2005.

[10] B. Lincoln, H. Erickson, S. Schinkinger, F. Wottawah, D. Mitchell, S. Ulvick, C. Bilby and J. and Guck, "Deformability-Based Flow Cytometry," *Cytometry Part A,* vol. 59A, pp. 203-209, 2004.

[11] N. Wandersee, "Increased erythrocte adhesion in mice and humans with herditary spherocytosis and hereditary elliptocytosis," *Blood,* vol. 103, pp. 710-716, 2004.

[12] C. Lim, "Experimental techniques for single cell and single molecule biomechanics," *Mat. Sci. Eng.,* vol. C 26, pp. 1278-1288, 2006.

[13] J. P. Mills, "Nonlinear elastic and viscoelastic deformation of the human red blood cell with optical tweezers," *Mech.Chem. Biosyst,* vol. 1, pp. 169-180, 2004.

[14] S. Suresh, "Connection between single cell biomechanics and human disease: gastrointestinal cancer and malaria," *Acta Biomater,* vol. 1, pp. 15-30, 2005.

[15] M. M. Brandao, "Optical tweezers for measuring red blood cell elasticity: application to the study of drug response in sickle cell disease," *Eur. J. Hematol,* vol. 70, pp. 207-211, 2003.

[16] G. B. Nash, "Mechanical properties of oxygenated red blood cells in sicklecell disease," *Blood,* vol. 63, pp. 73-82, 1984.

[17] M. R. Clark, "Osmotic gradient ektocytometry: comprehensive characterization of red cell volume and surface maintenance," *Blood,* vol. 61, pp. 899-910, 1983.

[18] V. Lulevich, T. Zink, H. Y. Chen, F. T. Liu and G. Y. Liu, "Cell mechanics using atomic force microscopy-based single-cell compression," *Langmuir,* pp. 8151-8155, 2006.

[19] A. A. L. Weisenhorn, A. M. Khorsand, A. S. Kasas, A. V. Gotzos and A. H. Butt, "Deformation and height anatomy of soft surfaces studied with an AFM," *Nanotechnology,* pp. 106-113, 1993.

[20] Y. Rabinovich, M. Esayanur, S. Daosukho, K. Byer, H. El-Shall and S. Khan, "Atomic force microscopy measurement of the elastic properties of the kidney epithelial cells," *Journal of Colloid and Interface Science,* pp. 125-135, 2005.

[21] M. Radmacher, "Measuring the elastic properties of biological samples with the AFM," *IEEE Engineering in Medicine and Biology Magazine,* pp. 47-57, 1997.

[22] M. Lekka, P. Laidler, D. Gil, J. Lekki, Z. Stachura and A. Z. Hrynkiewicz, "Elasticity of normal and cancerous human bladder cells studied by scanning force microscopy," *European Biophysical Journal,* pp. 312-316, 1999.

[23] J. Guck, R. Ananthakrishnan, T. J. Moon, C. C. Cunningham and J. Kas, "Optical deformability of soft biological dielectrics," *Physical Review Letters,* pp. 5451-5454, 2000.

[24] J. Guck, R. Ananthakrishnan, H. Mahmood, T. J. Moon, C. C. Cunningham and J. Kas, "The optical stretcher: a novel laser tool to micromanipulate cells," *Biophysical Journal,* pp. 767-784, 2001.

[25] J. Guck, S. Schinkinger, B. Lincoln, F. Wottawah, S. Ebert, M. Romeyke, D. Lenz, H. M. Erickson, R. Ananthakrishnan, D. Mitchell, J. Kas, S. Ulvick and C. Bilby, "Optical deformability as an inherent cell marker for testing malignant transformation and metastatic competence," *Biophysical Journal,* pp. 3689-3698, 2005.

[26] T. W. Remmerback, F. Wottawah, J. Dietrich, B. Lincoln, C. Wittekind and J. Guck, "Oral cancer diagnosis by mechanical phenotyping," *Cancer Research,* pp. 1728-1782, 2009.

[27] N. Mohandas and E. Evans, "Mechanical properties of the red cell membrane in relation to molecular structure and genetic defects," *Annual Review of Biophysics and Biomolecular Structure,* pp. 787-818, 1994.

[28] J. Y. Shao and J. B. Xu, "A modified micropipette aspiration technique and its application to tether formation from human neutrophils," *ASME Journal of Biomechanical Engineering,* pp. 388-396, 2002.

[29] R. M. Hochmuth, "Micropipette aspiration of living cells," *Journal of Biomechanics,* pp. 15-22, 2000.

[30] S. C. Tan, W. X. Pan, G. Ma, N. Cai, K. W. Leong and K. Liao, "Viscoelastic behavior of human mesenchymal stem cells," *BMC Cell Biology,* pp. 40-46, 2008.

[31] F. H. C. Crick and A. F. W. Hughes, "The physical properties of cytoplasm: a study by means of the magnetic particle method. Part I. Experimental," *Experimantal Cell Research,* pp. 37-80, 1950.

[32] F. Ziemann, J. Radler and E. Sachmann, "LOcal Measurements of viscoelastic moduli of entangled actin networks using an oscillating magnetic bead micro-rheometer," *Biophysical Journal,* pp. 2210-2216, 1994.

[33] M. Puig-de-Morales-Marinkovic, K. T. Turner, J. P. Butler, J. J. Fredberg and S. Suresh, "Viscoelasticity of the human red blood cells," *American Journal of Physiology-Cell Physiology,* pp. 597-605, 2007.

[34] N. Wang and D. E. Ingber, "Probing transmembrane mechanical coupling and cytomechanics using magnetic twisting cytometry," *Biochemistry and Cell Biology,* pp. 327-335, 1995.

[35] D. J. Ashkin A, "Optical trapping and manipulation of viruses and bacteria.," *Science Classic, Vol. 235 no. 4795,* pp. 1517-20, 1987.

[36] A. Ashkin, J. Dziedzic, J. Bjorkholm and S. Chu, "Observation of a single-beam gradient force optical trap for dielectric particles," *Optical Letter,* pp. 288-290, 1986.

[37] Y. Tan, D. Sun, J. Wang and W. Huang, "Mechanical Characterization of Human Red Blood Cells Under Different Osmotic Conditions by Robotic Manipulation With Optical Tweezers," *IEEE Transactions On Biomedical Engineering,* pp. 1816-1826, 2010.

[38] Y. Li, C. Wen, H. Xie, A. Ye and Y. Yin, "Mechanical Property Analysis of Stored Red Blood Cell Using Optical Tweezers," *Biointerfaces, 70,* pp. 169-173, 2009.

[39] G. Liao, P. Bareil, Y. Sheng and A. Chiou, "One-dimensional jumping optical tweezers for optical stretching of bi-concave human Red Blood CElls," *Opt. Expr,* pp. 1996-2004, 2008.

[40] A. Fontes, H. Fernandes, A. Thomaz Luiz, C. Barbosa and M. C. C. Barjas-Castro, "Measuring electrical and mechanical properties of Red Blood Cells with Double Optical Tweezers," *Journal of Biomedical Optics,* 2008.

[41] L. M. Walker, A. Holm, L. Cooling, L. Maxwell, A. Oberg, T. Sundqvist and A. El Haj, "Mechanical manipulation of bone and cartilage cells with optical tweezers," *FEBS Lett.,* pp. 39-42, 1999.

[42] J. L. Nascimento, E. L. Botvinick, L. Z. Shi, B. Durrant and M. W. Berns, "Analysis of Sperm Motility Using Optical Tweezers," *Biomed. Opt., 11,* pp. 044 001-044 008, 2006.

[43] N. Askenansy and D. Farkas, "Optical imaging of PKH labeled hematopoietic cells in recipient bone marrow in vivo," *Stem Cells,* pp. 501-513, 2002.

[44] H. Miyoshi, T. Sugiura and K. Minato, "Cell Palpation System Based on a Force Measurement by Optical Tweezers for Investigation of Local Mechanical Properties of a Cell Membrane," *Japanese Journal of Applied Physics, 48,* pp. 120223-120223-3, 2009.

[45] L. Jauffred, T. H. Callisen and L. B. Oddershede, "Viscoelastic membrane tethers extracted from Escherichia coli by optical tweezers," *Biophysics,* vol. 93, p. 4068–4075, 2007.

[46] K. Wang, J. Cheng, S. Cheng and D. Sun, "Probing cell biophysical behavior based on actin cytoskeleton modeling and stretching manipulation with optical tweezers," *Applied physics letters,* vol. 103, pp. 083706-1-4, 2013.

[47] R. Satcher and C. Dewey, "Theoretical estimates of mechanical properties of the endothelial cell cytoskeleton," *Biophysical Journal,* pp. 109-118, 1996.

[48] D. Stamenovic and D. Ingber, "Models of cytoskeletal mechanics of adherent cells," *Biomechanics and Modeling in Mechanobiology,* pp. 95-108, 2002.

[49] D. Stamenovic and M. Coughlin, "The role of prestress and architecture of the cytoskleton and deformability of cytoskeletal filaments in mechanics of adherent cells: a quantitative analysis," *Journal of Theoretical Biology,* pp. 63-74, 1999.

[50] R. De, A. Zemel and S. and Safran, "Theoretical concepts and Models of Cellular Mechanosensing," *Methods Cell Biol.,* vol. 98, pp. 143-175, 2010.

[51] A. Zemel, I. B. Bischofs and S. A. and Safran, "Active Elasticity of Gels with Contractile Cells," *Phys. Rev. Lett.,* vol. 97, no. 12, p. 128103, 2006.

[52] A. Mogilner and L. and Edelstein-Keshet, "Regulation of Actin Dynamics in Rapidly Moving Cells: A Quantitative Analysis," *Biophys. J.,* vol. 83, no. 3, pp. 1237-1258, 2002.

[53] R. Kaunas and H. J. ans Hsu, "A Kinematic Model of Stretch-Induced Stress Fiber Turnover and Reorientation," *J. Theor. Biol.,* vol. 257, no. 2, pp. 320-330, 2009.

[54] R. Kaunas and S. and Deguchi, "Multiple Roles for Myosin II in Tensional Homeostasis Under Mechanical Loading," *Cell. Mol. Bioeng.,* vol. 4, no. 2, pp. 182-191, 2011.

[55] F. J. Vernerey and M. and Farsad, "A Constrained Mixture Approach to Mechano-Sensing and Force Generation in Contractile Cells," *J. Mech. Behav. Biomed. Mater.,* vol. 4, no. 8, pp. 1683-1699, 2011.

[56] A. Yeung and E. Evans, "Cortical shell-liquid core model for passive flow of liquid-like spherical cells into micropipets," *Biophysical Journal,* pp. 139-149, 1989.

[57] C. Dong, R. Skalak and K. L. Sung, "Cytoplasmic rheology of passive neutrophils," *Biorhelogy,* pp. 557-567, 1991.

[58] R. Hotchmuth, H. Ting-Beall, B. Beaty, D. Needham and R. Tran-Son-Tay, "Viscosity of passive human neutrophilsundergoing small deformations," *Biophysical Journal,* pp. 1596-1601, 1993.

[59] M. A. Tsai, R. S. Frank and R. E. Waugh, "Passive mechanical behavior of human neutrophils: power-law fluid," *Biophysical Journal,* pp. 2078-2088, 1993.

[60] C. Dong, R. Skalak, K. L. Sung, G. W. Schmid-Schonbein and S. Chien, "Passive deformation analysis of human leukocytes," *Journal of Biomechanical Engineering,* pp. 27-36, 1988.

[61] G. W. Schmid-Schonbein, K. L. Sung, H. Tozeren, R. Skalak and S. Chien, "Passive mechanical properties of human leukocytes," *Biophysical Journal,* pp. 243-256, 1981.

[62] D. P. Theret, M. J. Levesque, M. Sato, R. M. Nerem and L. T. Wheeler, "The application of a homogeneous half-space model in the analysis of endothelial cell micropipette measurements," *Journal of Biomechanical Engineering,* pp. 190-199, 1988.

[63] G. N. Maksym, B. Fabry, J. P. Butler, D. Navajas, D. Tschumperlin, J. Laporte and J. Fredberg, "Mechanical properties of cultured human airway smooth muscle cells from 0.05 to 0.4 Hz," *Journal of Applied Physiology,* pp. 1619-1632, 2000.

[64] J. Alcaraz, L. Buscemi, M. Grabulosa, X. Trepat, B. Fabry, R. Farre and D. Navajas, "Microrheology of human lung epithelial cells measured by atomic force microscopy," *Biophysical Journal,* pp. 2071-2079, 2003.

[65] M. Wei, A. Zaorski, H. Yalcin, J. Wang, M. Hallow, S. Ghadiali, A. Chiou and D. Yang, "A comparative study of living cell micromechanical properties by oscillatory optical tweezers," *OPTICS EXPRESS,* vol. 16, no. 12, pp. 8594-8603, 2008.

[66] B. Fabry, G. Maksym, J. Butler, M. Glogauer, D. Navajas and J. Fredberg, "Scaling the microrheology of living cells," *Physical Review Letters,* 2001.

[67] B. Fabry, G. Maksym, J. Butler, M. Glogauer, D. Navajas, N. Taback, E. Millet and J. Fredberg, "Time scale and other invariants of integrative mechanical behavior in living cells," *Physical Review E,* 2003.

[68] J. Leterrier, "Water and cytoskeleton," *Cell and Molecular Biology (Noisy-le-grand),* pp. 901-923, 2001.

[69] V. Mow, S. Kuei, W. Lai and C. Armstrong, "Biphasic creep and stress relaxation of articular cartilage in compression? Theory and experiments.," *Journal of Biomechanical Engineering,* pp. 73-84, 1980.

[70] S. Khakshour, T. Beischlag, C. Sparrey and E. and Park, "Mechanical characterization of ART-treated Jurkat cells using optical tweezers," in *Proc IEEE EMBC*, Chicago, 2014.

[71] S. Khakshour, T. Beischlag, C. Sparrey and E. Park, "Probing mechanical properties of jurkat cells under the effect of ART using oscillating optical tweezers," *PLoS ONE,* vol. 10, no. 4, p. e0126548, 2015.

[72] A. Jemal, R. Siegel, E. Ward, T. Murray, J. Xu and M. Thun, "Cancer statistics," *CA. Cancer J. Clin.,* vol. 57, no. 1, pp. 43-66, 2007.

[73] M. Carin, D. B-Biesel, F. E-levy, C. Postel and a. D. C. Andrei, "Compression of of biocompatible liquid-filled HSA-Alginate capsules: determination of the membrane mechanical properties," *Biotechnology and Bioengineering,* vol. 82, pp. 207-212, 2003.

[74] Y. Tan, C. Kong, S. Chen, S. H. Cheng, R. Li and D. Sun, "Probing the mechanobiological properties of human embryonic stem cells in cardiac differentiation by optical tweezers," *JournalofBiomechanics,* vol. 45, pp. 123-128, 2012.

[75] C. Pozrikidis, "Deformed shapes of axisymmetric capsules enclosed by elastic membranes," *Journal of Engineering Mathematics,* vol. 45, pp. 169-182, 2003.

[76] V. Novozhilov, Thin shell theory, Groningen: P. Noordhoff, 1964.

[77] Y. Tan, D. Sun, W. Huang and S. H. Cheng, "Mechanical Modeling of Biological Cells in Microinjection," *IEEE Transactions On Nanobioscience,* pp. 257-267, 2008.

[78] K. Svoboda and a. S. Block, "Biological applications of optical forces," *Annual Review of Biophysics and Biomolecular Structure,* vol. 23, pp. 247-285, 1994.

[79] K. Asami, Y. Takahashi and S. Takashima, "Dielectric properties of mouse lymphocytes erythrocytes," *Biochim Biophys Acta.,* vol. 1010, no. 1, pp. 49-55, 1989.

[80] X. Cai, S. Gao, J. Cai, Y. Wu and a. H. Deng, "Artesunate induced morphological and mechanical changes of jurkat cell studied by AFM," *Scanning,* vol. 31, pp. 83-89, 2009.

[81] J. H. Baek, S. U. Hwang and a. Y. G. Lee, "Trap Stiffness in Optical Tweezers," in *Asian Symposium for precision Engineering and Nanotechnology*, 2007.

[82] K. C. Neuman and a. S. M. Block, "Optical Trapping," *Review of Scientific Instrument,* vol. 75, pp. 2787-2809, 2004.

[83] W. K. Purves, G. H. Orians and H. R. Heller, Life: The Science of Biology, Sinauer Associates Inc, 1994.

[84] H. Miyoshi, T. Sugiura and a. K. Minato, "Cell Palpation System Based on a Force Measurement by Optical Tweezers for Investigation of Local Mechanical Properties of a Cell Membrane," *Japanese Journal of Applied Physics,* vol. 48, pp. 1-3, 2009.

[85] B. Fabry, G. N. Maksym, J. P. Butler, M. Glogauer, D. Navajas, N. A. Taback, E. J. Millet and a. J. J. Fredberg, "Time Scale and other invariants of integrative mechanical behvior in living cells," *Physical Review,* vol. 68, pp. 1-18, 2003.

[86] S. Yamada, D. Wirtz and a. S. C. Kuo, "Mechanics of Living Cells Measured by Laser Tracking Microrheology," *Biophysical Journal,* vol. 78, pp. 1736-1747, 2000.

[87] S. G. Shroff and D. R. Saner, "Dynamic Micromechanical Properties of Cultured Rat Artial Myocytes Measured by Atomic Force Microscopy," *American Journal of Physiology,* vol. 269, pp. 286-292, 1995.

[88] W. H. Goldmann and R. M. Ezzell, "Viscoelasticity in Wild-Type and Vinculin-Deficient (5.51) Mouse F9 Embryonic Carcinome Cells Examined by Atomic Force Microscopy and Rheology," *Experimental Cell Research,* vol. 226, no. 1, pp. 234-237, 1996.

[89] G. N. Maksym, B. Fabry, J. P. Butler, D. Navajas, D. J. Tschumperlin, J. D. Laporte and a. J. J. Fredberg, "Mechanical Properties of Cultured Human Airway Smooth Muscle Cells From 0.05 to 0.4 Hz," *Applied Physiology,* vol. 89, pp. 1619-1632, 2000.

[90] L. Li, H. Zhang, S. Yuan, Z. Tian, L. Wang and a. Z. Sun, "Artesunate attenuates the growth of human colorectal carcinoma and inhibits hyperactive Wnt/beta-catenin pathway," *Int. J. Cancer,* vol. 121, pp. 1360-1365, 2007.

[91] A. Grzanka, D. Grzanka and M. Orlikowska, "Cytoskeletal Reorganization during process of apoptosis induced by cytostatic drugs in K-562 and HL-60 Leukemia Cell Lines," *Biochemical Pharmacology,* vol. 66, pp. 1611-1617, 2003.

[92] M. Levee, M. Dabrowska, J. Lelli and D. Hinshaw, "Actin polymerization and depolymerization during apoptosis in HL-60 cells," *American Journal of Physiology,* vol. 271, pp. 1982-1992, 1996.

[93] M. Labrecque, M. Takhar, J. Jagdeo, K. Tam, C. Chiu, T. Wang, G. Prefontaine, M. Cox and T. and Beischlag, "A TRIP230-retinoblastoma protein complex regulates hypoxia-inducible factor-1alpha-mediated transcription and cancer cell invasion.," *PLoS One,* vol. 9, p. e992, 2014.

[94] G. Soni, B. Ali, Y. Hatwalne and G. and Shivashankar, "Single particle tracking of correlated bacterial dynamics.," *Biophys J ,* vol. 84, pp. 2634-7, 2003.

[95] M. Labrecque, M. Takhar, R. Nason, S. Santacruz, K. Tam, S. Massah, A. Haegert, R. Bell, M. Altamirano-Dimas, C. Collins, F. Lee, G. Prefontaine, M. Cox and T. and Beischlag, "The retinoblastoma protein regulates hypoxia-inducible genetic programs, tumor cell invasiveness and neuroendocrine differentiation in prostate cancer cells.," *Oncotarget,* 2016.

[96] Z. Fan, C. Li, C. Qin, L. Xie, X. Wang, Z. Gao, W. T. Qiangbacuozhen, L. Yu and H. and Liu, "Role of the PI3K/AKT pathway in modulating cytoskeleton rearrangements and phenotype switching in rat pulmonary arterial vascular smooth muscle cells.," *DNA Cell Biol,* vol. 33, pp. 9-12, 2014.

[97] Y. Gan, C. Shi, L. Inge, M. Hibner, J. Balducci and Y. and Huang, "Differential roles of ERK and Akt pathways in regulation of EGFR-mediated signaling and motility in prostate cancer cells.," *Oncogene,* vol. 29, pp. 4947-58, 2010.

[98] D. Dworakowska, E. Wlodek, C. Leontiou, S. Igreja, M. Cakir, M. Teng, N. Prodromou, M. Goth, S. Grozinsky-Glasberg, M. Gueorguiev, B. Kola, M. Korbonits and A. and Grossman, "Activation of RAF/MEK/ERK and PI3K/AKT/mTOR pathways in pituitary adenomas and their effects on downstream effectors.," *Endocr Relat Cancer,* vol. 16, pp. 1329-38, 2009.

[99] M. Edwards, J. Aultman, G. Harber, J. Bhatt, E. Sztul, Q. Xu, P. Zhang, S. Michalek and J. and Katz, "Role of mTOR downstream effector signaling molecules in Francisella tularensis internalization by murine macrophages.," *PLoS One 8,* vol. 8, p. e83226, 2013.

[100] H. Irie, R. Pearline, D. Grueneberg, M. Hsia, P. Ravichandran, N. Kothari, S. Natesan and J. and Brugge, "Distinct roles of Akt1 and Akt2 in regulating cell migration and epithelial-mesenchymal transition.," *J Cell Biol ,* vol. 171, pp. 1023-34, 2005.

[101] I. Mavrommati, O. Cisse, M. Falasca and T. and Maffucci, "Novel roles for class II Phosphoinositide 3-Kinase C2beta in signalling pathways involved in prostate cancer cell invasion.," *Sci Rep,* vol. 6, p. 23277, 2016.

[102] S. Aggarwal, M. Singh, A. Kumar and T. and Mukhopadhyay, "SRD5A2 gene expression inhibits cell migration and invasion in prostate cancer cell line via F-actin reorganization.," *Mol Cell Biochem,* vol. 408, pp. 15-23, 2015.

[103] Y. Ahn, I. Shin, J. Kim, Y. Kim, C. Lee, S. Ju and W. and An, "Counteracting the activation of pAkt by inhibition of MEK/Erk inhibition reduces actin disruption-mediated apoptosis in PTEN-null PC3M prostate cancer cell lines.," *Oncol Lett,* vol. 6, pp. 1383-1389, 2013.

[104] G. Pawlak and D. and Helfman, "MEK mediates v-Src-induced disruption of the actin cytoskeleton via inactivation of the Rho-ROCK-LIM kinase pathway.," *J Biol Chem,* vol. 277, pp. 26927-33, 2002.

[105] A. Singh, S. Joshi, E. George and D. and Durden, "Anti-tumor effect of a novel PI3-kinase inhibitor, SF1126, in (12) V-Ha-Ras transgenic mouse glioma model.," *Cancer Cell Int ,* vol. 14:105, 2014.

[106] F. Xu, S. Ito, M. Hamaguchi and T. and Senga, "Disruption of cell spreading by the activation of MEK/ERK pathway is dependent on AP-1 activity.," *Nagoya J Med Sci,* vol. 72, pp. 139-44, 2010.

[107] S. Yu, X. Cai, C. Wu, L. Wu, Y. Wang, Y. Liu, Z. Yu, S. Qin, F. Ma, J. Thiery and L. and Chen, "Adhesion glycoprotein CD44 functions as an upstream regulator of a network connecting ERK, AKT and Hippo-YAP pathways in cancer progression.," *Oncotarget,* vol. 6, pp. 2951-65, 2015.

[108] D. Chen, Y. Xia, K. Zuo, Y. Wang, S. Zhang, D. Kuang, Y. Duan, X. Zhao and G. and Wang, "Crosstalk between SDF-1/CXCR4 and SDF-1/CXCR7 in cardiac stem cell migration.," *Sci Rep,* vol. 5, p. 16813, 2015.

[109] E. Niba, H. Nagaya, T. Kanno, A. Tsuchiya, A. Gotoh, C. Tabata, K. Kuribayashi, T. Nakano and T. and Nishizaki, "Crosstalk between PI3 kinase/PDK1/Akt/Rac1 and Ras/Raf/MEK/ERK pathways downstream PDGF receptor.," *Cell Physiol Biochem,* vol. 31, pp. 905-13, 2013.

[110] C. Yu, Z. Liu and L. and Cantley, "ERK negatively regulates the epidermal growth factor-mediated interaction of Gab1 and the phosphatidylinositol 3-kinase.," *J Biol Chem,* vol. 277, pp. 19382-8, 2002.

[111] K. Moelling, K. Schad, M. Bosse, S. Zimmermann and M. and Schweneker, "Regulation of Raf-Akt Cross-talk," *J Biol Chem,* vol. 277, pp. 31099-106, 200.

[112] T. Kodaki, R. Woscholski, B. Hallberg, P. Rodriguez-Viciana, J. Downward and P. and Parker, "The activation of phosphatidylinositol 3-kinase by Ras.," *Curr Biol ,* vol. 4, pp. 798-806, 1994.

[113] R. Zoncu, A. Efeyan and D. and Sabatini, "mTOR: from growth signal integration to cancer, diabetes and ageing.," *Nat Rev Mol Cell Biol ,* vol. 12, pp. 21-35, 2011.

[114] S. Cho, Y. Wang, M. Rodriguez, K. Tan, W. Zhang, J. Luo, D. Li and M. and Liu, "Haploinsufficiency in the prometastasis Kiss1 receptor Gpr54 delays breast tumor initiation, progression, and lung metastasis.," *Cancer Res,* vol. 71, pp. 6535-46, 2011.

[115] D. Cvetkovic, M. Dragan, S. Leith, Z. Mir, H. Leong, M. Pampillo, J. Lewis, A. Babwah and M. and Bhattacharya, "KISS1R induces invasiveness of estrogen receptor-negative human mammary epithelial and breast cancer cells.," *Endocrinology ,* vol. 154, pp. 1999-2014, 2013.

[116] M. Pampillo, N. Camuso, J. Taylor, i. J. Szereszewsk, M. Ahow, M. Zajac, R. Millar, M. Bhattacharya and A. and Babwah, "Regulation of GPR54 signaling by GRK2 and {beta}-arrestin.," *Mol Endocrinol ,* vol. 23, pp. 2060-74, 2009.

[117] C. Goertzen, M. Dragan, E. Turley, A. Babwah and M. and Bhattacharya, "KISS1R signaling promotes invadopodia formation in human breast cancer cell via beta-arrestin2/ERK.," *Cell Signal,* vol. 28, pp. 165-76, 2016.

[118] S. An, C. Pennella, A. Gonnabathula, J. Chen, N. Wang, M. Gaestel, P. Hassoun, J. Fredberg and U. and Kayyali, "Hypoxia alters biophysical properties of endothelial cells via p38 MAPK- and Rho kinase-dependent pathways.," *Am J Physiol Cell Physiol,* vol. 289, pp. C521-30, 2005.

[119] M. Coughlin and J. and Fredberg, "Changes in cytoskeletal dynamics and nonlinear rheology with metastatic ability in cancer cell lines.," *Phys Biol ,* vol. 10, p. 065001, 2013.

[120] A. Hesse, E. Levent, A. Zieseniss, M. Tiburcy, W. Zimmermann and D. and Katschinski, " Lights on for HIF-1alpha: genetically enhanced mouse cardiomyocytes for heart tissue imaging.," *Cell Physiol Biochem ,* vol. 34, pp. 455-62, 2014.

[121] J. Wang, Z. Wan, W. Liu, L. Li, L. Ren, X. Wang, P. Sun, L. Ren, H. Zhao, Q. Tu, Z. Zhang, N. Song and L. and Zhang, "Atomic force microscope study of tumor cell membranes following treatment with anti-cancer drugs.," *Biosens Bioelectron ,* vol. 25, pp. 721-7, 2009.

[122] E. Dreaden, Y. Kong, S. Morton, S. Correa, K. Choi, K. Shopsowitz, K. Renggli, R. Drapkin, M. Yaffe and P. and Hammond, "Tumor-Targeted Synergistic Blockade of MAPK and PI3K from a Layer-by-Layer Nanoparticle.," *Clin Cancer Res,* vol. 21, pp. 4410-9, 2015.

[123] C. Vogel, M. Smit, G. Maddalo, P. Possik, R. Sparidans, S. vander Burg, E. Verdegaal, A. Heck, A. Samatar, J. Beijnen, A. Altelaar and D. and Peeper, "Cooperative induction of apoptosis in NRAS mutant melanoma by inhibition of MEK and ROCK.," *Pigment Cell Melanoma Res ,* vol. 28, pp. 307-17, 2015.

[124] S. Mijailovich, M. Kojic, M. Zivkovic, B. Fabry and J. and Fredberg, "A finite

element model of cell deformation during magnetic bead twisting," *J. Appl. Physiol.,* vol. 93, pp. 1429-36, 2002.

[125] S. Khakshour, T. Beischlag, C. Sparrey and E. and Park, "Probing mechanical properties of Jurkat cells under the effect of ART using oscillating optical tweezers," *PLoS One,* vol. 10, p. e0126548, 2015.

[126] W. Driessche, P. Smet and G. and Raskin, "An automatic monitoring system for epithelial cell height," *European Journal of Physiology,* vol. 425, pp. 164-171, 1993.

[127] G. Gonzales, S. Miranda, J. Nieto, G. Fernandez, S. Yucra, J. Rubio, P. Yi and M. and Gasco, "Red maca (Lepidium meyenii) reduced prostate size in rats," *Reprod. Biol. Endocrinol.,* vol. 3(5), 2005.

[128] S. Liu, M. Yen and Y. and Fung, "On measuring the third dimension of cultured endothelial cells in shear flow," *Proc. Natl. Acad. Sci.,* vol. 91, pp. 8782-86, 1994.

[129] T. Efferth, H. Dunstan, A. Sauerbrey, H. Miyachi and C. Chitambar, "The anti-malarial artesunate is also active against cancer," *Int. J. Oncol,* vol. 18, no. 4, pp. 763-773, 2001.

[130] T. Efferth, M. Giaisi, A. Merling, P. Krammer and a. A. M. Li-Weber, "Artesunate induces ROS-mediated apoptosis in doxorubicin-resistant T leukemia cells," *PLOS One,* vol. 2, no. 8, pp. 693-693, 2007.

[131] D. Goldstein., "The effects of drugs on membrane fluidity," *Ann. Rev. Pharmacol. Toxicol.,* vol. 24, pp. 43-64, 1984.

[132] C. X. Wang, L. Wang and a. C. R. Thomas, "Modeling the mechanical properties of single suspension-cultured tomato cells," *Annals of Botany,* vol. 93, pp. 443-453, 2004.

[133] Y. Tan, D. Sun, W. Huang and S. H. Cheng, "Mechanical modeling of biological cells in microinjection," *IEEE Transactions On Nanobioscience,* pp. 257-267, 2008.

[134] T. Sohail and B. Nadler, "On the Contacr of an inflated spherical membrane-fluid

structure with a rigid conical indenter," *Acta Mech,* pp. 225-235, 2011.

[135] B. Alberts, A. Johnson, J. Lewis, M. Raff, K. Roberts and P. Walter, Molecular Biology of the Cell, New York: Garland Science, 2007.

[136] D. A. Fletcher and R. D. Mullins, "Cell mechanics and the cytoskeleton," *Nature,* vol. 463, pp. 485-492, 2010.

[137] M. A. Jordan and L. Wilson, "Microtubules and actin filaments: dynamic targets for cancer chemotherapy," *Current Opinion in Cell Biology,* vol. 10, no. 1, pp. 123-130, 1998.

[138] V. M. Esteban, D. Charron, C. Gelin and a. N. Mooney, "Chemotherapeutic Agents Targeting the Tubulin Cytoskeleton Modify LPS-induced Cytokine Secretion by Dendritic Cells and Increase Antigen Presentation," *Immunather,* vol. 33, pp. 364-370, 2010.

[139] W. A. Lam, M. J. Rosenbluth and D. A. Fletcher, "Chemotherapy Exposure Increase Leukemia Cell Stiffness," *Neoplasia,* vol. 109, pp. 3505-3508, 2007.

[140] S. C. Wuang, B. Ladoux and C. T. Lim, "Probing the Chemo-Mechanical Effect of an Anti-Cancer Drug Emodin on Brast Cancer Cells," *Cellular and Molecular Bioengineering,* vol. 4, no. 3, pp. 466-475, 2011.

[141] J. R. Stehn, N. K. Haass and T. Bonello, "A Novel Class of Anticancer Compounds Targets the Actin Cytoskeleton in Tumor Cells," *Cancer Research,* vol. 73, pp. 5169-5182, 2013.

[142] P. Knudsen, B. Hanna, S. Ohl, L. Sellner, T. Zenz, H. Dohner, S. Stilgenbauer, T. Larsen, P. Lichter and a. M. Seiffert, "Chaetoglobosin A Preferentially Induces Apoptosis in Chronic Lymphocytic Leukemia Cells by Targeting the Cytoskeleton," *Leukemia,* vol. 28, pp. 1289-1298, 2014.

[143] P. G. Cai, Y. Mizutani, M. Tsuchiya, J. M. Maloney, B. Fabry and K. J. V. Vliet, "Quantifying cell-to-cell Variation in Power-Law Rheology," *Biophysical Journal,* vol. 105, pp. 1093-1102, 2013.

[144] M. Puing-De-Morales, M. Grabulosa, J. Alcaraz, J. Mullol, G. N. Maksym, J. J. Fredberg and a. D. Navajas, "Measurement of Cell Microrheology by

Magnetic Twisting Cytometry with Frequency Domain Demodulation," *Journal of Applied Physiology,* vol. 91, pp. 1152-1159, 2001.

[145] P. Kollmannsberger, C. T. Mieke and B. Fabry, "Nonlinear viscoelasticity of adherent cells is controlled by cytoskeletal tension," *Soft Matter,* vol. 7, pp. 3127-3132, 2011.

[146] J. Chang and J. Erler, "Hypoxia-mediated metastasis.," *Adv Exp Med Biol,* pp. 772:55-81, 2014.

[147] P. Subarsky and l. R. and Hil, "The hypoxic tumour microenvironment and metastatic progression.," *Clin Exp Metastasis,* vol. 20, pp. 237-50, 2003.

[148] H. Yamaguchi and J. and Condeelis, "Regulation of the actin cytoskeleton in cancer cell migration and invasion.," *Biochim Biophys Acta ,* vol. 1773, pp. 642-52, 2007.

[149] D. Gilkes, S. Bajpai, P. Chaturvedi, D. Wirtz and G. and Semenza, "Hypoxia-inducible factor 1 (HIF-1) promotes extracellular matrix remodeling under hypoxic conditions by inducing P4HA1, P4HA2, and PLOD2 expression in fibroblasts.," *J Biol Chem,* vol. 288, pp. 10819-29, 2013.

[150] D. Gilkes, L. Xiang, S. Lee, P. Chaturvedi, M. Hubbi, D. Wirtz and G. and Semenza, "Hypoxia-inducible factors mediate coordinated RhoA-ROCK1 expression and signaling in breast cancer cells.," *Proc Natl Acad Sci U S A,* vol. 111, pp. 384-93, 2014.

[151] T. H. D. A. Park JE, R. Lai, H. Zhang, W. Meng, S. Lim and S. and Sze, "Hypoxic tumor cell modulates its microenvironment to enhance angiogenic and metastatic potential by secretion of proteins and exosomes.," *Mol Cell Proteomics,* vol. 9, pp. 1085-99, 2010.

[152] S. Vogel, M. Wottawa, K. Farhat, A. Zieseniss, M. Schnelle, S. Le-Huu, M. von Ahlen, C. Malz, G. Camenisch and D. and Katschinski, "Prolyl hydroxylase domain (PHD) 2 affects cell migration and F-actin formation via RhoA/rho-associated kinase-dependent cofilin phosphorylation.," *J Biol Chem,* vol. 285, pp. 33756-63, 2010.

[153] L. Gonzalez-Mariscal, R. Tapia and D. and Chamorro, "Crosstalk of tight junction components with signaling pathways.," *Biochim Biophys Acta,* vol. 1778,

pp. 729-56, 2008.

[154] H. Lee, J. Ryu, Y. Jung, S. Oh, S. Lee and H. and Han, "Novel Pathway for Hypoxia-Induced Proliferation and Migration in Human Mesenchymal Stem Cells: Involvement of HIF-1alpha, FASN, and mTORC1.," *Stem Cells,* vol. 33, pp. 2182-95, 2015.

[155] L. Ostergaard, U. Simonsen, Y. Eskildsen-Helmond, H. Vorum, N. Uldbjerg, B. Honore and M. and Mulvany, "Proteomics reveals lowering oxygen alters cytoskeletal and endoplasmatic stress proteins in human endothelial cells.," *Proteomics,* vol. 9, pp. 4457-67, 2009.

[156] C. Veith, S. Schmitt, F. Veit, B. Dahal, J. Wilhelm, W. Klepetko, G. Marta, W. Seeger, R. Schermuly, F. Grimminger, H. Ghofrani, L. Fink, N. Weissmann and G. and Kwapiszewska, "Cofilin, a hypoxia-regulated protein in murine lungs identified by 2DE: role of the cytoskeletal protein cofilin in pulmonary hypertension.," *Proteomics ,* vol. 13, pp. 75-88, 2013.

[157] M. Vogler, S. Vogel, S. Krull, K. Farhat, P. Leisering, S. Lutz, C. Wuertz, D. Katschinski and A. and Zieseniss, "Hypoxia modulates fibroblastic architecture, adhesion and migration: a role for HIF-1alpha in cofilin regulation and cytoplasmic actin distribution," *PLoS One,* vol. 8, p. e69128, 2013.

[158] M. Labrecque, G. Prefontaine and T. and Beischlag, "The aryl hydrocarbon receptor nuclear translocator (ARNT) family of proteins: transcriptional modifiers with multi-functional protein interfaces.," *Curr Mol Med,* vol. 13, pp. 1047-65, 2013.

[159] D. Chan and A. and Giaccia, "Hypoxia, gene expression, and metastasis.," *Cancer Metastasis Rev,* vol. 26, pp. 333-9, 2007.

[160] Y. Tsai and K. and Wu, "Hypoxia-regulated target genes implicated in tumor metastasis.," *J Biomed Sci,* vol. 19, p. 102, 2012.

[161] T. Beischlag, R. Taylor, D. Rose, D. Yoon, Y. Chen, W. Lee, M. Rosenfeld and O. and Hankinson, "Recruitment of thyroid hormone receptor/retinoblastoma-interacting protein 230 by the aryl hydrocarbon receptor nuclear translocator is required for the transcriptional response to both dioxin and hypoxia.," *J Biol Chem,* vol. 279, pp. 54620-8, 2004.

[162] H. Hayashi, Y. Tsuchiya, K. Nakayama, T. Satoh and E. and Nishida, "Down-regulation of the PI3-kinase/Akt pathway by ERK MAP kinase in growth factor signaling.," *Genes Cells,* vol. 13, pp. 941-7, 2008.

[163] C. Choi and D. and Helfman, "The Ras-ERK pathway modulates cytoskeleton organization, cell motility and lung metastasis signature genes in MDA-MB-231 LM2.," *Oncogene,* vol. 33, pp. 3668-76, 2014.

[164] J. Bereiter-Hahn, H. Karl and M. and Voth, "Mechanical basis of cell shape: investigations with the scanning acoustic microscope," *Biochem Cell Biol.,* vol. 73, pp. 337-348, 1995.

[165] C. Chen, M. Mrksich, S. Huang, G. Whitesides and D. and Ingber, "Geometric control of cell life and death," *Science,* vol. 276, pp. 1425-1428, 1997.

[166] M. Chicurel, R. Singer, M. C. and D. and Ingber, "Integrin binding and mechanical tension induce movement of mRNA and ribosomes to focal adhesions," *Nature,* vol. 392, pp. 730-733, 1998.

[167] B. Fabry, G. Maksym, J. Butler, M. Glogauer, D. Navajas, N. Taback, E. Millet and J. and Fredberg, "Time scale and other invariants of integrative mechanical behavior in living cells," *Physical Review,* vol. 68, pp. 1-18, 2003.

[168] P. Cai, Y. Mizutani, M. Tsuchiya, J. Maloney, B. Fabry and K. and Vliet, "Quantifying cell-to-cell variation in power-law rheology," *Biophysical Journal,* vol. 105, pp. 1093-1102, 2013.

[169] M. Puing-De-Morales, M. Grabulosa, J. Alcaraz, J. Mullol, G. Maksym, J. Fredberg and D. and Navajas, "Measurement of cell microrheology by magnetic twisting cytometry with frequency domain demodulation," *Journal of Applied Physiology,* vol. 91, pp. 1152-1159, 2001.

[170] S. Yamada, W. D. and S. and Kuo, "Mechanics of living cells measured by laser tracking microrheology," *Biophysical Journal,* vol. 78, pp. 1736-1747, 2000.

[171] S. Kollmannsberger, C. Mieke and B. and Fabry, "Nonlinear viscoelasticity of adherent cells is controlled by cytoskeletal tension," *Soft Matter,* vol. 7, pp. 3127-3132, 2011.

[172] J. Ohayon and P. and Tracqui, "Computation of adherent cell elasticity for critical cell-bead geometry in magnetic twisting experiments," *Annals of Biomedical Engineering,* vol. 33(2), pp. 131-141, 2005.

[173] H. Karcher, J. Lammerding, H. Huang, R. Lee, R. Kamm and M. and Kaazempur-Mofrad, "A three-dimensional viscoelastic model for cell deformation with experimental verification," *Biophysical Journal,* vol. 85, pp. 3336-3349, 2003.

[174] T. Niu and G. and Cao, "Power-law rheology characterization of biological cell properties under AFM indentation measurement," *RSC Adv.,* vol. 4, pp. 29291-9, 2014.

[175] H. Irie, R. Pearline, D. Grueneberg, M. Hsia, P. Ravichandran, N. Kothari, S. Natesan and J. and Brugge, " Distinct roles of Akt1 and Akt2 in regulating cell migration and epithelial-mesenchymal transition," *J Cell Biol ,* vol. 171, pp. 1023-34, 2005.